AAPM REPORT NO. 54

STEREOTACTIC RADIOSURGERY

Report of Task Group 42
Radiation Therapy Committee

Michael C. Schell (Chairman)
Frank J. Bova
David A. Larson (Consultant)
Dennis D. Leavitt
Wendell R. Lutz
Ervin B. Podgorsak
Andrew Wu

June 1995

Published for the
American Association of Physicists in Medicine
by the American Institute of Physics

Further copies of this report ($10 prepaid) may be obtained from:

American Association of Physicists in Medicine
One Physics Ellipse
College Park, MD 20740-3843

International Standard Book Number: 1-56396-497-X
International Standard Serial Number: 0271-7344

Published by the American Institute of Physics, Inc.
500 Sunnyside Blvd., Woodbury, NY 11797

Printed in the United States of America

STEREOTACTIC RADIOSURGERY

Table of Contents

I. INTRODUCTION

A. Clinical Introduction

Stereotactic radiosurgery (SRS) of an intracranial lesion, or radiosurgery, combines the use of a stereotactic apparatus and energetic radiation beams to irradiate the lesion with a single treatment. Stereotactic Radiotherapy (SRT) utilizes the stereotactic apparatus and radiation beams for multiple fractions or treatments. SRS and SRT are essentially two-step processes consisting of: (1) accurately defining the shape and location of the lesion and the neuroanatomy in the reference frame of a stereotactic frame system with CT, MRI or angiography; and (2) developing and delivering the planned treatment. The treatment techniques produce a concentrated dose in the lesion with steep dose gradients external to the treatment volume. The rapid dose falloff from the edge of the treatment volume provides dramatic sparing of normal brain tissues.

SRS was first developed by Leksell in the late 1940s to destroy dysfunctional loci in the brain using orthovoltage x rays (Leksell, 1951). Heavy charged particles, gamma rays, and megavoltage x rays have been used in the intervening decades to irradiate arteriovenous malformations as well as benign and malignant tumors.

This report describes the techniques for stereotactic external beam irradiation with heavy charged particles from cyclotrons, x rays from electron linear accelerators (Linacs) with nominal beam energies between 4- and 18-MV, and gamma rays from the "gamma knife" using 201 ^{60}Co sources. The first three-dimensional treatment of a brain lesion with a megavoltage unit took place in April 1948 (Kerst, 1975). The first combined use of an x-ray unit and stereotactic frame occurred in 1950 (Leksell, 1951, 1983). This report is written primarily for clinical medical physicists who are considering acquisitioning and commissioning of a SRS program at their facility. It is extremely important to understand the importance of quality assurance in every step of the SRS treatment process. As with brachytherapy, the dose with SRS is administered in one or a few applications. However, the dose rate for SRS is such that the dose is typically delivered in less than one hour from the start of treatment, unlike low-dose-rate brachytherapy, which is typically administered over several days. It is imperative therefore that a thorough and methodical quality assurance program for SRS be developed at each institution. Safety precautions include the implementation of interlocks on the patient support assembly (couch) motion and the gantry motion, which limit the arc or rotation of the equipment and prevent patient injury. No therapy department should consider undertaking SRS without the presence of at least one clinical medical physicist (as defined by the AAPM, 1985) at each procedure. The quality assurance requirements demand that every step be checked by a physicist and independently rechecked by a

second expert (clinical medical physicist or a board-eligible medical physicist). A joint statement has been issued on this subject by The American Association of Neurological Surgeons and The American Society for Therapeutic Radiology and Oncology (Lunsford *et al.*, 1994). The statement defines radiosurgery, but also recommends that training be received by the radiation oncologist and physicists. It also specifies that the oncologists and physicists be board certified or eligible for board certification.

Typical abnormalities that are treated with SRS are single metastasis (Sturm *et al.*, 1987), solitary primary brain tumors (Larson *et al.*, 1990), arteriovenous malformations (Betti *et al.*, 1989; Colombo *et al.*, 1987; Fabrikant *et al.*, 1985 and1984; Kjellberg *et al.*, 1986; Saunders *et al.*, 1988; and Steiner, 1986) and benign conditions (Barcia-Salorio *et al.*, 1985) or tumors, such as pituitary adenoma and acoustic neuroma (Kamerer *et al.*, 1988). Overviews of clinical applications of SRS/SRT have been presented by Flickinger and Loeffler (1992), Luxton *et al.* (1993), McKenzie *et al.* (1992), and Podgorsak *et al.* (1987, 1988, 1989, 1990, and 1992). SRS generally consists of identifying a target in the patient's brain that is to be irradiated by the intersection of one or more heavy charged particle beams, by multiple noncoplanar arcs with a linac, by dynamic rotation with a linac, or by the intersection of ^{60}Co beams at the isocenter of the gamma knife.

Target identification begins with the fixation of a stereotactic frame to the patient's skull. Imaging techniques, such as computerized tomography (CT), magnetic resonance imaging (MRI) and/or angiography, pinpoint the target within the stereotactic frame. The location and geometry of the target is then transferred to a treatment planning system that calculates dose distributions in three dimensions. The treatment planning system must be capable of computing dose distributions from either the combination of noncoplanar arcs or the intersection of the ^{60}Co beams. For linac-based radiosurgery, the arc geometry can be varied to provide a concentrated dose to the selected target while minimizing the dose to critical structures surrounding the target. The gamma knife achieves similar results by selective "plugging" of holes in the helmet (Flickinger, 1990).

The clinical rationale or indications for radiosurgery are discussed in Section II. Factors contributing to the net uncertainty of the SRS treatments are reviewed in Section III, which describes the tolerances encountered in each SRS technique. A brief introduction to the radiosurgical techniques is presented in Section IV and detailed synopses of five techniques are in the appendices. Acceptance testing requirements for the pedestal-mounted and couch-mounted frames are contained in Section V. The beam and dosimetry requirements are described in Section VI. Requirements of quality assurance programs for the hardware, software, and treatment procedure are reviewed in Section VII. Current research efforts in SRS are summarized in Section VIII.

B. Introduction For Administrators

Table I contains time estimates for various tasks that are involved with commissioning a linac-based radiosurgery procedure. These time estimates deal solely with the time requirements for collecting the physical data and testing the hardware and software of a radiosurgery installation. For example, it is estimated that it would take approximately 10 weeks for a department with a scanning film densitometer and the appropriate ionization chambers to commission a commercial radiosurgery package. Such packages are currently available from RSA, Inc. (Brookline, MA) and Leibinger and Fischer LP (Metairie, LA). To fabricate the treatment hardware (the tertiary collimation system) for the stand or the couch mount systems would take approximately 0.7 yr. To install a prefabricated hardware system and write a treatment planning software package for radiosurgery would take 2.3 yr. To design the entire system in-house and install the hardware and software would require almost 3 yr. These time estimates do not include the background efforts regarding the coordination of the disciplines of radiation oncology, neurosurgery, and neuroradiology. A considerable amount of time

TABLE I. Time Estimates for Commissioning a Radiosurgery Program.
Estimated Project Times (weeks)

TASK	TIME
Stereotactic Equipment Evaluation	2 wks
Treatment Planning System	
a) Evaluate commercial package	1 wk
b) Develop treatment planning	2 yrs
Dosimetry Measurements	2 wks
Treatment Delivery Hardware	
a) Setup commercial package	3 wks
b) Adapt a prefabricated system	12 wks
c) Design & fabricate	28 wks
Final System Test	2 wks
Routine QA	0.5 days/month
Plan and Treat a Radiosurgery Case	8–12 hr/patient (Depending on Complexity)
TIME ESTIMATES FOR FOUR OPTIONS:	
Commercial Package	10 wks
Adapt a Prefabricated System and Write Software	2.3 yrs
Fabricate Hardware/Buy Software	0.7 yrs
Design and Fabricate Hardware/ Write Software	2.7 yrs

is invested in coordinating the quality assurance programs of each department and establishing the team required to execute a radiosurgery procedure. Finally, there are time estimates for planning and treating a typical radiosurgery patient. It usually requires 8 hr of 1.5 physicists and dosimetrists to plan and treat the patient. This begins with acquiring imaging data early in the day, entering the data sets into the computer, establishing the appropriate contours and surfaces of the tumor and normal tissue structures, developing a plan, and reviewing the plan with the radiation oncologists, the neurosurgeons, and finally treating the patient. The routine QA of radiosurgery hardware and software requires approximately 0.5 days per month.

In summary, the time requirements for installing and commissioning a radiosurgery procedure are substantial. The time requirements for treating a typical patient per week amounts to 20% of a typical weekly patient load. **This procedure represents a significant increase in the staffing requirements of the physics section of the department of radiation oncology. We recommend an additional 0.3 FTE medical physicists/patient/week (board-certified or board-eligible radiotherapy medical physicist) to support an ongoing radiosurgery program.** We recommend a minimum of 0.2 FTE medical physics years be allotted for the acceptance and commissioning of a commercial linac-based SRS system. Radiosurgery is a very time-consuming procedure requiring a high degree of attention to detail. The consequences of understaffing and misadministration are a significant and grave risk to the patient.

II. RATIONALE FOR RADIOSURGICAL TREATMENTS

Radiosurgery has been used to treat a variety of benign and malignant lesions as well as functional disorders. In many categories, however, only a small number of cases have been treated. Results have not been reported and indications are far from established. Kihlstrom reported 1311 gamma knife unit radiosurgical procedures performed at Karolinska Hospital between 1968 and 1986 (Kihlstrom, 1986). The most frequent reasons for treatment were arteriovenous malformations (AVM) (41%), acoustic neuroma (14%), and functional radiosurgery (14%). Chierego *et al.* (1988) listed 150 patients treated with a linac-based system in Vicenza. The most frequent categories were AVM (44%) and malignancy (33%). The natural history of inoperable arteriovenous malformations may be favorably influenced by radiosurgery as discussed below. The risk of hemorrhage is 2–3% per year and 6% immediately posthemorrhage. The nidus of the AVM is a blood steal from the adjacent parenchyma. Hence, it is generally assumed that the adjacent tissues are dysfunctional and that radiation damage to this tissue would result in minimal additional neurological deficits.

A. Nonmalignant Lesions

Stereotactic radiosurgery has been used for nonmalignant lesions such as arteriovenous malformations and acoustic neuromas. Arteriovenous malformations are congenital anomalies that develop from aberrant connections within the primitive arterial and venous plexus overlying the developing cortical mantle. During embryological maturation, this region of abnormal vasculature is incorporated into the brain parenchyma. Initially, the cerebral vasculature adjacent to the AVM develops normally. However, because AVMs lack a normal capillary bed and the associated hemodynamic resistance, local blood flow through the AVM is increased and vascular dilation gradually ensues. This shunting of blood through the AVM may result in a blood steal phenomenon. The lack of a normal capillary bed implies that the vessels of the AVM provide no nutritive function. Therefore, tissues deep within the AVM may be nonfunctioning and sclerotic. The approximately 2–3% per year risk of bleeding is the primary reason for treating the AVM. The standard treatment is surgical resection, if it can be performed safely. The immediate goal is to eliminate the risk of hemorrhage. In cases where the AVM is relatively inaccessible, especially if centrally located in the speech area or in the brain stem, radiosurgery may be considered.

The radiosurgical principles applicable to the treatment of AVMs are evolving, and thus far are similar to established surgical principles: (1) Within the nidus of the AVM, radiosurgery may be destructive because there is usually little normally functioning tissue therein; (2) One should not pursue arteries or veins beyond their normal attachment to the nidus to avoid damaging normal tissue: (3) Obliterating a final feeding artery only improves tissue nutrition whereas obliterating any other artery only worsens tissue nutrition; and (4) Total obliteration of the AVM is of vastly greater benefit than partial obliteration. Usually the obliteration of AVMs after radiosurgery is not complete for 1–3 years.

Stereotactic radiosurgery for small-volume AVMs appears to achieve a high obliteration rate at the end of 2 years with a low complication rate (Alexander *et al.*, 1993). There are several limitations or disadvantages to stereotactic radiosurgery for the treatment of AVMs. The obliteration of the larger AVMs is not readily achievable with stereotactic radiosurgery with a 2-yr follow-up. Microembolization in conjunction with stereotactic radiosurgery is currently under evaluation for treatment for the larger AVMs. Other sites of treatable benign lesions include pituitary adenomas, acromegaly Cushings disease, and Nelson's syndrome (Levy *et al.*, 1989 and Alexander *et al.*, 1993). [See also Friedman (1993); and Hosobuchi (1987).]

B. Malignancies

It may be argued that radiosurgery as the sole treatment modality, with its dose localization characteristics, is contraindicated in the treatment of

primary malignant intracranial lesions, where tumor cells are known to infiltrate beyond the borders of abnormalities seen on CT or MRI (Halperin *et al.*, 1989; Hochberg and Pruitt, 1980; and Wallner *et al.*, 1989). The role of radiosurgery in radiation oncology may be analogous to that of interstitial brain implants as a high-dose boost following the standard course of external beam therapy (Halperin *et al.*, 1989). Mehta *et al.* (1993) have performed a prospective analysis of the toxicity and efficacy of stereotactic radiosurgery boost when combined with external beam radiotherapy for the treatment of newly diagnosed glioblastoma (GBM). External beam radiation therapy was delivered to 54 Gy with 1.8 Gy per fraction times 30 fractions. The stereotactic radiosurgery boost ranged from a maximum of 25–35 Gy. Their preliminary findings were that no significant toxicities were encountered and the necrosis rate was 10% at a follow-up of 13.5 months. The data evinces at best a minimal improvement in survival. SRS application to the treatment of metastases has been found to provide improved local control if applied in conjunction with whole brain irradiation (Fuller *et al.*, 1992). Further discussion of the use of SRS for malignancies is located in Section IV.

III. THE ACCURACY OF STEREOTACTIC RADIOSURGERY

Accuracy limits not only reflect the technical limitations of the frames and treatment units, but also reflect the current knowledge of the neurological abnormality and its radiation response. Two SRS techniques report uncertainties in target alignment with the beam focus of 0.2–0.4 mm in patient position, whereas the linac setup uncertainty is 1.0 mm (Friedman and Bova, 1989 and Wu *et al.*, 1990). Although the techniques differ in accuracy, it is unclear whether the difference is clinically significant. The uncertainty in dose delivery is a result of two processes: (1) target definition and (2) the machine tolerances of the dose delivery apparatus (including the frame). A reasonable perspective on accuracy requirements for SRS should include (1) the current accuracy in external beam therapy; (2) the net result of uncertainties in SRS; (3) the resolution of the target image; and (4) the relationship of the image to the lesion itself, macroscopic and microscopic.

The accuracy of patient setup in conventional external beam therapy has been investigated by several groups, including that of Rabinowitz *et al.* (1985). The variation in setup was determined from the differences between simulation and port films. The standard deviation in treatment-to-treatment variation was 3 mm. However, the average discrepancy between the simulation films and port films was 5 mm when the brain was the treatment site. The mean deviation exceeded 7 mm. Hence, the benefit of stereotactic localization and treatment is the ability to plan and treat a target with reduced position uncertainty.

The definition of a tumor with CT (or AVM with angiography) depends on the resolution of the image and the relationship of the macroscopic image with the microscopic extent of the disease. The first factor is a consequence of the dimensions of the voxel. The pixel dimensions are typically 0.7 mm by 0.7 mm, and the separation between slices is not less than 1.0 mm. Therefore, an object's location cannot be known better than to within 1.5–2.0 mm. The mechanical position uncertainty in any orthogonal axis of a stereotactic frame is 0.6 mm. The gantry rotation axis, collimator rotation axis, and table rotation axis should coincide within a sphere of 1 mm radius. The net uncertainty in target localization and treatment delivery is then 2.0 mm for an AVM and 2.4 mm for a tumor when summed in quadrature (Table II). Note that the net uncertainty increases to 3.7 mm when a CT slice separation of 3 mm is employed. This net uncertainty is far less than the clinical knowledge of the AVM or neoplasm.

AVM definition can be limited by factors other than the detector resolution. The nidus of an AVM may be partially obscured by arteries or veins. In this case, the location of the nidus may only be known to within 5 mm. In the absence of this uncertainty, orthogonal angiograms permit the location of an AVM in the stereotactic frame coordinates to within 1 mm. The 1-mm limit derives from the radiologists ability to identify a unique point from two views. However, the extent of the nidus cannot be determined from the orthogonal radiographs, preventing the optimum plan of irradiating the target while sparing normal tissue.

Similar uncertainties exist for certain brain tumors, but it is caused by the invasive nature of the malignancies. The relationship of the macroscopic CT image with the primary brain tumor is a matter of current study (Halperin *et al.*, 1989; Hochberg and Pruitt 1980; Kelly *et al.*, 1987; and Wallner *et al.*, 1989). Halperin *et al.* obtained antemortem CT scans of glioblastoma multiforme (GBM) tumors in 11 patients. In nine cases, autopsies indicated that the tumor extended beyond a 1-cm margin around the contrast-enhancing areas. Furthermore, the differences between survival rates for whole brain irradiation versus partial brain irradiation are not statistically signifi-

TABLE II. Achievable Uncertainties in SRS

Stereotactic Frame	1.0 mm	1.0 mm
Isocentric Alignment	1.0 mm	1.0 mm
CT Image Resolution	1.7 mm	3.2 mm
Tissue Motion	1.0 mm	1.0 mm
Angio (Point Identification)	0.3 mm	0.3 mm
Standard Deviation of Position Uncertainty (by Quadrature)	2.4 mm	3.7 mm

cant. This lack of difference between treatments is a result of the failure of external beam therapy to control bulky disease. Current external irradiation techniques alone are insufficient for tumor eradication; "focal" (brain implants or SRS) treatment is required to help eliminate the original tumor. It is further speculated that when the primary tumors are controlled, many patients will have recurrent GBM outside the abnormal region as shown by CT or MRI.

The uncertainties in dose delivery by any of the above SRS techniques are significantly less than the clinical knowledge of the location and extent of the lesion as determined by CT or MRI. The accuracy in dose delivery to the target of linac-based radiosurgery is a significant improvement over conventional techniques and approaches that of the heavy-charged-particle facilities. Until technology affords accurate target localization, the differences in position accuracy will have minimal impact on treatment delivery. However, the impact of the net position accuracy on the planning process should be foremost in the minds of the oncologist and physicist. Table II illustrates the uncertainties in SRS delivery for two cases: (1) 1-mm slice thickness and (2) 3-mm CT slice thickness.

IV. STEREOTACTIC RADIOSURGERY TECHNIQUES

SRS is a nonstandard radiation therapy technique by nature of the means of delivery of the target dose. Two basic approaches have been taken in the past: (1) modification of standard linear accelerators with the addition of tertiary collimation and stereotactic frame system or (2) the use of a dedicated ^{60}Co unit. Linac-based radiosurgery delivers a narrowly collimated x-ray beam while rotating about the target. The target is positioned at the center of linac rotation. The process is repeated for a number of treatment couch angles. Thus, the target is caught in a cross fire of x-ray beams which deliver a lethal dose to the target and a sublethal dose to the surrounding normal tissues. The gamma knife unit delivers a comparable dose by means of the simultaneous irradiation from 201 cobalt beams. The dose distribution is concentrated in a localized small volume by the intersection of beams from up to 201 ^{60}Co sources (gamma knife unit shown in Figure 1) or of the multiple arcs from a linear accelerator. The small treatment volume and rapid dose falloff are also characteristic of brain implants, yet the technical aspects of SRS are considerably different from those of brachytherapy.

Figure 2 illustrates the beam entry patterns for (1) the gamma knife unit; (2) a single 360° arc in the transverse plane of the patient; (3) a four noncoplanar arc geometry; and (4) the dynamic radiosurgery approach (b, a, e, and g, respectively in Figure 2). These four approaches produce isodose surfaces with shapes that are unique to the SRS. The dose-volume histograms have been found to be approximately equivalent among the four approaches (Phillips *et al.*, 1989; Schell *et al.*, 1991; and Serago, 1992). Stan-

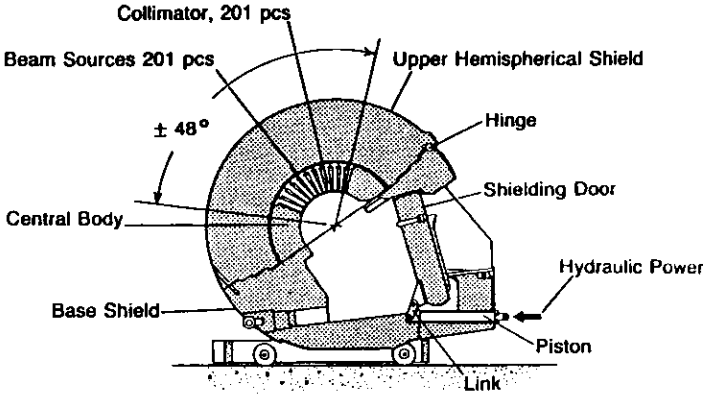

THE RADIATION UNIT

FIGURE 1. The cross-sectional view of the gamma knife irradiator. The 201 sources are focused at one locus. The stereotactic frame positions the target at the intersection of the beams. (Wu *et al.*, 1990.)

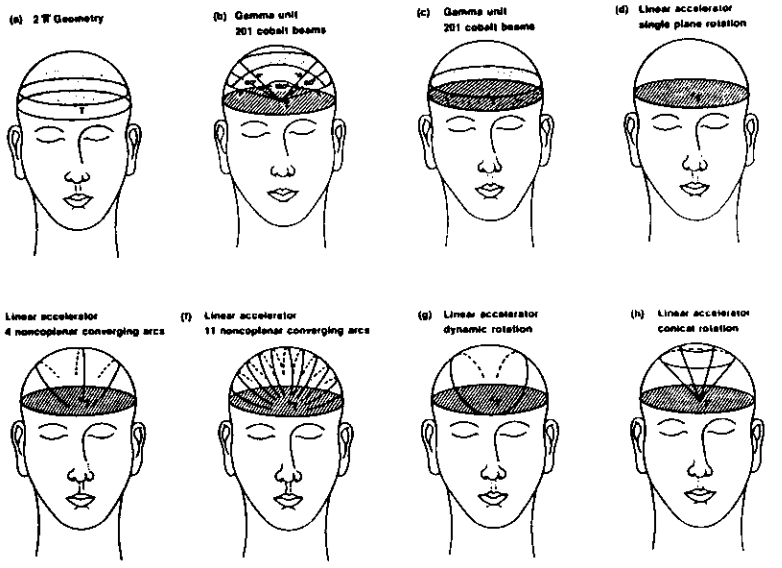

FIGURE 2. Beam-entry patterns on a patient's skull for various radiosurgical techniques. (Podgorsak, E.B. Physics for radiosurgery with linear accelerators, in "Stereotactic Radiosurgery", Chapter 2, pp. 9–34, Neurosurgery Clinics of North America, Vol. 3, edited by D. Lunsford, W.B. Saunders Company, Philadelphia, PA, 1992.)

dard arc geometries were routinely used for many lesions in the mid-1980s. Advances in treatment planning software allow for beam's-eye-view planning which facilitates dose optimization to the target and avoidance of critical normal tissues. The shapes of the isodose surfaces can be modified to minimize the dose to critical structures by changing the arc geometry with linacs. The gamma knife unit collimators can be plugged to prevent beam passage through vital tissue. At most centers, each treatment plan geometry is adjusted to minimize normal-tissue dose and maximize target dose, as is the case with conventional external beam planning. Irregularly shaped lesions are treated with multiple isocenters with linacs and the gamma knife unit. The range in collimator size differs between linacs and the gamma knife unit. Linacs use collimator sizes in the range of 5–40 mm diameter, whereas the gamma knife unit has four collimator diameters: 4 mm, 8 mm, 14 mm, and 18 mm. Large lesions require more isocenters with the gamma knife unit than with linacs.

The irradiation geometry for heavy charged particles varies between centers. LBL (Lawrence Berkeley Lab) only irradiated through the hemisphere with the lesion; a four-port geometry is normally employed. The Harvard Cyclotron Therapy Center treats with seven to eleven ports. Heavy charged particle beams have the advantage of stopping at the distal edge of the target. Consequently, the integral dose is approximately a factor of two less than with photon therapy beams. The beam shaping of heavy charged particle beams eliminates the need for multiple isocenters.

Figure 3 compares the beam profiles for helium ions with 6-MV x rays with 1.27- and 1.25-cm beam diameters. The helium beam yields a more uniform dose profile than the 6-MV x rays. However, the two modalities have comparable profiles. An 8-mm diameter lesion would receive a zero % dose gradient from helium ions and a 10% dose gradient with 6-MV x rays if a prescription were based solely on profile data. This comparison suggests that the primary advantage of heavy ion therapy is in normal tissue sparing, due principally to the finite range of the particles in tissue. Since the late 1940s (Wilson, 1946), the advantages of delivering heavy charged particles in concentrated doses to tumors while sparing normal tissue have been acknowledged. Since the high cost of heavy ion therapy limits its use, most institutions rely on the gamma knife unit or modified linacs. However, new x-ray-based techniques, such as PEACOCK and ACCU-RAY, have the potential to enhance the dose delivery of x-ray beams and narrowing the gap between x rays and heavy charged particle approaches (see Section VIII).

Three groups have compared photon-SRS techniques. The first comparison used the steepest and shallowest dose gradients as criteria (Podgorsak *et al.*, 1989). More recently, Schell *et al.* (1991) and Serago *et al.* (1992) have used dose-volume histogram analysis to compare linac-based SRS techniques. The differences in dose-volumes between the approaches were clinically insignificant when the total arc traversal exceeded 400° of gantry rotation.

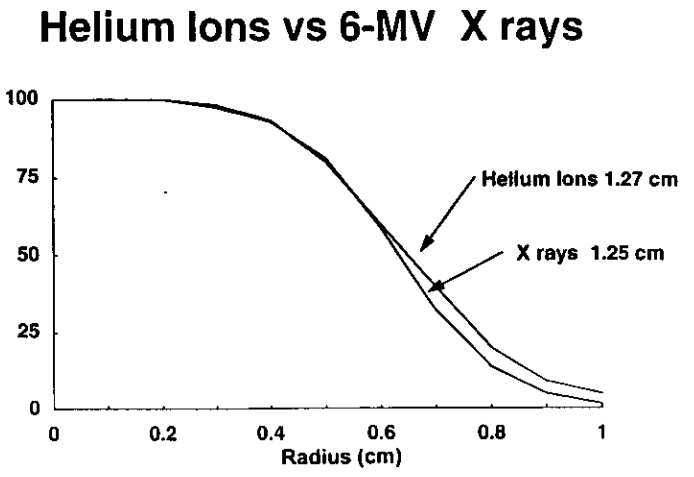

FIGURE 3. The dose profile of a 230 MeV/u helium ion beam is compared with the dose profile of a 6-MV x-ray beam.

Schell *et al.* (1991) demonstrated that the differences in techniques disappeared at the 5% dose level as the collimator sizes exceeded 2.0 cm when the geometry of the cranium became the limiting factor. Detailed information on five SRS techniques is contained in Appendix IV.

V. ACCEPTANCE TESTING

A. Introduction

The basic requirements for SRS are: (1) accurate localization, (2) mechanical precision, (3) accurate and optimal dose distribution, and (4) patient safety. These four requirements are common to linac-based radiosurgery and the gamma knife unit. Some tests are unique to the gamma knife unit and are discussed at the end of this section.

B. Accurate Localization

The stereotactic localization techniques shall be able to determine the coordinates of a well-defined object (pointer or a ball bearing in a phantom) in the frame coordinate system to within 1 mm for angiography, and 2 mm for CT and MRI. A localization test is described in the System Verification Test section.

C. Mechanical Precision

An essential element of stereotactic therapy is the alignment of the patient-frame-based coordinate system with the LINAC coordinate system. The alignment procedure puts the treatment target position specified in the

patient-frame coordinate system at the LINAC isocenter. The alignment procedure typically relies on rigid mechanical devices, including pedestal and couch-mounted devices, or on registration of patient-based markers. A prerequisite of this report is that the radiation oncology department abide by the recommendations of AAPM Reports 40 and 45 with regard to quality assurance and quality improvement of equipment and procedures. AAPM Report 40 focuses on comprehensive QA for radiation oncology and AAPM Report 45 deals specifically with the code of practice for radiotherapy accelerators and machine tolerance limits. Adherence to the recommendations of the aforementioned reports forms the foundation for the SRS QA procedures delineated below.

1. Linac Gantry, Collimator, and Couch (PSA)

The overall stability of the isocenter under rotation of all axes—couch, gantry, and collimator—needs to be established before commencing any stereotactic therapy program. These axes shall coincide within a 1-mm radius sphere for all possible gantry, collimator and PSA angles. (Hartmann *et al.*, 1994) Caution: Some centers correct for the precession of the PSA axis by changing the target coordinates as a function of PSA angle in order to center the lesion during treatment. We recommend correcting the mechanical precession problem (e.g., PSA bearing replacement) prior to commissioning the SRS procedure. PSA precession correction requires at least two coordinate adjustments for each PSA angle. These corrections could be misapplied and place the lesion further away from the linac isocenter.

A couch-mount system requires a mechanically stable couch. The most critical mechanical property is the stability of the couch rotation axis under rotation. It is not necessary for the couch to be infinitely rigid, as such a requirement is unattainable, even in principle. It is necessary, however, for the couch to be stable under rotation, i.e., as the couch rotates, the mechanical forces on it should not change the torque on the couch. A couch can be mechanically stabilized by external supports to increase the stiffness if needed.

2. Lasers

The most practical room-based reference system is afforded by wall-mounted lasers. A set of three lasers—two on opposite sides lateral to the LINAC and one in the ceiling—suffices. These lasers must cross accurately at the isocenter and must be as parallel as possible. These requirements imply that the laser-mounting brackets must allow very fine movement to allow mechanical movement of the complete laser assembly. The lasers should coincide within 1 mm of axes locus. The lasers should be routinely checked for drift.

3. Patient Docking Device

The patient docking device couples the frame to the treatment machine, either the pedestal or the couch-mount bracket. The patient docking device must be as mechanically rigid as possible. Notably, the docking position on the frame should minimize torque caused by the patient. For the pedestal-mounted frame system, the origin of the pedestal's coordinate system should be aligned to within 1.0 mm of the gantry/collimator/PSA axes' locus. For the couch-mounted frame, the patient is brought in alignment with the LINAC isocenter using the standard couch motors. These motors, however, are not accurate or sensitive enough to assure accurate positioning. The patient docking device thus must allow a vernier-based or fine adjustment system to precisely align the patient at the desired isocenter/target position. It is the experience of the task group members that the frame system can be aligned to within 1 mm of the linac coordinate system.

4. Frame System

The performance of the components relating to the frame coordinate system must be verified as to compliance with the manufacturer's specifications. For example, the BRW pedestal and phantom base axes should be accurate to within ± 0.6 mm for each axis. The CT, MRI, and angiographic localization procedures must yield target coordinates that differ by less than the total uncertainty of the frame system and imaging procedures over the coordinate domain of the frame system.

5. Target Verification Devices

The target verification devices ensure that the patient is treated at the correct target coordinate, that the target coordinate is aligned with the isocenter, and that the patient is aligned with the isocenter. These devices are calibrated with respect to the frame-based coordinate system. This calibration needs to be verified and documented upon acceptance.

6. SRS System Verification Test

Before a particular radiosurgery system is considered ready for patient treatments, we recommend testing the entire system/procedure (localization through treatment) for geometric accuracy. This comprehensive method to obtain quantitative results involves the use of hidden targets (steel or lead balls) placed in a head phantom. These hidden targets are localized by CT and planar angiograms (MRI may require a more careful selection of phantom and targets) under conditions and with the same equipment used for patients. These targets are next "treated" with a number of fixed beams representing entrance points spread over the upper hemisphere of the skull.

A port-film exposure is made for each beam. The displacement of the image of the steel ball from the center of the field is measured for each of the beams. From this information, the geometric error in treatment (i.e., the displacement of the center of the radiation distribution from the target center) can be calculated. A summary of the geometric error in the "treatment" of 18 hidden targets is given below (Lutz *et al.*, 1988):

Localization Method	Average Error in Treatment (mm)
Computed Tomography	1.3 ± 0.6
Plane Film Angiography	0.6 ± 0.2

These results agree with the uncertainties ascertained by Yeung *et al.* (1993) and determine a margin (in the absence of medical uncertainty) which can be used between the prescription isodose surface and the target boundary that assures target coverage for a particular confidence level desired.

It is also possible to measure the accuracy of localization alone via CT or planar radiography, in the absence of medical uncertainty, using the test targets (plastic or steel balls) that are attached, respectively, to the CT and angiographic localizer frames. The coordinates of the balls can then be measured directly by mounting the appropriate localizer to the BRW phantom base and comparing with the coordinates found using the treatment planning program.

$$Localization\ Error = \sqrt{(\Delta AP)^2 + (\Delta Lat)^2 + (\Delta Vert)^2}$$

where ΔAP, for example, is the difference between a phantom base measurement and a computer calculation.

If you use digitally reconstructed planar radiographs or MRI, test the procedure thoroughly to ensure the images are free of distortions throughout the volume of interest. Positional errors as large as 4 mm can occur when digitally reconstructed radiographs are used for localization.

One interesting observation is that if the linac and the radiosurgery apparatus are accurately aligned and mechanically stable, then the average measured errors in "treatment" (hidden targets in a phantom) will be approximately the same size as the measured localization errors. The fact that localization and treatment errors presented here are exactly the same is just a coincidence. Furthermore, these results do not suggest that the treatment apparatus does not introduce error. Rather, they suggest that for a *well aligned system*, errors introduced through the treatment apparatus are smaller and randomly directed with respect to the errors in localization (particularly CT localization). Furthermore, uncertainties in measurements of the test target coordinates by the phantom base contribute to the "localization error".

D. Dose Delivery

- The accuracy of the absorbed dose (beam calibration) to the target shall be uncertain by less than 5%, in accord with AAPM Report 21.
- The dose delivery to the simulated radio-opaque target shall be aligned to within 1 mm for all gantry, collimator, and PSA angles.
- The tertiary collimator system shall reproducibly collimate the beam with a variation in the full-width at half maximum of 2 mm.
- The dose gradient in the beam penumbra (from 80% to 20%) shall be greater than or equal to –60%/3 mm.

E. Patient Safety/Machine Interlocks

The linac should be interlocked to:

- Limit gantry rotation as a function of PSA position in order to prevent injury to the patient, by means of either software or hardware.
- Set the secondary collimators to the treatment position. **If the SRS treatment occurs with the jaws opened beyond the tertiary collimator, the normal brain tissue will receive an excessive and unacceptable dose.**
- Disable power and immobilize the PSA during the SRS treatment. An interlock system for certain linacs has been developed to satisfy the above requirements (DeMagri *et al.*, 1994).

F. Gamma Knife Acceptance Tests

- Radiation Survey of the Facility
- Radiation Leakage Test
- Radiation Wipe Test
- Timer Constancy and Linearity Tests
- Timer Accuracy Test
- Timer On-Off Error
- Safety and QA checks:
  a) Door interlock
  b) Emergency-off switches
  c) Beam on-off lights
  d) Audio-visual system
  e) Couch movement
  f) Micro switches verify the helmet alignment with the ^{60}Co source locus to ± 0.1 mm.
  g) Hydraulic system. The hydraulic system is designed to withdraw the patient/couch from the gamma knife unit and close

the gamma unit door in the event of a power failure. A hand pump serves as a backup in case of hydraulic fluid pressure loss. These systems must be tested.

h) Dose profiles of each helmet shall be measured by plugging 200 of the 201 collimators in each helmet. Film dosimetry is used to obtain the beam profile and background radiation. The background radiation is measured with all 201 collimators plugged. The background is then subtracted from the first film.

i) Relative helmet factors. A small ion chamber should be cross-calibrated against an ion chamber which has a calibration traceable to NIST. The cross-calibrated ion chamber is used in a small phantom to calibrate the 18-mm helmet, with the chamber centered at the beam locus. Film, diodes and/or TLDs should be used to calibrate the 4-, 8-, and 14-mm helmets.

j) Availability of operating manual and safety posting.

VI. DOSIMETRY

A. Linac Systems

1. Dose Measurements

The dosimetry of small x-ray fields is complicated by two factors: the relationship between detector size and field dimensions and the lack of equilibrium in lateral charged particles. Figures 4 (a)–(c) and 5 illustrate the beam profiles for both the linac and gamma knife as a function of collimator diameter. The large dose gradients in the typical SRS penumbra relative to the conventional fields require dosimetry techniques with higher spatial resolution.

Dose distributions for stationary fields have been determined in water baths and polystyrene slabs with ion chambers, TLDs, and film (Friedman and Bova, 1989; Rice *et al.*, 1987; Wu *et al.*, 1990; and Olsson *et al.*, 1992). The effect of detector size on penumbra width has been reported by Dawson *et al.* (1986) and Rice *et al.* (1987). Beam profile measurements with a detector diameter of 3.5 mm or less can reproduce the penumbra width to within 1 mm. Dawson *et al.* investigated the penumbra width as a function of ion chamber diameter for large photon fields. Extrapolation to zero detector diameter provided a correction factor for the 90%–10% width of the penumbra. Rice *et al.* (1987) determined that the corrections to penumbra widths ranged from 0.3–1.0 mm when beam profiles (1.25–3.0 cm in diameter) were measured with a 3.5-mm diameter detector.

Transient electronic equilibrium exists at the point of measurement when the measurement point is farther from the beam edge than the maximum

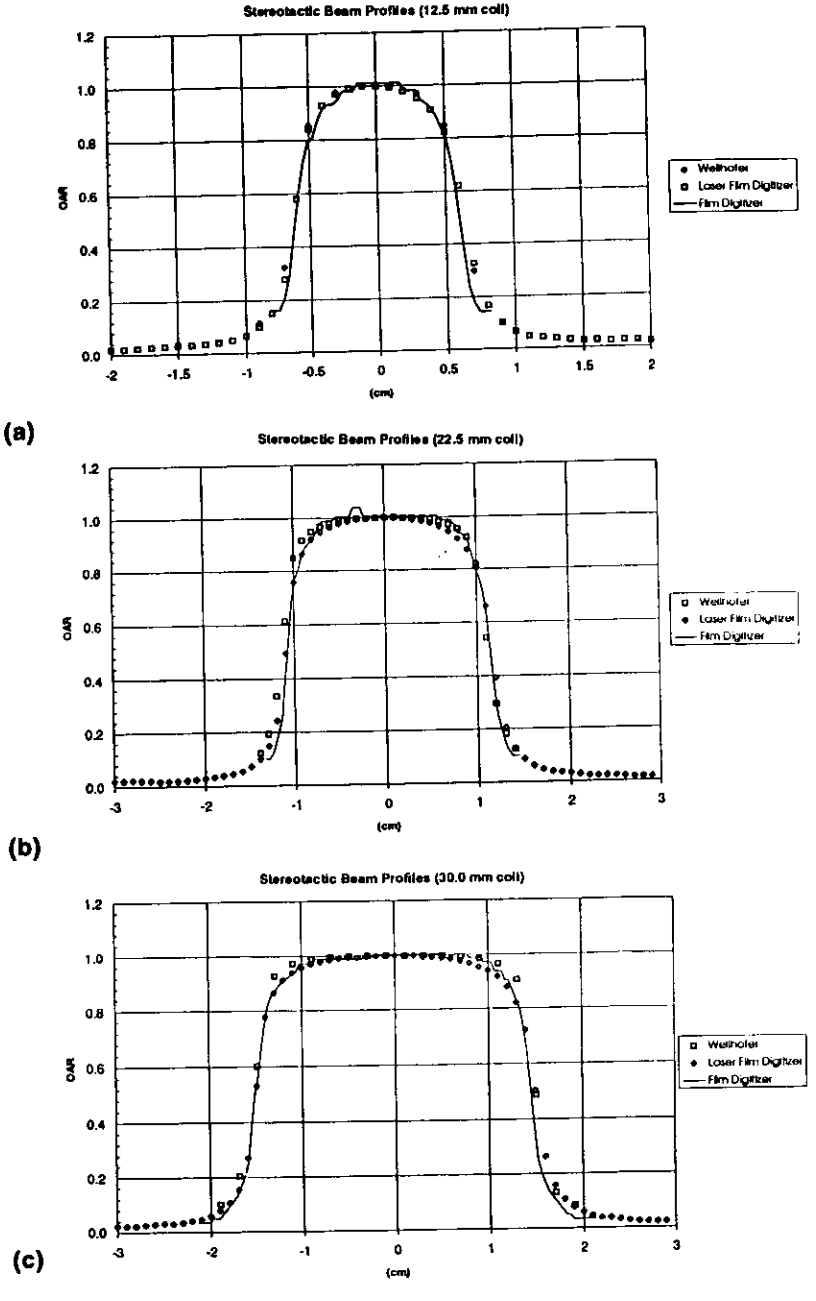

FIGURE 4 (a)–(c). Beam profiles for 12.5-, 22.5-, and 30-mm diameter fields. The beam profiles were measured with three densitometry systems (Welhofer, Lumisys laser film digitizer and the Truvel film scanner). Note that the beam profiles are essentially equivalent. These data are not to be substituted for actual beam data by the reader.

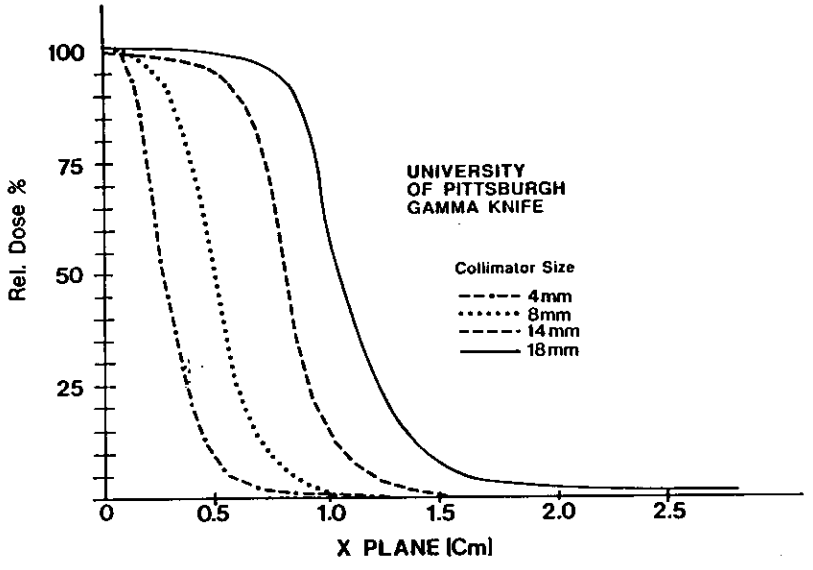

FIGURE 5. The beam profiles are illustrated for the four beam diameters of the Gamma Unit (4, 8, 14 and 18 mm).

range of electrons. However, effective transient equilibrium is observed because the x-ray beam has a continuous photon energy distribution, weighted toward the lower energies, and the secondary electrons are forward peaked. Bjarngard *et al.* (1990), measured the dose on the central axis as a function of field diameter from 0.7 mm to 8.5 mm. They determined that the electron fluence for the 8.5-mm field was measured correctly when the detector diameter was 2 mm or less. For field sizes 12.5 mm and greater, the central axis dose measurement can be achieved with a parallel plate ionization chamber such as the PTW Model N23342 (PTW Freiburg, Germany), which has a 3-mm diameter collecting volume. Dose calibration can also be achieved with the RMI plastic scintillation detector (RMI, Middleton, WI) (Beddar *et al.*, 1992 and Meger–Wells *et al.*, 1993).

The field-size dependence of output factors has been measured from 12.5–35 mm with cylindrical and parallel-plate chambers. The inner ion chamber diameters of 3.5 mm and 5.4 mm, small compared to the 12.5-mm field diameter, enable output factors to be measured accurately to within 0.5% (Rice *et al.*, 1987) and related to the dose calibration of the linac (AAPM Task Group 21 Report, 1983).

Figures 4, 6, and 7 are plots of the beam profiles, tissue maximum ratios (TMRs), and output factors for field collimator sizes of 12.5, 22.5, and 30

mm for a 6-MV x-ray beam. It shall be noted that these TMR values, beam profiles, and output factors are representative for a 6-MV x-ray beam, but shall not be substituted for the reader's beam data. The beam profile film data were measured with three instruments. The first instrument is a laser film digitizer with an effective aperture of 0.5 mm. The second instrument is a scanning film densitometer by Truvel with an aperture of 1 mm. The third densitometer is the Wellhofer with an effective aperture of 0.8 mm. Note that the beam profiles obtained with the laser film densitometer, Wellhofer and the Truvel densitometry system are comparable to within a millimeter. It is estimated that the uncertainty in position in the beam profile (edge) is approximately ± 1.0 mm (Schell *et al.*, 1993). It is important to directly calibrate each scanner using the film calibration that is performed at the time of each measurement since the response can vary between the scanning densitometer and the manual densitometer. Therefore, each densitometer must be calibrated separately.

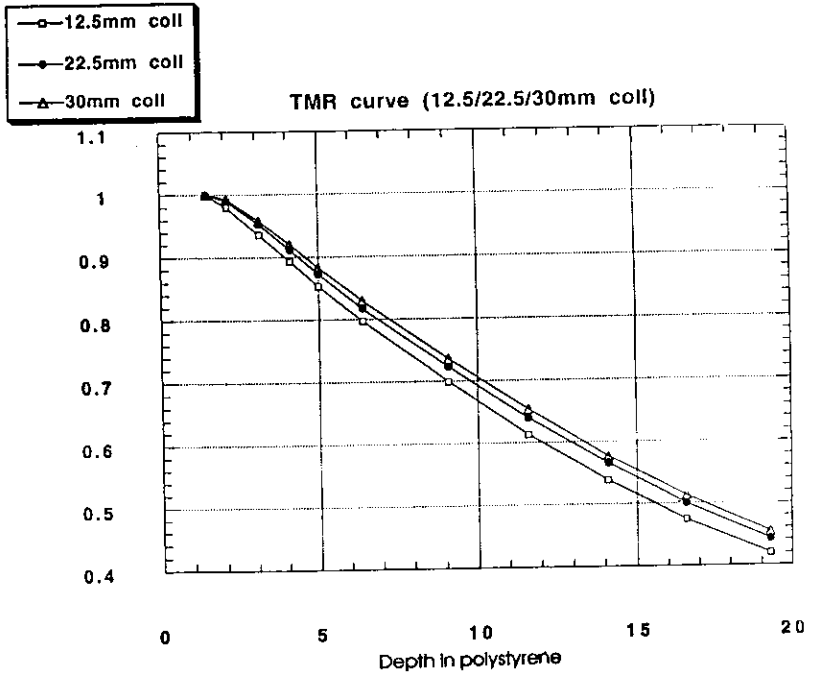

FIGURE 6. 6-MV TMR data are shown for the 12.5-mm, 22.5-mm, and 30.0-mm collimators for depths between 1.5 cm and 20 cm. Note the TMR increases 8% at d=10 cm as the field diameter increases from 12.5 to 30.0 mm.

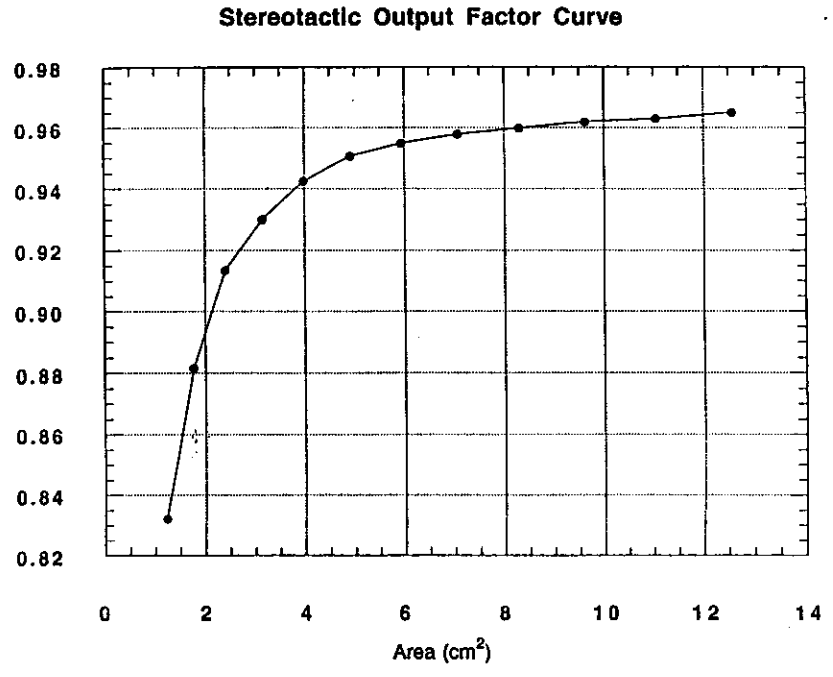

FIGURE 7. 6-MV output factors at isocenter and at d_{max} for collimator diameters 12.5–40.0 mm.

The following data acquisition procedures are adequate for field diameters greater than or equal to 10 mm. Beam profiles require high spatial resolution and film has been shown to be the most efficient dosimeter. Film analysis can be performed by a scanning isodensitometer with an aperture of 1 mm or less or with a laser film digitizer. These approaches yield equivalent results to high-resolution TLDs. The uncertainty of the beam radius measurements can be greater than 1 mm. This uncertainty should be minimized. Tissue maximum ratios and output factors should be acquired with parallel plate or thimble ionization chambers that have small collecting volume diameters, e.g., 3 mm or less. The phantom material should be within the guidelines of the TG-21 Report of the AAPM.

• *Off-Axis Ratios*

Off-axis ratios (OAR) have been measured for 6-MV x-ray beams as a function of depth in a polystyrene phantom and in air. The variation of the scaled profile with depth (constant SDD) is less than 2% (Rice *et al.*, 1987). Hence, some radiosurgery computer codes (Schell *et al.*, 1991) use OAR tables for each collimator which scale with the geometric projection of the beam. Figures 4 and 5 illustrate the beam profiles for the 6-MV linac and gamma knife unit.

• *Scatter Correction Factors*

The total scatter correction factor, S_t, as a function of field size is a product of the collimator scatter, S_c, and the phantom scatter, S_p (Khan *et al.*, 1980). Phantom scatter factors are inferred from the total scatter and collimator scatter factors.

• *Collimator Scatter*

The dose in phantom is independent of collimator scatter from the tertiary collimator for a 6-MV x-ray beam (Bjarngard *et al.*, 1990). Collimator scatter is dependent on the secondary collimator setting and independent of the tertiary collimator diameter. S_c is illustrated in Figure 7 for the 6-MV beam. The data were obtained with a PTW Model N23342 parallel plate chamber. The chamber volume is 0.02 cm^3 and a collecting volume diameter of 3 mm.

• *Tissue-Maximum Ratios*

The variation of tissue-maximum ratios (TMR) with collimator diameter at large depths is approximately 10% for 6 MV and 9 MV x rays (Arcovito *et al.*, 1985; Rice *et al.*, 1987; Houdek *et al.*, 1983; Serago *et al.*, 1992; and Jani, 1993) for field diameters in the interval between 0 cm and 4 cm. The principal diminution is from the lack of lateral electronic equilibrium. The TMR data in Figure 6 were acquired with the PTW parallel plate chamber.

B. Measurement Summary

1. Linacs

- Measure beam profiles with film, diodes, plastic scintillators, thermoluminescent dosimeters or ionization chambers. Film is the dosimeter of choice. The detector dimensions must be 2 mm or less. Diodes must be used with caution, due to the angular response of the detector.
- Measure tissue-maximum ratios and total output factors (S_c) with ionization chambers with diameters less than or equal to 3 mm.
- Use phantom materials and calibrate in accordance with the AAPM Protocol: TG-21: a protocol for absorbed dose from high-energy beams.
- The PTW Model N23342 parallel plate chamber and the Capintec

cylindrical 0.07 cm^3 chamber (with the cylindrical axis aligned with the beam axis) are examples of detectors for TMR and output factor measurement (see Kalend *et al.*, 1993).

2. Gamma Knife Units

- The aforementioned dosimeter types are appropriate for the gamma knife unit if the dimensions are no greater than 1 mm × 1 mm × 1 mm.

3. Phantoms

Polystyrene (Rice *et al.*, 1987 and Wu *et al.*, 1990), anthropomorphic (Serago *et al.*, 1992 and Smith *et al.*, 1989), water, and water-equivalent plastic have been used to measure the dose output and dose distributions of small fields (dose verification). Existing anthropomorphic phantoms usually require measurement modifications for the smaller field sizes that are encountered in SRS (Smith *et al.*, 1989); additional adaptations are required for use with the frame. Finally, anthropomorphic phantoms vary in size and heterogeneity between institutions. For these reasons, members of the task group (Schell and Wu) have modified the gamma knife unit phantom design to accommodate field sizes encountered with the linacs as well as the gamma knife unit. The phantom design is depicted in Figures 8 (a) and (b). The film cassette must be opaque to Cerenkov radiation in order for the film response to be a result of x-ray radiation absorbed dose.

The dose distributions for rotating fields can be acquired with spherical phantoms. Dose rate calibration and dose distributions for the gamma knife units have been determined with a 16-cm diameter polystyrene phantom which can contain a cassette for TLDs or film. Cassettes for TLDs and sheet film accommodate field sizes from 4–18 mm. This film cassette design was modified to accommodate field diameters up to 35 mm. Water-equivalent plastic (WEP) by RMI was used to construct a 16-cm diameter sphere and cassettes for TLD and film dosimetry, (see Figure 8). This phantom design can be used with both linac and gamma knife units. The standard WEP-based design enables dose distribution for the two SRS techniques to be compared and minimizes dosimetry corrections.

4. Dosimetry Calculation

The approximately spherical geometry of the human head and its tissue densities make the dose calculation algorithm relatively simple yet accurate to within 2.5% for cylindrically symmetric fields. The dose algorithm reported by Rice *et al.* (1987) incorporates off-axis ratios to represent the

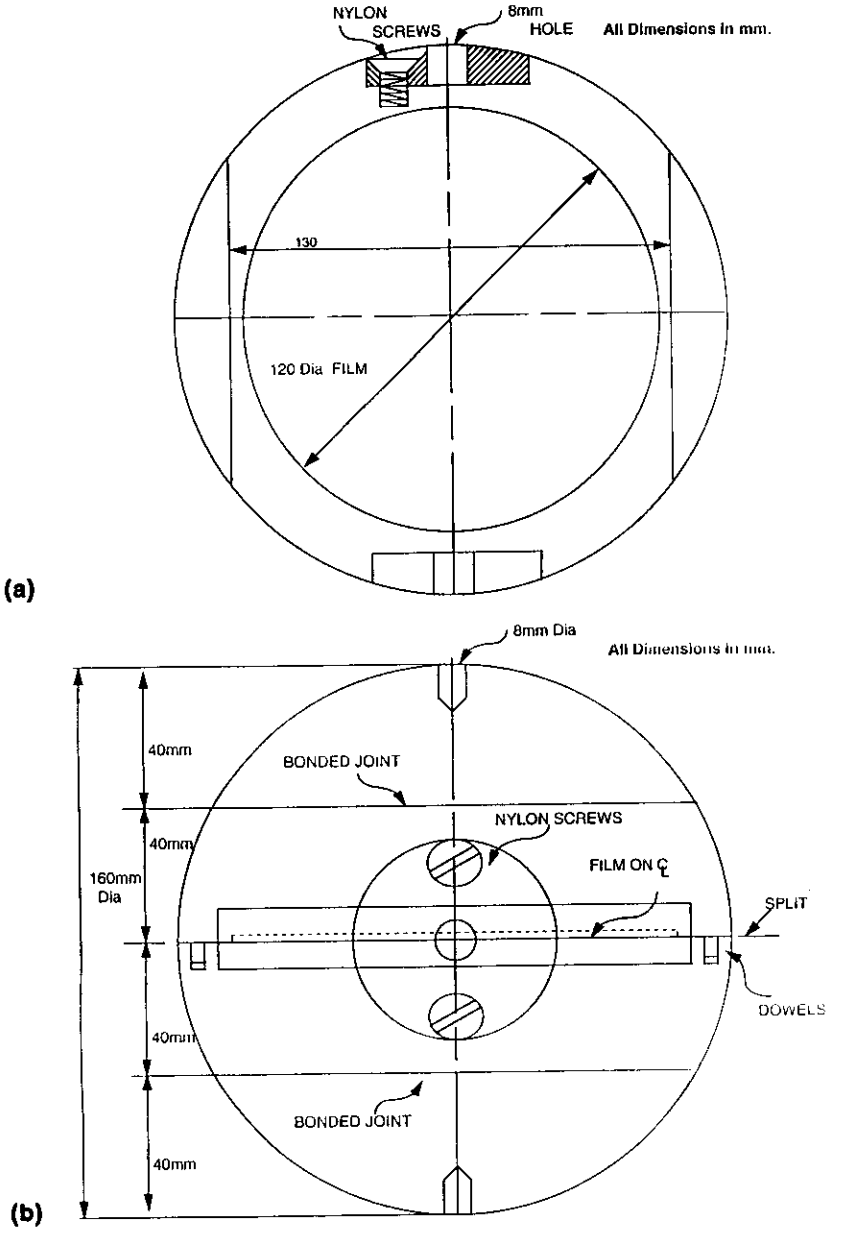

FIGURE 8 (a)–(b). The side and top views of the water-equivalent phantom are shown in (a) and (b), respectively. The large film cassette allows for the linac-produced dose distributions to be measured as well as the smaller gamma knife fields. The film cassette also accommodates TLD ribbons for output calibration.

beam profile at depth, tissue attenuation, inverse-square/fall-off of dose, and dose output versus field size. Tissue heterogeneity occurs from bone tissue. The dose perturbation for beam energies between 4 MV and 10 MV is 1–2% for a beam passing through the skull. The current arc geometries and gamma knife source arrangement minimize the effect of oblique beam incidence on the measured dose distribution by entering the surface over 2π steradians. The algorithm by Pike *et al.* (1987) is based on the Milan and Bentley (1974) two-dimensional algorithm but provides the radiosurgical dose distribution in three orthogonal planes through the machine isocenter.

Factors contributing to the net uncertainty of the dose delivery to the target have been reviewed in Table II. The principle factors are the uncertainty in the frame, the dose delivery system, movement of the brain within the skull, and the resolution of the target by the imaging modalities. Total uncertainty is on the order of 2.4 mm. The appropriate choice of the dose calculation grid size has been addressed by Niemierko and Goitein, 1989. The analysis of factors affecting the accuracy of dose estimation were divided into two factors: dose accuracy and position accuracy. Beam profile was represented by the Fermi function and it was shown that the limiting factor is the accuracy in the dose, whereas the accuracy in the position was normally less demanding. It was also shown that the maximum uncertainty does not occur at the midpoint of the penumbra, but at the 80% and 20% isodose lines—the shoulder and heel of the beam profile. This is particularly pertinent to linac-based radiosurgery because the dose prescription is normally in the neighborhood of the 80% isodose surface. Given these factors, the appropriate grid size has been shown to be on the order of 2 mm. A 2-mm grid spacing will produce a 1–2% uncertainty in the dose, whereas a 4-mm grid spacing will produce approximately 3–4% uncertainty in the dose (Niemierko and Goitein, 1989).

The planning code should directly overlay the dose distributions on the appropriate CT image (transverse slice or reformatted), MRI or angiographic image. Reformatted CT images in the plane of each arc are recommended. This reconstruction allows the user to visualize the peak dose in the plane of the arc. The multiple arc geometries are simulated in treatment planning software codes by many stationary beams (usually the stationary beams are separated by angles of 5–10°). The complex beam geometries can make conventional treatment plan calculation times intolerably long. The task group recommends the use of software packages that are capable of calculating the dose distributions on ten CT images from five noncoplanar arcs (500° total traversal) in 1 min or less. This time requirement will reduce the total planning time to less than 1 hr.

• *Planning Parameters*

The definition of the patient geometry is obtained from CT scans with

slice separations typically between 3 and 10 mm. Target definition requires smaller slice separations (CT and MRI) of 1–3 mm depending on the size of the lesion. Target definition is the enhancing region or the surgical defect in the tumor bed. The treatment volume, depending on the radiation oncologist, can be the target volume with the margin of overall uncertainty of dose delivery (Lutz *et al.*, 1988 and Winston and Lutz, 1988). When the uncertainty in dose delivery exceeds the separation of the target from a critical structure, there are occasions when the patient should be treated with a more accurate technique (heavy ions, surgery, etc.). Size and location of AVMs is determined from paired angiograms (Siddon and Barth, 1987).

The dose to extracranial critical organs has been measured and was reported relative to the isocentric dose for the gamma knife by Walton *et al.* (1987) and for linac-based radiosurgery by Podgorsak *et al.* (1992):

Organ	Dose (%)
Eyes	2.5
Thyroid	0.2
Breast	0.06
Gonads	0.02

Dose-volume histograms (DVH) have been used to compare various SRS modalities (Phillips *et al.*, 1989; Schell *et al.*, 1991; Serago *et al.*, 1992). The DVH analysis complements the treatment planning process. Software packages such as XKNIFE and PINNACLE are capable of calculating dose-volume histograms of the lesion and normal structures with sufficient speed so as to serve as a guide in optimizing the plan. Since fast 3-D dose algorithms are required for critical treatment plan evaluation, a maximum time limit for DVH calculation should be 30 seconds.

The tissue response, normal or otherwise, as a function of dose and volume is not well known. Consequently, DVH analysis is valuable for the understanding of tissue response in clinical studies. Lyman and Wolbarst (1987) have proposed an algorithm based on DVH analysis to estimate complication rates as a function of dose in normal tissues. Flickinger *et al.* (1990) have used DVH analysis to model complication rates in normal tissue and have shown that these rates follow the trend reported by Kjellberg (1983 and 1992). An RTOG protocol (#90-05) has been designed and implemented to determine the radiotoxicity of single fraction radiosurgery as a function of dose and volume.

• *Gamma Knife*

In addition to the X, Y, and Z coordinates of the target and the gamma angle, the distances from the center of the stereotactic frame to 24 preselected points on the surface of the skull are measured with a special plastic helmet

attached to the frame. Based on these measurements, three-dimensional simulation of the skull inside the stereotactic frame is created by the treatment planning computer. Treatment planning is accomplished with a computer and a graphic plotter and printer. Isodose distributions are calculated for the X-Y transverse plane view, X-Z coronal plane, and Y-Z sagittal plane and can be displayed or plotted with the proper magnification or reduction for superimposing on radiographic images. The dose delivered by each of 201 radiation beams is calculated in a 31 × 31 matrix of points centered in the region of interest. Spacing between the points on the matrix can be verified by altering the grid size.

Dose calculation for a single beam requires defining the skull configuration, transverse radiation profiles, a specified collimator size, and the dose reference point in a water phantom. The source to focus distance (SFD) is 40.3 cm. The cylindrical beam symmetry allows for simplification in the dose calculation algorithm. Assuming axial symmetry, the dose at a point in the skull can be calculated using the inverse square law, off-axis ratios, and linear attenuation exponential formulas of a single beam. The off-axis ratio is obtained from the dose profile. The linear attenuation coefficient of a ^{60}Co beam is used. Contributions from all 201 sources are summed for each point within the matrix, providing no sources are occluded. Determining an absolute dose at a given point allows the normalization and display of isodose distributions in the matrix volume. Isodose distributions can be displayed in any plane parallel to the three principal planes (transverse, sagittal, and coronal) by specifying the desired coordinates.

When multiple irradiation isocenters are considered, the contribution from each is weighted and summed to yield the final integrated dose distribution. Calculation of the treatment time for each irradiation session is based on the weight given to that irradiation, the relative output of the selected collimator helmet, and the output of the unit at the focus for a given skull configuration.

VII. QUALITY ASSURANCE

A. Introduction

Quality assurance in SRS is necessarily a multidisciplinary program not only for radiation oncology but radiology and neurosurgery as well (Schell and Kooy, 1994). The following section focuses solely on medical physics QA. The Quality Assurance design applies to three stages: (1) the SRS procedure design methodology, which is based on probable risk analysis; (2) the QA for each treatment; and (3) the routine QA tests, which occur at fixed time intervals, such as the examples in Appendix III, (a) and (b).

B. Probable Risk Analysis and QA

Probable risk analysis is helpful in designing the SRS procedure and QA program (Jones, 1994). The variation in the constraints on each institution from resources, physical plant layout, etc., prohibits the development of a universal QA program or a universal SRS procedure. Therefore, some attention will be devoted to Prospective QA or Probable Risk Analysis. Prospective QA or Probable Risk Analysis (PRA) pertains to methodologies for the Fault Hazard Analysis (FHA) of a system and the subsequent measures taken to minimize the risk of injury or mistreatment of the patient. The prospective analysis can be applied to both the design of the SRS procedure and to the design of the QA program. Risk analysis techniques were initially developed for the aircraft industry and NASA, where trial and error techniques would produce unacceptable losses. FHA is performed prior to the first patient treatment. FHA consists of modeling each step of the procedure, in addition to actual tests or system trials. Attention is focused on procedural steps where injury can occur. The probability of injury is assessed. The procedure is redesigned to reduce the risk when the initial probability is excessive. The PRA is helpful for designing the individual system within each institution and yields an institution-specific QA procedure. The definition of excessive risk should also be defined by each institution.

Technical aspects of SRS include accuracy in target localization and in target position during dose delivery, dosimetry, quality assurance, and patient safety. Examples of the application of fault hazard analysis are shown in Appendices I and II. Appendix I indicates the steps on a flow chart listed in order for a typical radiosurgery procedure. Each step can be reviewed and prioritized in terms of the risk to the patient. In this simple example (Appendix II), there are three levels of risks and they are signified in the second table by an increasing order of risks. The lowest risk category is signified by the ordinary font. The second level of risk is signified by bold letters and the highest risk level to the patient is signified by bold and capital letters. The lowest risk level includes instances where if an error occurred, it would have a minor impact on the treatment or the error would not allow treatment to proceed. For example, if the localization rods were not visible in the CT scans, one could not calculate the coordinate transformation between CT and to BRW reference frame. If this occurred, the patient would have to be rescanned. The second level is exemplified by the check on the alignment of gross anatomy with the isocenter. This is a back-up to the check on the coordinates and does not have the accuracy of the coordinate check, but it is a visual confirmation that the isocenter is in the correct place, for example, in the correct hemisphere. The highest priority is exemplified by checking that the collimator is the right size and that the coordinates are correct on the pedestal mount or the couch mount.

Quality assurance procedures for linac-based radiosurgery have been developed for a variety of frame/linac configurations (Lutz *et al.*, 1988; Podgorsak *et al.*, 1992; Drzymala, 1991; Serago *et al.*, 1991; and Tsai *et al.*, 1991). The principal features of the QA programs are (1) verification of the mechanical tolerances, (2) x-ray/light field/laser alignment with isocenter, and (3) verification of the target/tumor with the isocenter prior to treatment.

The QA program at the Joint Center for Radiation Therapy was designed initially by Lutz and augmented by Tsai. Three tests can complement a quality assurance program for target verification. The localization algorithm/software can be tested by determining the frame coordinates of a target with a previously known coordinate. For these purposes a test case can be archivally stored for routine software QA. The BRW frame system features an arc assembly that employs four angles and the depth to uniquely identify a target in BRW space. The arc assembly has been used to mark the scalp as a function of angles and depth to identify frame slippage between the time of image acquisition and treatment. The BRW stereotactic frame system includes a verification device known as the phantom base (Figure 9). The phantom base was designed for verification of tumor localization in neurosurgery. Lutz used the phantom base to set a target (a radio-opaque steel sphere) at the BRW coordinates of the tumor. The alignment of the sphere at the isocenter with the x-ray beam confirms the coordinate selection on the BRW pedestal (Figure 10). The patient is then positioned on the Patient Support Assembly (PSA) and the frame is attached to the pedestal. The treatment configuration of the linac and pedestal mount is shown in Figure 2.

Similar attention should be focused on the graphics display of the treatment planning system. The position of color-coded isodose contours relative to the target image are a function of the color gun alignment. Misalignment of the color guns in the graphics display unit can displace color-coded isodose curves relative to the target by more than 1 mm and mislead the planning process. Each step of the SRS procedure must be examined for the consequences of failure.

C. Treatment QA

1. Checklists

Because of the complexity of radiosurgery treatments, the QA program must include a treatment procedure checklist. The checklist will reflect the treatment step sequence and should be written in sufficient detail so as to minimize risk of misadministration or injury. Some sample items are: jaw setting, proper diameter collimator inserted, couch disabled, anti-collision switches in place, external target test acceptable, head ring check accept-

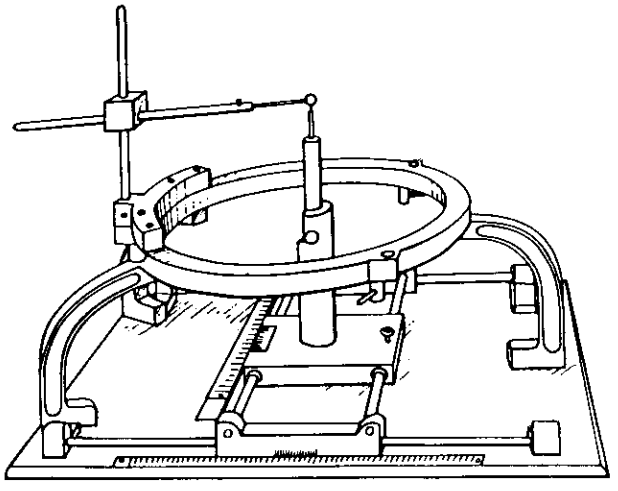

FIGURE 9. The target simulator (steel ball) is shown attached to the BRW phantom base. The phantom coordinate system is identical to the coordinates of the BRW stand. The pointer is set to position the target simulator at the lesion's coordinates. The BRW phantom is also used in QA procedures to verify the angiographic box localization in SRS. (Lutz *et al.*, 1988.)

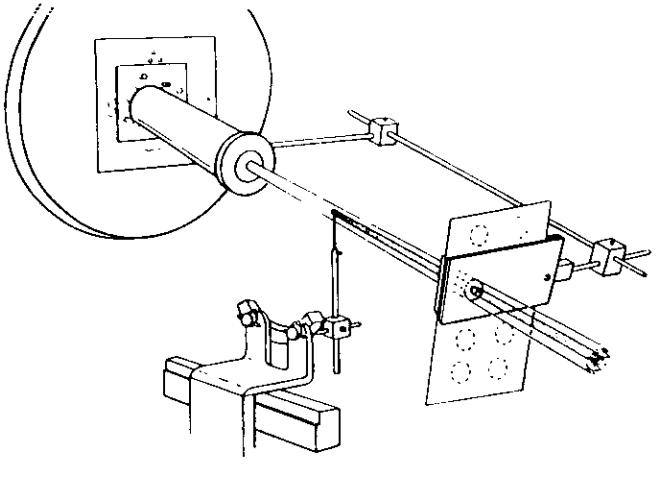

FIGURE 10. The target simulator is mounted on the pedestal to verify the target alignment with the SRS x-ray beam as a function of table and gantry angles. (Lutz *et al.*, 1988.)

able, target coordinates checked, target simulator film acceptable (or comparable test), laser alignment of patient verified, patient strap in place, etc. In general, the critical steps in a radiosurgery treatment procedure should require confirmation by at least two people. Sample procedures are shown in the Appendix IV. Note that one sign-off includes the detachment of the frame from the pedestal before restoring the capability of vertical motion to the patient support assembly.

2. Target Position Verification

Verification of the target position in the beam prior to irradiation has been developed at the heavy charged particle therapy centers [Goitein *et al.* (1982) and Lyman *et al.* (1989)]. A pre-treatment radiograph is obtained from the beam's-eye view and compared to the digitally reconstructed radiograph of the treatment plan. When the positioning differences are less than 1 mm, patient irradiation is initiated. Similar efforts have been reported by Serago *et al.* (1991), using orthogonal port films. Jones *et al.* (1989) used fiducial markers embedded in the scalp as a stereotactic frame. A linac-mounted x-ray tube/simulator has been used to verify patient position prior to treatment by means of the angiographic localizer (Schell *et al.*, 1991). Methods for target coordinate verification are described below for the pedestal-mounted and couch-mounted frame approaches.

3. Laser Check

A couch mount system derives its accuracy from lasers fixed in the room. The first check confirms that the lasers indeed intersect with the isocenter within the desired tolerance.

The initial laser alignment procedure is best performed using a calibrated mechanical pointer. The Joint Center for Radiation Therapy uses a Mechanical Isocenter Standard (MIS) that bolts on the base plate of the PSA. The MIS is also used in the initial morning check to verify visually check the alignment of the lasers.

The test involves aligning a radio-opaque marker to the point marked by the crosspoint of the lasers. This alignment procedure depends on the particulars on the stereotactic hardware. A set of films taken at various gantry-couch angle combinations allows a determination of the alignment between the radio-opaque marker and the isocenter, and the centricity of the radiation field. A film test with the calibrated MIS allows a quantification of any misalignment of the three axes of rotation and the shift of the MIS itself. The film test before a patient treatment thus becomes a second test and documentation of the alignment.

The films become part of the treatment record and document that the laser intersection point corresponds to the LINAC isocenter within a desired

tolerance, and that the radiation field is centered around the isocenter and beam axis.

4. Pedestal Mount System

Three primary tests and one secondary test are suggested to assure the positional accuracy of a patient treatment.

- "Known" target test during localization.
- Head ring movement check.
- Rigorous verification of treatment set-up.
- A secondary, less quantitative test, which to some extent supplements the three main tests.

These tests will be illustrated with the Joint Center for Radiation Therapy approach to radiosurgery (Lutz *et al.*, 1988) which utilizes BRW stereotactic biopsy equipment and patient head support independent of the couch. In particular, the first and third tests utilize the BRW phantom base which can position a pointer at any desired target coordinate relative to a head ring.

5. "Known" Target Test During Localization: Recommendation to SRS Manufacturers

The requisite equipment for this test is not available commercially. The task group recommends that the SRS system manufacturers modify the frame systems to accommodate this coordinate transformation algorithm test. The localization test, which checks the process, involves placing a target of "known" coordinates external to the skull, but relatively near the internal target, during angiographic or CT localization procedures. The external target is attached to the localization frame (CT or angiography). Following CT or angiography, the frame, with the external target attached, can be placed on the BRW phantom base. The phantom base is then used to measure the coordinates of the external target. These results are the "known" coordinates. The coordinates of the external target are also calculated using the same films or CT slices, computer hardware and software as used to calculate the patient's treatment target coordinates. Only when these external target coordinates compare favorably with the BRW phantom base measurements ("known" coordinates), would one proceed with the calculation of the patient's target coordinates. **Note, this test is valid only if the localizer is correctly affixed to the frame during the imaging acquisition. An incorrectly attached localizer will produce incorrect target coordinates.**

The coordinates of the patient's treatment target should be calculated independently by at least two people or by two independent software programs. If possible, two different methods and/or computers should be used and compared. If the target is localized by CT, the thinnest possible slices, consistent with the use of contrast, should be taken through the target to

minimize the localization error. The size and shape of the target needs to be carefully evaluated so that treatment planning decisions (number of isocenters, collimator diameters, pattern of arcs, etc.) are meaningful. It should be noted that two planar radiographs are often inadequate to determine either the exact shape or size of a target (Bova and Friedman, 1991).

6. Head Ring Movement Test

The BRW arc system (or its equivalent in another system) can be used to insure that the BRW head ring has not moved between its initial placement and treatment (Tsai *et al.*, 1991). After the head ring is secured, the BRW arc system is attached. Using the arc system and its pointer, three or four points on the scalp are marked at specific values of α, β, γ, Δ, and depth. Choose "easy" numbers for the angles, since the only constraint is that the points be distributed. Just prior to treatment, the arc system is again attached to the head ring with the patient's head in the same position as before. The three or four marked scalp points are then confirmed to be at the same values of α, β, γ, Δ, and depth, thus establishing that the head ring has not moved.

7. Verification of Treatment Setup

In the BRW based system, the target simulator test (Lutz *et al.*, 1988) verifies that the treatment equipment is set up correctly to the target coordinates and that the entire system is properly aligned. Alignment and setup are verified by simulating the patient's lesion with a small steel sphere positioned at the target coordinates and making radiographic exposures with the gantry and couch in eight representative positions (Lutz *et al.*, 1988). After the collimator and the BRW floor stand are secured in place, one person aligns the floor stand to the correct coordinates while a second person sets the phantom base to the identical coordinates. The BRW phantom base allows the precise mechanical identification of the target's position in BRW space. Next the target simulator is attached to the BRW phantom base (Figure 9). The target simulator contains a section of head ring that attaches to the top of the phantom base ring. The steel sphere on the arm of the simulator is then centered using a magnifying glass as a visual aid on the tip of the phantom base's pointer. The vertical coordinate must be adjusted for the radius of the spherical target and for the thickness of the head ring, which should now overlay the phantom-simulated head ring. Next, the target simulator is removed from the phantom base and attached to the BRW floor stand in the same manner that a patient's head ring would be attached (Figure 10). The simulator's spherical target then represents the patient's lesion with its center located precisely at the "best compromise" isocenter, if no errors have been made.

The film holder is attached to the collimator and the film is exposed with the accelerator's beam at eight standard turntable/gantry positions. This film verifies the alignment of the entire system over the range of possible gantry and turntable movements. If the steel sphere is centered within the acceptable limits of all eight exposures, it is reasonable to conclude that the set-up has been correctly aligned for the treatment of the lesion at the specified location.

This verification procedure will detect subtle problems with the linac as well as misalignment of the supplemental collimator or BRW floor stand, and mistakes such as incorrectly setting the intended coordinates. This verification procedure checks all positioning aspects of the treatment subsequent to determination of the target coordinates. After verification, the target simulator is removed and the patient is attached via the BRW head ring to the floor stand without making any alterations.

The target simulator test cannot detect an error in the target coordinates regardless of the cause of that error. Nor can this test detect an error caused by slippage of the head ring on the patient's head. These potential problems were covered in the first two tests.

An equally rigorous test for target positioning for a couch-mount system during set-up in which the patient's head is supported on the couch is described by Serago *et al.* (1991).

8. Secondary Test

A general, less quantitative supplemental test can be used which checks for errors in the localization process and/or treatment setup, providing the target can be visualized on CT. At the CT console, distances from the lesion center to the head surface, along the three principal axes, are measured. These measurements are made from two CT slices: one through the center of the lesion (or nearly so) and one through the top of the head. (The difference in table position between these two slices is the "Lesion Center to Superior" distance.) These measurements are made as part of the localization process and carefully recorded. At the time of treatment, after the patient has been secured in the treatment position, these same three distances can be measured reasonably accurately (maybe ± 6 mm) on the patient using the lateral and ceiling lasers and a couple of rulers. Successful completion of this test, even with its limited accuracy, can be very reassuring.

D. Stereotactic Couch Mount

1. Overview

A stereotactic couch mount fixates the patient on the couch and relies on an external reference to define the LINAC or treatment coordinate system.

The main advantage of the couch mount is complete access to any point in the patient's cranium, especially for plain transverse arcs and access to the posterior as shown in Figure 11. Elements of a couch mount include:

- Couch locking devices—Stabilize the couch to ensure mechanical stability and to disable all motions.
- Lasers—Provide room-based fixed reference.
- Patient docking device—Rigidly attaches to the couch and allows the patients frame to be uniquely positioned on the couch.
- Isocenter/target verification devices—Allow verification of the correct target coordinate and its alignment with the LINAC isocenter.

2. Target Verification/The Joint Center for Radiation Therapy

The following procedure is specific to the Radionics couch mount assembly and reflects the quality assurance procedure as performed at the Joint Center for Radiation Therapy (Tsai *et al.*, 1991).

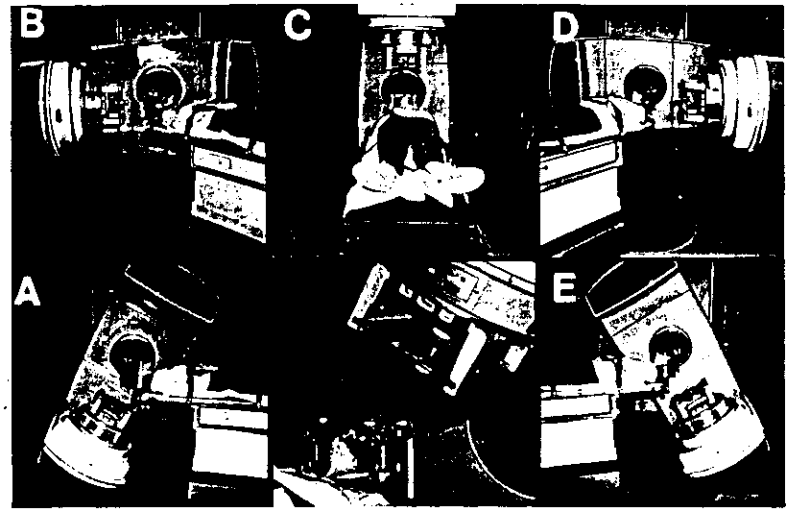

FIGURE 11. A dynamic stereotactic radiosurgical procedure starts with the couch at +75° and the gantry at 30°, as shown in part (A). During the treatment the couch rotates 150° from +75° to −75°, while the gantry simultaneously rotates from 30° to 330°. Several successive positions through which the couch and gantry move during the complete radiosurgical procedure are shown, starting (A) with the gantry and couch angels of 30° and 75°, respectively, through (B) 90° and +45°, respectively, (C) 180° and 0°, respectively, (D) 270° and −45°, respectively, and (E) stopping at 300° and −75°, respectively. (Souhami, L.; Olivier, A.; Podgorsak, E.B.; Pla, M.; Pike, G.B. Radiosurgery of cerebral arteriovenous malformations with the dynamic stereotactic irradiation. Int. J. Radiat. Oncol. Biol. Phys. 19:775–782, 1990.)

The alignment hardware consists of two assemblies: a rectilinear phantom base (RLPB) and a laser target localizer frame (LTLF). Both devices are calibrated with respect to the BRW coordinate system and have scales that allow a coordinate to be entered given the AP, LAT, and VERT positions. The RLPB mounts on the couch-mount docking device and allows a pointer to be precisely positioned to the isocenter using the couch motors and verniers on the docking device.

Two people should execute the procedure. The first person sets the target coordinate on the RLPB and the second person sets the target coordinate on the LTLF. The RLPB is aligned to the isocenter. Couch motions, except the vertical movement, are locked and stabilizers applied if needed. The above laser test is performed. The LTLF is placed on the RLPB. If the lasers are parallel, and if the target coordinate on both the LTLF and the RLPB are identical, then the lasers will align with the markers on the LTLF. This procedure thus documents the alignment of the target with isocenter through the film test and that the target coordinate is indeed the correct coordinate through the redundant entry on both devices.

In practice, the lasers never are truly parallel even though they cross at the isocenter, and small deviations will exist. The alignment markers on the LTLF are a macroscopic distance from the isocenter, and any divergence of the lasers is magnified by this distance. Thus when the LTLF is placed on the RLPB, a small deviation will be observable. This deviation should be below an acceptable tolerance. If not, adjust the LTLF to exactly align the lasers at the LTLF. Note that this means that the coordinate AP, LAT, and VERT values now will slightly differ from the prescription coordinates. It is important to note the objectives of these steps. First, the RLPB/LTLF combination verifies that the physicists/therapists correctly entered the target coordinate on the RLPB. Secondly, the small adjustments on the LTLF allow an exact calibration of the state of the lasers with respect to the target coordinate. Thus the critical element is not that the lasers are perfectly collinear; instead the critical element is that they are stable from the time the treatment procedure starts until the treatment is over.

The exact calibrated positions of the LTLF for a given target position are recorded prior to the actual patient treatment. For a patient treated with multiple isocenters, individual LTLF positions for each target are re-entered on the LTLF without requiring the patient to be taken off the couch. This much improves the ease of patient setup and throughput.

3. Patient Alignment

The RLPB is removed from the couch docking device, the couch is lowered, and the patient is positioned on the couch and locked in the docking device. The couch is raised to its original height during the above test. The patient's weight, however, will induce an unavoidable shift even in the most

mechanically stable system. The LTLF is placed on the patient's frame, and is aligned to the lasers once again using the couch docking device verniers. Note that the LTLF prior to placement on the patient was calibrated to the exact configuration of the lasers for the treatment coordinate. Thus this alignment of the LTLF once again will align the target coordinate to the lasers and thus to the isocenter. The LTLF thus affords a direct method to assess the patient-weight induced effect on the mechanical assembly and a method to correct for this effect. This procedure thus reduces torque effects and increases the mechanical accuracy.

4. Alignment Verification of a Couch-Mounted Frame (McGill)

The collimator alignment is a critical step in treatment because the precision of the treatment itself depends heavily on the accuracy of the collimator placement. The collimator is placed onto the linac tray holder, which is attached to the linac head. The proper collimator position is obtained with the help of ceiling- and wall-mounted lasers that are periodically calibrated to indicate accurately the linac isocenter location. The alignment procedure is as follows: The couch table top is raised to the isocenter and the gantry positioned off-vertical, so that the dot produced by the vertical ceiling laser to indicate the couch rotation axis is clearly visible on the table top. The position of the dot is marked on the table top, the gantry is placed vertically, and the collimator position is centered with the help of the light-field localizer lamp around the mark on the table top representing the couch rotation axis. The collimator plate is then immobilized with four pressure screws.

The alignment of the collimator is verified with radiographic film in three steps. First, a film is suspended horizontally at the isocenter and exposed to a parallel-opposed beam with the gantry at 0° and 180°. Next, another film is placed vertically through the isocenter and exposed to a parallel-opposed beam with the gantry at 90° and 270°. Finally, a third film is placed horizontally through the isocenter onto the couch table top and rotated with the couch during irradiation with a vertical beam. With the three-step process above, any misalignment of the collimator can be easily detected with the radiographic film. The radiosurgical treatment is not given unless the results of the alignment procedure are within the accepted tolerances.

An example of the radiographic films obtained during an alignment procedure for a 1-cm diameter collimator is given in Figures 12 and 13. Part (a) of both figures represents the radiographic image of a single, vertical 1-cm diameter beam. Images of vertical parallel-opposed beams (first step) are shown in Figure 12 (b) and (d), while images of horizontal parallel-opposed

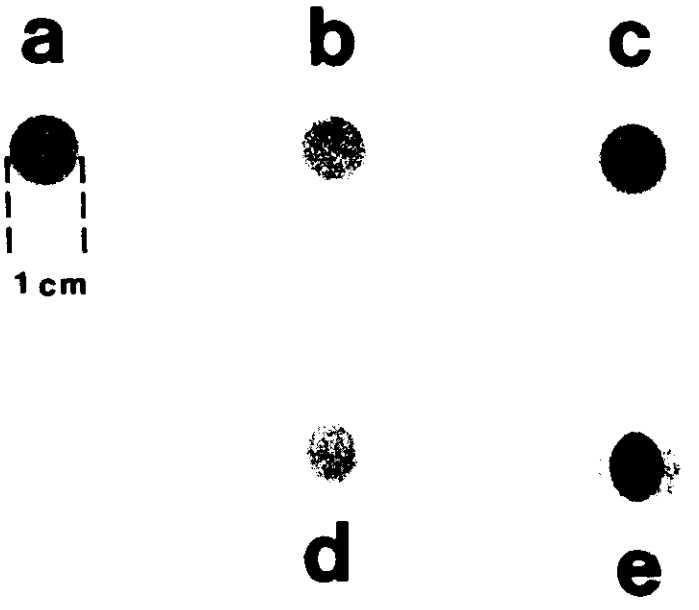

FIGURE 12. Verification films illustrating collimator alignment. Collimator diameter: 1 cm, film at isocenter, perpendicular to the beam. Image (a) is for a single vertical beam, images (b) and (d) are for two parallel-opposed vertical beams (gantry angles: 0° and 180°), and images (c) and (e) are for two parallel-opposed horizontal beams (gantry angles: 90° and 270°). Images (b) and (c) result from a well-aligned collimator, and images (d) and (e) result from a collimator shifted 1 mm laterally from the optimal position.

beams (second step) are shown in Figure 12 (c) and (e). Parts (b) and (c) of Figure 12 are for a well aligned collimator, while parts (d) and (e) represent a collimator shifted 1 mm out of alignment. It is evident from Figure 12 that even a slight misalignment of the collimator can be easily detected with the radiographic test procedure involving two parallel-opposed beams.

Figure 13 represents the third step of the alignment test, which checks the coincidence of the couch rotation with the collimator alignment. Part (b) results from a couch (film) rotation in a vertical beam from an aligned collimator and shows an excellent coincidence between the couch rotation axis with the vertical beam axis. Part (c) results from a couch (film) rotation in a vertical beam from a collimator shifted by about 1mm from the aligned position. The misalignment of the couch rotation axis with the beam vertical axis is easily noticeable, and the treatment would not be given under

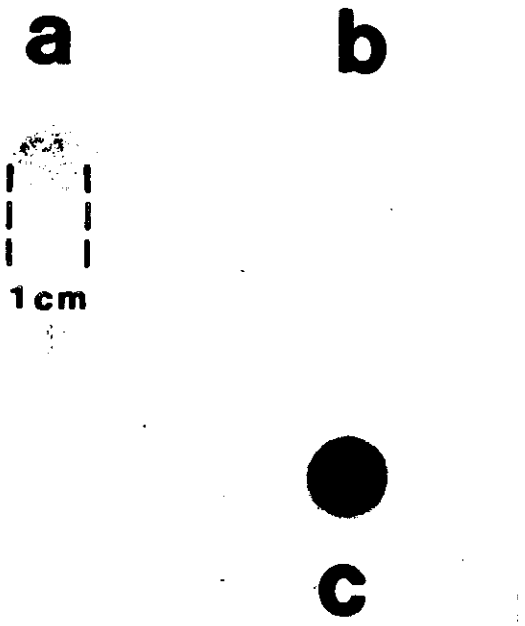

FIGURE 13. Verification films illustrating couch alignment. Collimator diameter: 1 cm, film at isocenter, perpendicular to the beam. Image (a) is for a single vertical beam and images (b) and (c) are for couch (film) rotating from 75° to –75° in a vertical beam. Image (b) results from a well-aligned collimator, and image (c) results from a collimator shifted 1 mm from the optimal position.

these circumstances. Alignment of the lesion with isocenter is achieved by positioning the patient such that the lasers align with the x, y, and z coordinates on the localizer grid.

E. Routine QA

The QA program at any SRS installation should routinely inspect the hardware/software performance to ensure compliance with the original specifications. Several QA protocols have been or are about to be published for radiation oncology (AAPM Report No. 13; ACMP Report No. 2, Svensson, 1990; AAPM Report No. 40; AAPM Report No. 45; and Van Dyk *et al.*, 1993). These existing QA protocols for radiation oncology should guide the institution's QA program for SRS. Such a program should also include all aspects of the planning and treatment process. The QA program involves

several disciplines, and the equipment is likely to be used by a variety of health professionals in different departments (Schell and Kooy, 1994). Therefore, the task involves coordinating personnel as well as QA of apparatuses and procedures. The QA program should include:

Stereotactic Frame:	Phantom base + pointer or analogous devices CT localizer Angiographic localizer Target pointer and frame pedestal or couch mount
Therapy Machine:	Dose calibration Frame alignment with gantry and couch eccentricity or precession X-ray field alignment with isocenter beam profiles
Software:	Dose calculation Frame coordinate/image coordinate transformation Digitizer linearity Graphics display image alignment Film imager distortion 1) Gamma Knife dose overlay 2) DRR distortion for charged particles

F. QA Program for a Gamma Knife

The quality assurance (QA) program is divided between daily, monthly, semi-annual and annual checks.

Before the patient is ready to be treated each day, door interlock, both the elapsed-time timer and the remaining-time timer, audio-visual systems, emergency-off buttons, console lamp test, radiation monitors and hydraulic pressure must be checked for safety purposes.

The timer constancy, timer linearity, timer accuracy, on-off error, trunnion centricity, radiation output, and the relative helmet factors need to be checked. The timer constancy, linearity and accuracy are checked over the range of clinical use. An ionization chamber coupled with an electrometer is placed at the center of an 80-mm radius polystyrene spherical phantom and the focus of the beams. Multiple exposures are made using different time intervals and the 18-mm collimator helmet with all collimators open.

A spread of the electrometer readings of a constant time setting determines the constancy and reproducibility of the timer and the dosimetric system. A plot of the average electrometer readings versus time intervals determines the timer's linearity. The "On-Off" error calculation, (α), is based on the same method used in a teletherapy machine, where $\alpha = [nR_2 - R_1]/n[(R_1) - R_2]$. This procedure is repeated monthly at the University of Pittsburgh.

The radiation output of the machine is measured using an electrometer with an NIST-traceable ion chamber placed at the center of an 80-mm radius sphere of tissue equivalent material which is positioned at the focus of the 18-mm collimator. At the University of Pittsburgh, a Capintec Model PR05P ion chamber was used with a Capintec Model 192 electrometer. The dose output measured for the gamma knife is referred to the dose to water. The percent discrepancy between the measured output and the anticipated output should be within ± 3%. The relative helmet factors are verified using diodes or thermoluminescent dosimeters. The diode (PTW 9111), or LiF chip is placed at the center of the spherical phantom and the focus of the radiations. The ratios of the readings obtained from the 4-, 8-, and 14-mm helmets to the reading for 18-mm helmet are determined as the relative helmet factors. This procedure is repeated annually.

Trunnion centricity is checked using the trunnion test tool supplied by the manufacturer. The trunnions are responsible for the accurate placement of a target in the X dimension. The trunnion test tool is a cross-shaped apparatus that is attached to the interior of the collimator helmet. The trunnions should read 100 when they are fully inserted and come in contact with the center of test tool. This procedure is performed monthly.

Radiation/mechanical isocenter coincidence is checked by irradiation of a film in a specially designed tool. The mechanical/radiation isocenter tool is basically a light-tight aluminum film cassette, containing a small piece of film (2.3 × 2.5 cm). At the center of the cassette, a pin is used to pierce a tiny hole on the film which indicates the mechanical isocenter of the machine. The film is irradiated, and then scanned with a densitometer. Figure 14 shows the position of the pinhole as the mechanical center, and the center of the radiation profile measuring by the half-width of the half-maximum. The discrepancies between the two centers along X, Y, and Z directions were approximately 0.25 mm.

The engagement of two microswitches located at the base surface of the helmet indicates the proper positioning of the helmet. To test their sensitivity, a special tool, which is simply a ring that simulates the helmet docking with the central body, is provided by the manufacturer. After seating the tool on the helmet's four anchor posts, a small sheet of brass approximately 0.1 mm thick is inserted into the space between the top surface of the helmet base and the bottom of the tool to create a 0.1-mm gap. This small gap causes misalignment of the docking of the helmet and improper engage-

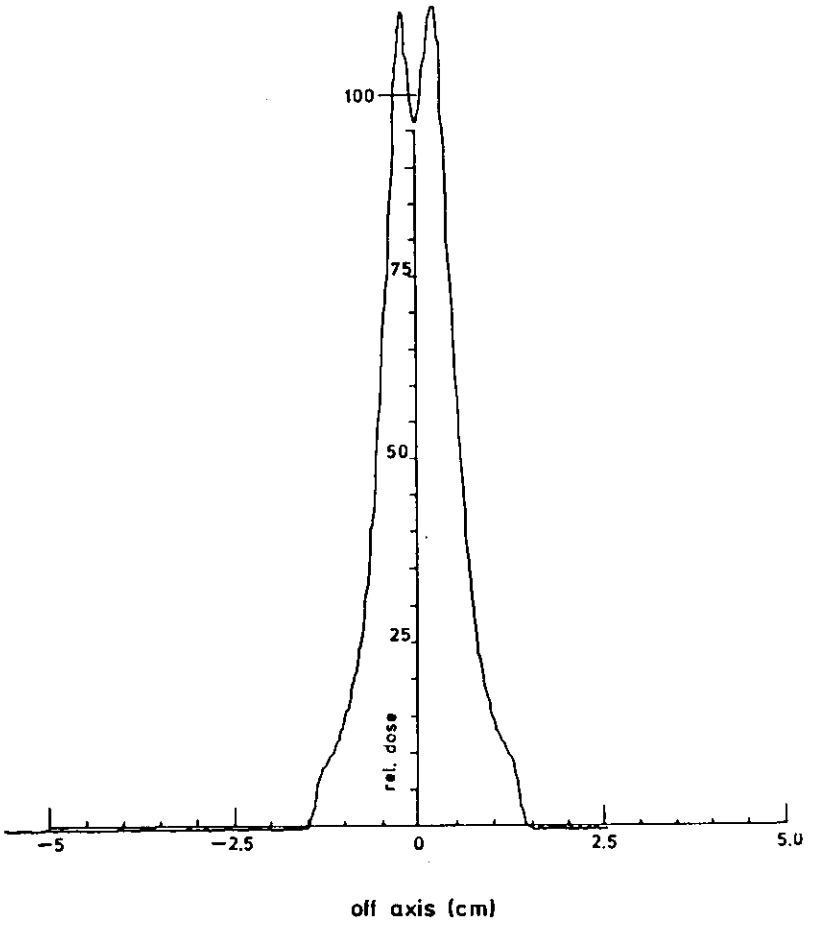

FIGURE 14. The X-axis dose profile of a film exposed with the 8-mm collimator helmet. The film was punctured with a pin to indicate the center of mechanical focus (the dip at the center of the profile). (Wu *et al.*, 1990).

ment of the microswitches. As a result, the control console should stop the treatment. This test should be performed monthly.

Couch movement time is the interval time during which the patient may be exposed to radiation in the case where treatment is interrupted right after it is initiated. When the treatment is interrupted, the couch moves the patient out of the unit, and the shielding door closes completely. The couch travel time is adjusted to the minimum, typically within 30–40 sec. This test is performed monthly.

Furthermore, the treatment planning aspects of quality assurance should

include the computer output check, and relative collimator helmet factor verifications. This procedure is performed monthly. Also, on a semi-annual basis leak testing of the source is required. Dose profiles should also be verified on acceptance or after a source change.

G. Stereotactic Frames and Quality Assurance

The majority of SRS applications use one of five stereotactic frames: Brown–Roberts–Wells, Tipal, Leksell, Gill–Thomas–Cosman, or Riechert/Mundinger. Excellent reviews of the technical aspects of the stereotactic frames are presented by Galloway and Maciunas (1990) and Maciunas *et al.* (1994). The stereotactic frames must be assessed for accuracy as they are actually used. One point made in Maciunas's article is that phantom tests do not stress the stereotactic frames in the same manner as do actual patient treatments and that "clinically encountered levels of weight-bearing by stereotactic frames may have a pronounced effect on their mechanical accuracy." The consequence of this factor is an introduction of an error that is not appreciated by the general community. For example, a mean error for a 4-mm slice thickness in the BRW frame system is 2.7 mm, with a 95% confidence level of 4.8 mm. These numbers decrease to 1.9 mm for the mean error and 3.6 mm for a 95% confidence level for a 1-mm slice thickness. These numbers also do not take into account the uncertainty in the treatment delivery in the linac system or that introduced in the planning process of the radiosurgery software. The overall uncertainty is larger when these numbers are included and are representative of the numbers in Table II. All frames serve the same function: to accurately guide surgical instruments or small radiotherapy x-ray beams to a locus in the brain. Frame accuracy has been found to vary between serial numbers of the same manufacturer. As with other apparatuses in radiation oncology, the frame system must be tested initially and routinely for accuracy.

The task group strongly recommends to the manufacturers that all frame systems use the positive valued quadrant of the Cartesian coordinate system. This convention eliminates the accidental omission/substitution of a negative-valued coordinate. Elimination of negative values therefore reduces the possibility of misplacing the target.

All frame systems provide localizing devices for angiography, CT, and MRI. Some angiographic localizers have radiotranslucent scales that allow for direct deduction from the film image of the target coordinates. Other frame systems rely on fiducial markers and require more complex algorithms for obtaining the target position. Similarly, certain CT localizers enable direct calculation of the target coordinates, others do not. Simplicity in localizer function and design facilitates target-setup verification on the treatment machine.

VIII. FUTURE DIRECTIONS

This section delineates areas of development which have yet to be standardized. Five areas are described: (1) image correlation (CT and MRI), (2) multiple fractionation, (3) real-time portal imaging, (4) conformal radiosurgery and, (5) a robot-guided linac.

A. Image Correlation

MRI contains distortions which impede direct correlation with CT data at the level required by SRS (Sumanaweera *et al.*, 1994). Three approaches are cited below. Magnetic resonance imaging (MRI) and magnetic resonance angiography (MRA) are capable of resolving tissues 1 mm in diameter or less. The difficulty in MRI stems from the fact that inhomogeneities in the magnetic field and eddy currents produced within the patient can distort the images and produce warping or displacements in the image relative to the stereotactic frame coordinate system. Two general precautions can be taken to minimize this. The first is placing the volume of interest in the center of the main magnetic field. Displacements of 20 cm or more from the center of the magnetic field can produce gross distortions in the MR image. This precaution will reduce the typical uncertainty in the anomalous displacement of the image to 4 mm.

A quantitative analysis of the distortion in MR has been reported by Schad *et al.* (1992) and Ehricke *et al.* (1992). This group has devised two phantoms to assess warping in the MR image. The first phantom is two-dimensional and quantifies the pin cushion distortion in the phantom. The second phantom is three-dimensional and quantifies the displacement and warp and tilt of the image plane. Correction of the pin cushion distortion is reported to reduce displacements on the order of 1 mm using a fourth order two-dimensional polynomial correction. Minimization of the warp and displacement of the MR plane is achieved by adjusting the gradient-shimming currents of the magnetic field until the image of the three-dimensional phantom is a faithful reproduction of the three-dimensional phantom structure. Both of these corrective procedures are time-consuming and require a rigorous QA program of the MR unit prior to each radiosurgical procedure, resulting in the reduction of the MRI uncertainty from 4 mm to approximately 1 mm.

A second effort has been presented by Kessler and Carson (1992) which includes the development of a test object for determining the geometric distortion in three-dimensional MRI and other three-dimensional imaging systems. The phantom consists of sets of three spiral-filled rods which cross-correlate with the array of simulated images. The position of the rods and the phase change of the rods allow for the determination of the position of a point in absolute three-dimensional space and determine the conformal map

to the three-dimensional image coordinate system. The differences between the coordinates are due to the distortion by imperfections in the magnetic field of the imaging system. This phantom accesses distortion by the imaging system, but not the distortion from the perturbation of the magnetic field by the patient.

A third effort has been presented by Kooy *et al.* (1993), which utilizes an automated method for image fusion of CT and MRI volumetric image data sets. The approach uses a chamfer-matching algorithm which ensures quality assurance of the procedure and eliminates the requirement for stereotactic fixation of the patient during the MRI study. The accuracy is improved from approximately 6 mm to 1 mm using the image-fusion technique based on the chamfer-matching method.

B. Multiple Fractionation

From the beginning, SRS has been a multidisciplinary effort to deliver a large radiation dose to a well localized, small volume in the brain through stereotaxis. Although Leksell originally intended to induce lesions with a single fraction to eliminate functional disorders (Leksell, 1951, 1983, and 1987), subsequently SRS has been mainly used to treat AVMs and neoplasms. Furthermore, many treatments pioneered by the heavy-charged-particle therapy groups have not yet been widely incorporated into the x-ray SRS techniques. These treatments include multiple fractionation, conformal radiation therapy, beam's-eye-view treatment planning, and real-time imaging verification of the patient setup.

Conventional experience indicates that several fractions of SRS will enhance tumoricidal effects while minimizing normal tissue sequelae. Guidelines for fractionated stereotactic radiotherapy have been published for producing the tumoricidal effect of 70-Gy low-dose-rate ^{125}I interstitial implants (Brenner *et al.*, 1991). However, little is known about the benefits and risks of SRS. An RTOG protocol (#90-05) has been initiated to determine the radiotoxicity as a function of volume. Future protocols will compare the effectiveness of single versus multiple-fraction SRS and SRS versus brain implantation versus external beam irradiation.

These studies will require the development of stereotactic frames that accommodate multiple applications with minimal degradation of patient repositioning accuracy, as well as minimal personnel time. Several devices have been reported: (1) the stereotactic frame/mask designed at Lawrence Berkeley Laboratory (Lyman *et al.*, 1989); (2) the Laitinen frame (Hariz *et al.*, 1990); (3) the Schwade–Houdek frame (Schwade *et al.*, 1992); and (4) the Gill–Thomas–Cosman frame (Sofat *et al.*, 1992). The first two devices are noninvasive, whereas the third frame is attached to the patient's skull for 1–2 weeks. None of these have been widely used in SRS at this time. The Gill–Thomas–Cosman frame has completed beta testing and is currently

marketed with the RSA XKNIFE system. (See Loeffler: Stereotactic Radiotherapy: Rationale, Techniques and Early Results in Stereotactic Surgery and Radio Surgery," MPPC Press, 1993, pp 307–320.)

Repositioning the patient relative to the linear accelerator can be accomplished by several techniques. Standard techniques involve a BRW stereotaxic floor stand or laser-line intersections with the patient's head ring. New innovations in patient repositioning include the use of a low-frequency magnetic field generated by a special source in the accelerator gantry with the patient's spatial coordinates digitized by a field-sensor that is an integral part of the stereotaxic head ring (Houdek *et al.*, 1990). Another repositioning scheme embeds three gold radiographic markers into the scalp. Orthogonal radiographic films locate the three markers in space during the first patient set-up. Subsequent patient repositioning then requires the three markers to be oriented in the same locations. This orientation is accomplished through repeat radiographs coupled with computer programs that determine the movements required to provide the correct position (Jones *et al.*, 1989). Likewise, repositioning schemes using Moiré patterns or laser-constructed repositioning planes can be investigated. A repeat-fixation system is offered by MEDCO (Cinnaminson, NJ) for multiple fractionation in SRT. This system will be marketed with a stereotactic frame and a variable attenuation cylindrical collimation system.

C. Real-Time Portal Imaging

Real-time imaging (Meertens, 1985) should be adapted for verifying patient position to within 1.5 mm of the desired target position with respect to the machine isocenter. The skull affords many anatomical landmarks. The use of the natural landmarks, image reconstruction from the CT treatment planning data in the beam's-eye view, and real-time imaging will allow for frameless SRS or high-precision radiation therapy. Several digitally reconstructed radiographs (DRR) can be compared with the corresponding real-time images to align the skull with the treatment machine's coordinate system. Again, this is an enhancement of positioning techniques developed at LBL and other charged-particle therapy facilities (Lyman *et al.*,1989). See also Adler:"Frameless Radiosurgery," *Stereotactic Surgery and Radiosurgery*. Med. Phys. Pub. Co. 1992, pp 237–248.

D. Conformal SRS

Conformal SRS (CSRS) is the use of an adjustable collimator to conform the beam profile to the target cross-section in the beam's-eye view and is analogous to the collimation of the charged-particle beam to the BEV of the target for each beam port. Conformal SRS would improve the dose delivery in approximately 40–70% of the SRS caseload. The absence of CSRS can

prevent treatment in instances such as a large nonspherical target within 5 mm of a critical structure. For the remaining SRS candidates, CSRS reduces the irradiated volume of normal tissue (Nedzi *et al.*, 1993; Nedzi *et al.*, 1991; and Leavitt *et al.*, 1989). A second benefit of CSRS results in the elimination of one or more multiple isocenters. Most targets are nonspherical. If the target is elongated, conventional SRS techniques reduce the dose to normal tissue through the use of more than a single isocenter (Nedzi *et al.*, 1990 and Serago *et al.*, 1990). Nonetheless, two overlapping spheres are not likely to conform to the typical tumor. CSRS will permit an additional 25% reduction of the normal tissue volume between the 50–80% dose levels. The end result should be the reduction of complications. Difficulties experienced with the multiple-isocenter technique include the increased time required to determine the location of isocenters, field sizes, determination of the arc geometry to achieve an adequate treatment plan, and the increased treatment time required to double or triple the treatment arcs.

Several techniques to implement field shaping have been proposed. One technique attempts to shape a single elliptical aperture that can be applied across an entire arc without field shape modification during the arc (Serago *et al.*, 1990 and Otto–Oelschlager *et al.*, 1994). The single elliptical aperture is chosen when it is necessary to encompass the maximum projection of the target volume throughout all angles of all arc segments used in treatment. This technique will be expanded through the development of control software that allows the major axis of the elliptical aperture to be rotated about the beam axis during rotation to more closely conform the aperture to the target shape. Additionally, the elliptical aperture insert can be removed manually from the collimation system and be replaced by a different insert for each arc to improve conformation to the target volume. However, in many cases the projected cross-sectional shape of asymmetric lesions changes markedly during a single arc as well as from one arc to the next, thereby making dynamic field shaping necessary to optimize dose distributions. Existing multi-vane collimation techniques can be applied to small-field irradiation. However, this application requires a large number of very thin vanes to achieve the required resolution in field shapes.

An alternate design uses four independent computer-controlled jaws, each having translational motion (in-out) and circular rotation (around the target-to-isocenter axis) to conform the field shape projected by the standard circular collimator more closely to the target projection at each increment of arc (Leavitt *et al.*, 1991).

The key feature of the dynamic field-shaping design is the use of independently controlled collimating vanes to shape the circular field defined by the standard aperture. Thus, the vanes can be reduced in size and mass because they must only "trim" the existing circular field, rather than provide all the primary beam attenuation across the entire larger field defined by the primary photon collimators. Figure 15 illustrates the prototype collimator assembly at the University of Utah. With the photon collimator jaws of the linear accelerator set to define a field 6 cm × 6 cm at isocenter, an aperture is inserted at the bottom of the stereotactic collimator to define a circular field of the desired diameter at isocenter, which will encompass the maximum target volume projection plus a clinically determined margin. This aperture is chosen from a complete series of aperture inserts that define the field diameter from 1 cm to 5 cm in 0.25-cm increments. These inserts preserve the small geometric penumbra of the standard circular aperture. Immediately upstream (relative to the photon beam) from the circular aper-

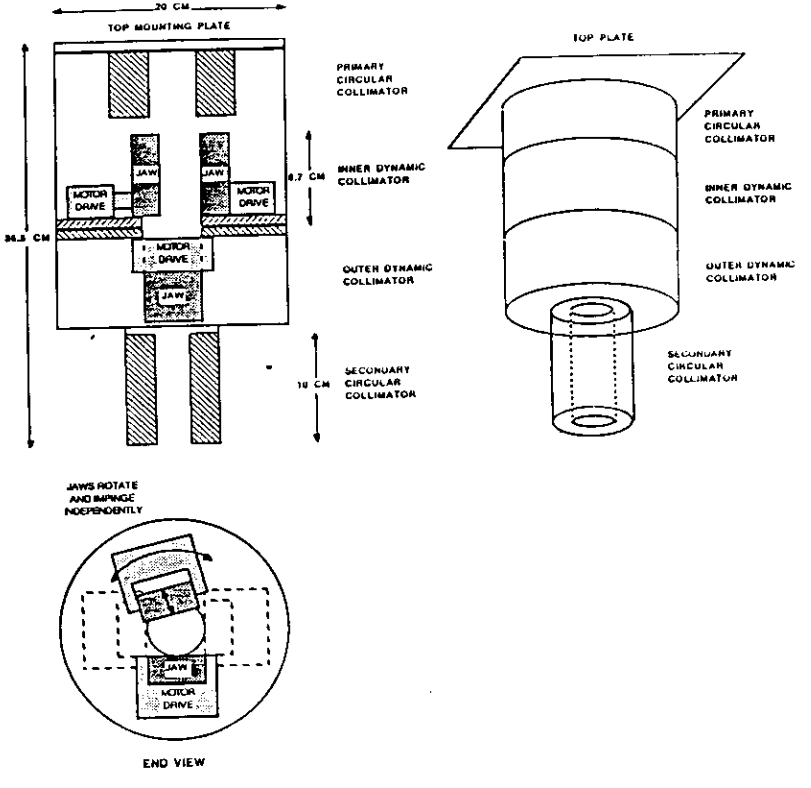

FIGURE 15. Upper right: A limited perspective of the collimator housing for dynamic field shaping. Upper left: A schematic view of the secondary circular collimator, the two layered identical dynamic collimator sub-assemblies, and the primary circular collimator (6 cm in diameter). One collimator vane is extended into the field, while the other is retracted. Lower left: An end view illustrating that each motor drive and its respective collimator jaw is rotated independently and the independent in-out movement of the jaws. (Leavitt *et al.*, 1991.)

ture, two pairs of independently controlled tungsten vanes and their associated linear-motion, screw-drive motors mount on two concentric movable rotating tables driven by belt attachment to motors with integral quadrature-count encoders for sensing angular position. The vanes, concentric mounting plates, and potentiometers are controlled and driven by a microprocessor-based, four-axis controller. The required range of linear motion of each vane is limited to only 2 cm, corresponding to the distance from the outer diameter of a 5 cm (at isocenter) aperture to the midline of the aperture. The angular range of motion can extend to 360°, subject to the anti-collision constraints imposed by the second concentrically mounted vane. Immediately upstream again, this two-vane configuration is repeated on a second set of two concentric movable rotation tables. This second set of independent vanes complements the first set to define field shapes of four straight sides (a field smaller than the circular aperture), one to four straight sides, and one to four curved sides (circular aperture clipped by one to four of the vanes), or circular (all four vanes withdrawn to the edge of the circular aperture).

The above-described four-vane collimation system is unable to match the projected cross-sectional concave view of some target shapes, such as a crescent or peanut shape. In these cases, improved conformation to the target cross-section may be achieved through the use of multiple narrow vanes, each moving independently to describe a curved treatment field boundary. Efforts are now in progress to develop specialized multi-vane collimators for radiosurgery in which the projected width of each vane will be reduced to 2 mm (Nedzi *et al.*, 1991). This capability, coupled with rotation of the entire collimator assembly about the principal beam axis, may improve the dose conformation in selected clinical cases.

Dynamic dose-rate control features on new-generation linear accelerators allow the continuous adjustment of dose delivered per degree. This feature may be incorporated into dose delivery in radiosurgery. During treatment planning, a large number of treatment arcs would be defined. Each arc would then be broken into a number of segments; for each segment the conformal collimator shape would be determined, and the dose contribution within the target volume and the surrounding normal tissue would be calculated for a fixed number of monitor units. Optimization routines would determine the monitor units to be delivered during each segment, based on evaluation of differential and integral dose volume histograms, which are weighted by the biological predictors of tumor control probability (TCP) and normal tissue control probability (NTCP) (Lyman and Wolbarst, 1987). Additionally, computer control of the patient couch rotation during treatment suggests additional possibilities for optimizing the dose distribution by adding simultaneous couch rotation to conformational vane positioning and computer-controlled dose rate modulation. The potential advantages of

simultaneous control and adjustment of these parameters requires considerable study.

NOMOS Corp. has also introduced a complete conformal SRT planning and treatment delivery system (PEACOCK). The treatment-planning algorithm is based on the filtered backprojection techniques which generate the dose distribution by beam intensity modulation and dynamic collimator-jaw movement. The treatment volume is irradiated in slices. The net result is a dose distribution which conforms to the tumor and minimizes normal tissue dose. The PEACOCK system is entering beta testing at Baylor and the University of California at San Francisco. Similarly, TOMOTHERAPY strives to achieve the same dose delivery goals by means of a redesign of the entire treatment delivery system (linac) by mounting the electron waveguide/target on a ring perpendicular to the patient axis (Mackie *et al.*, 1993). Temporally-modulated collimators and beam intensity modulation would conform the dose distribution to the tumor as the beam spirals down the axis of the patient. This technique has the theoretical advantage of delivering a homogeneous dose to the target (Carol, 1993).

E. Robot-Guided Linac

A mini-linac has been mounted on a robotic arm and configured for frameless SRS (Cox *et al.*, 1993). The system, Neurotron 1000, can vary the source-axis distance as well as the beam path by angle, distance and speed. The Neurotron 1000 tracks the image of the patient anatomy in real-time and continuously guides the robot arm during the treatment. Consequently, conformal SRS can be affected by beam manipulation as opposed to complex collimation.

In summary, dynamic conformational field shaping, improved imaging techniques, expanded treatment planning techniques, the incorporation of dose-volume histogram and biological predictive data, and patient positioning techniques will be extensively investigated. Progress in these areas will undoubtedly lead to further advances in stereotactic radiosurgery.

IX. SUMMARY

Stereotactic radiosurgery has evolved to the point where commercial systems, such as XKNIFE, LEIBINGER AND FISCHER LP, the GAMMA-KNIFE and the BRAIN LAB are available to the oncology community. The basics of these systems will not change significantly with the exception of image correlation and immobilization techniques. Stereotactic radiosurgery (SRS) and stereotactic radiotherapy (SRT) present the same accuracy requirements in dosimetry and patient positioning and are at the millimeter level. The introduction of the SRS/SRT hardware and software is a complex

process which must be configured to the institution at the interdepartmental level as well as to the SRS apparatus. The system will be used by a team of radiation oncologists, neurosurgeons, medical physicists, and neuroradiologists. The following basic sequence for its introduction is recommended:

1) Establish a multidisciplinary team to determine the treatment goals.
2) Determine the accuracy required and present in existing equipment. For example, the rotational axes of the gantry, collimator and PSA should intersect within a 1-mm radius sphere.
3) Select the SRS apparatus and perform a prospective risk analysis of the SRS procedure.
4) Establish an acceptance test.
5) Acquire the beam-profile data with a maximum detector dimension of 1–2 mm for the linac and 0.5 mm for the gamma knife unit.
6) Acquire dose calibration with a detector dimension of 3 mm or less for the linac (12.5–40.0 mm diameter fields) and 1 mm × 1 mm × 1 mm for the gamma knife unit.
7) Establish a treatment procedure and routine treatment QA schedule (daily, quarterly and annual).
8) Interlock the gantry/PSA to prevent collisions.

Appendix III contains a representative or generic QA schedule for a linac-based installation. Examples of the gamma knife unit and linac QA schedules are shown in Appendix IV. Each institution should modify the above guidelines to optimize the accuracy of treatment delivery at that particular facility.

X. ACKNOWLEDGMENTS

The task group would like to express their appreciation for the assistance afforded by Drs. Steven Leibel, Hanne Kooy, Robert Kline, Patrick Stafford, Jatinder Palta, Martin Weinhous, Steven Goetsch, Robert Dryzmala, and Douglas Rosenzweig. Dr. Leibel provided considerable insight into the treatment of primary brain lesions. Dr. Kooy assisted with the QA procedure for the couch-mounted system. Dr. Rosenzweig as well as Kathi Burton were integral in preparing the manuscript for publication.

XI. APPENDIX I

PROBABLE RISK ANALYSIS FLOWCHART: EXAMPLE 1

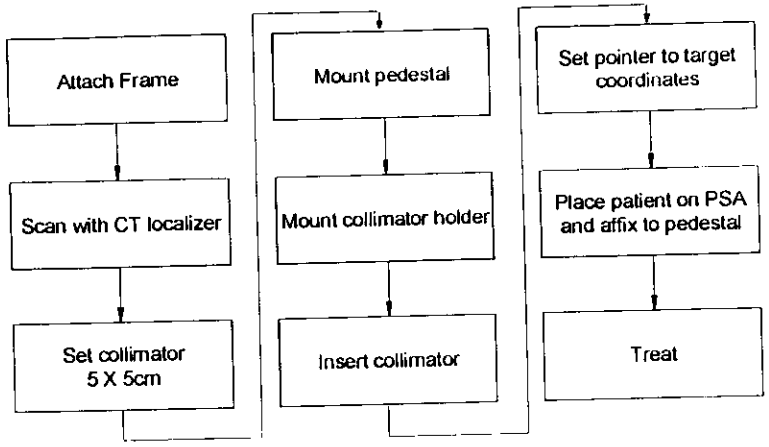

XII. APPENDIX II

PROBABLE RISK ANALYSIS FLOWCHART: EXAMPLE 2

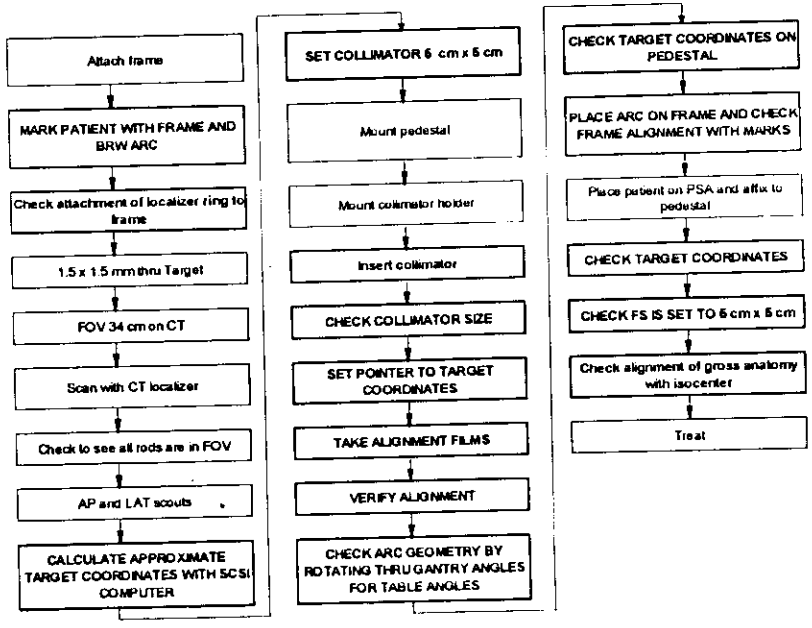

XIII. APPENDIX IIIA: SRS QA SCHEDULE

PROCESS TEST	PERIODICITY
I. INPUT DIGITIZER, OUTPUT PLOT	
• Square contour	Weekly*
II. CT SCAN TRANSFER	Quarterly**
III. PHOTON BEAMS	
1) Point doses ($d = d_{max}$, 5, 10)	Semi-annually*
2) Lateral profiles	Semi-annually*
• Open ($d = d_{max}$, 10) (12.5 mm, 30.0 mm)	
IV. FRAME SYSTEM	
1) CT Localization Performance	
2) Angiographic Performance	Quarterly
3) MRI Performance	
V. SYSTEM LOCALIZATION	
1) CT Phantom Target	Quarterly
2) Beam Target on Linac	
VI. SUMMATION ALGORITHMS	
1) Arc pair	
• Equally weighted	
• Unequally weighted	Semi-annually*
2) 5 arc	
• 270°, 230°, 190°, 10°, 50°	
VII. MACHINE SETTINGS	
1) Single stationary	Semi-annually*
2) 4 arcs on sphere	

*At minimum frequency indicated or after software changes.
**At minimum frequency indicated or after any software or hardware changes on the CT scanner or treatment planning system.

XVI. APPENDIX IIIB: LINAC QA SCHEDULE

HARDWARE TEST	PERIODICITY
I. DOSIMETRY OF THE LINAC	
a) Dose calibration	monthly
b) x-ray/light field alignment	bi-weekly
II. ALIGNMENT OF GANTRY COLLIMATOR AND PSA AXES	annually
III. STABILITY OF THE BEAM SPOT	annually
IV. SAFETY OF PATIENT SUPPORT ASSEMBLY	monthly
V. ARC THERAPY TEST	quarterly
VI. LASER ALIGNMENT	
a) Pedestal mount	weekly
b) Couch mount	prior to each treatment

XV. APPENDIX IV

STEREOTACTIC RADIOSURGERY TECHNIQUES

A. Heavy-Charged-Particle Therapy

R. R. Wilson first proposed the use of heavy charged particles for radiotherapy in 1946 (Wilson). Heavy charged particle therapy has been available for several decades (Goitein *et al.*, 1982). The therapy facility at the Donner Lab/Lawrence Berkeley Lab is presented as an example of the efforts in heavy-charged particle therapy. The treatment philosophies at LBL are not identical to those at other facilities. For example, as many as eight ports through both hemispheres may be used to treat intracranial lesions at the Harvard Cyclotron, compared to four ports through one hemisphere at LBL.

1. Heavy Ions—LBL

Although the initial stereotactic irradiation at LBL occurred in the early 1960's, the current SRS design was developed in 1980 (Lyman *et al.*, 1989). The principal criteria for SRS with a helium ion beam were (1) a uniform field between 10 mm and 40 mm; (2) a range in penetration depth between 40 mm and 140 mm; (3) the ability to shift the Bragg peak over a 40-mm interval; (4) sharply defined lateral and distal borders; and (5) a dose rate greater than 2 Gy/min.

2. ISAH: Irradiation Stereotactic Apparatus for Humans

Irradiation Stereotactic Apparatus for Humans (ISAH) is a patient-positioning device for heavy-charged-particle therapy (Lyman and Chong, 1974). ISAH maneuvers the patient with 5 degrees of freedom: three mutually orthogonal translations and two rotations. The base of ISAH is a 0.5-m thick granite slab, polished to tolerances of 0.5 microns. The slab can be adjusted vertically and horizontally to within 5 cm. A patient module is mounted on the slab and can rotate on two orthogonal axes. Position accuracy is 0.01 cm and rotational position is uncertain by 0.10 degrees. All motions are effected by computer-controlled stepping motors. Should the difference between the actual patient position and the computed position exceed the 1-mm or 1° limits, treatment is halted until the position error is corrected.

3. Beam Characteristics

Beam energy degradation and modulation occurs 3.8 m upstream from the patient (Figure 16). Consequently, the beam has negligible divergence. The peak-to-plateau dose ratio equals 3.09. The distal beam penumbra drops from 90% peak dose to 10% in less than 6 mm (Figure 17).

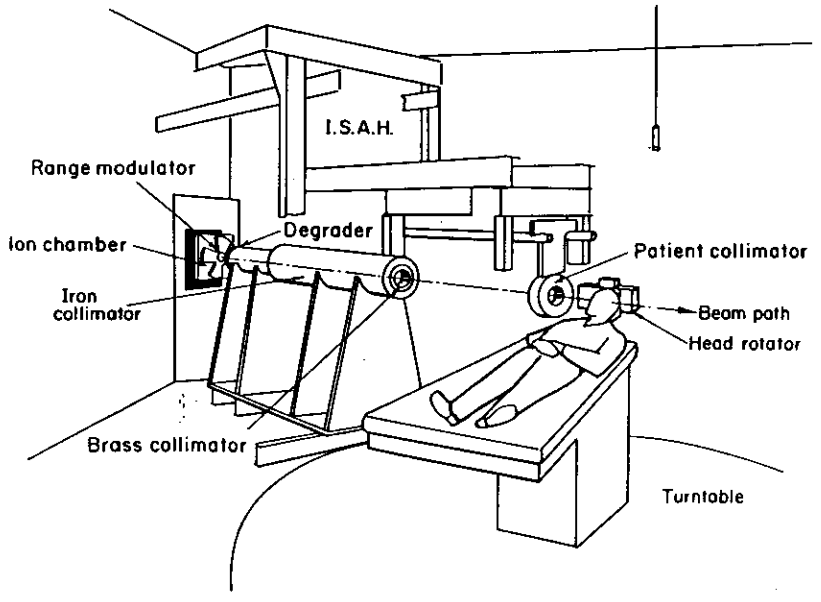

FIGURE 16. The helium ion beam delivery line is shown in relation to the ISAH. An x-ray uytube (not shown) is positioned between the patient and beam line to obtain BEV radiographs for position verification. (Lyman *et al.*, Med. Phys. 13:695–699, 1986.)

Figure 3 is a comparison of dose profiles of a 230-MeV/u helium ion beam and a 6-MV x-ray beam with beam apertures of 1.27 cm and 1.25 cm, respectively. The two beam profiles are remarkably similar. The principal clinical advantage of the charged particle beams over x rays is the finite range of charged particles. The charged particle beams can be range-modulated such that the Bragg peak coincides with the distal side of the target, thus sparing the normal tissue behind the lesion.

4. LBL Stereotactic Frame

A noninvasive frame has been developed at LBL for stereotactic neuroradiological studies (CT, MRI, and angiography), (Lyman *et al.*, 1989). The frame consists of a plastic mask, a Lucite/graphite mounting frame, fiducial markers, and a fixation interface to the imaging couches (Figure 18). The frame allows the patient to be repositioned to within 1 mm in each of three orthogonal planes.

The frame is mounted to the ISAH and positioned for the desired beam entry and inclination. A radiograph is taken to provide a beam's-eye view (BEV) of the treatment port. The radiograph is compared with a digitally reconstructed radiograph (DRR) also reconstructed from the BEV, as calcu-

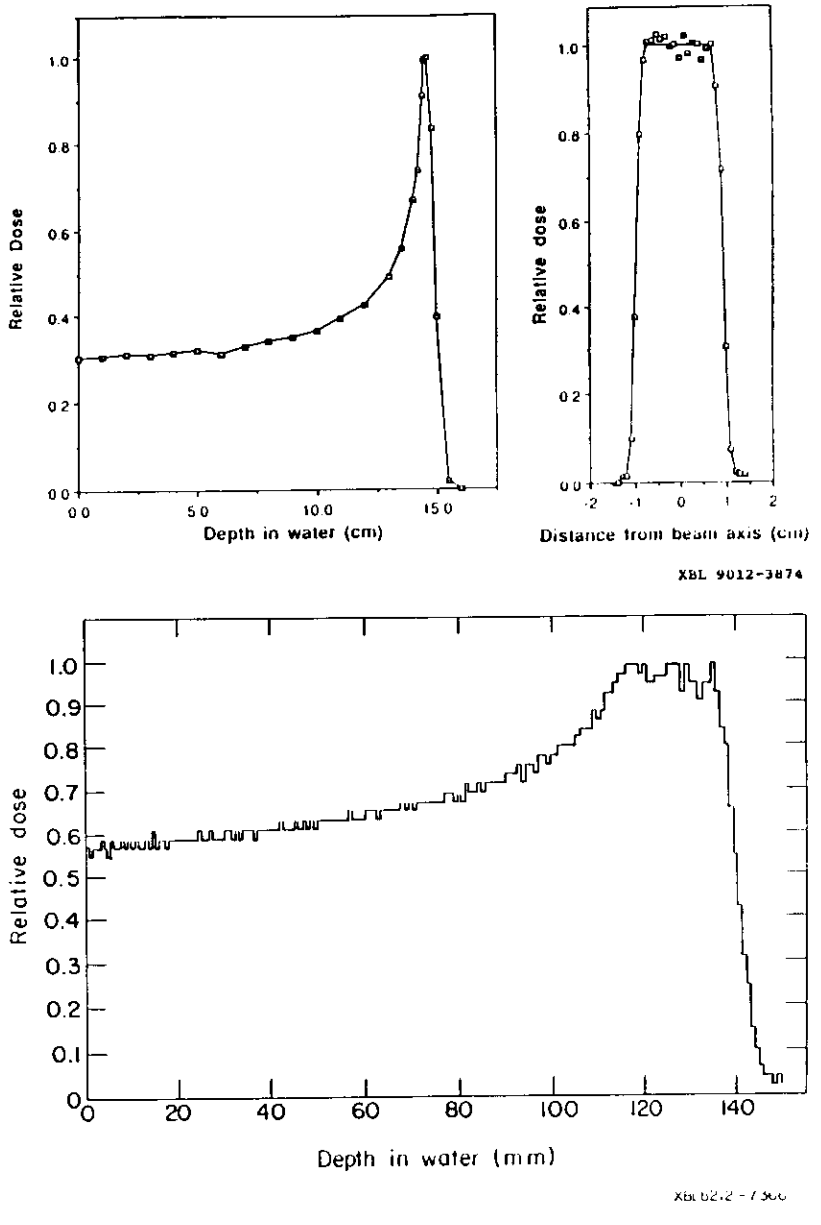

FIGURE 17. The depth dose profiles in water are shown for (a) an unshifted 230 MeV/u helium ion beam and (b) a range-modulated beam (stopping region is 21.6 mm). The beam cross-section is shown in (c) for the 12.7 mm aperture. (Lyman *et al.*, Med. Phys. 13:695–699, 1986.)

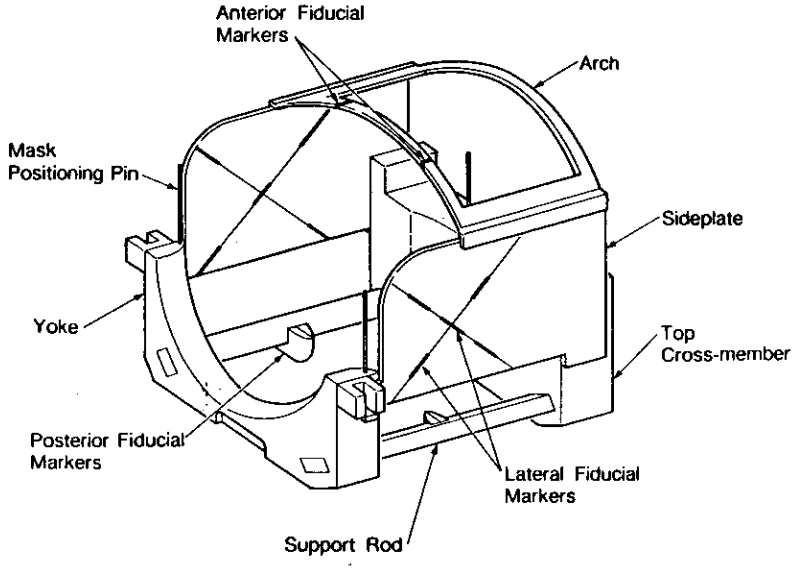

FIGURE 18. The LBL noninvasive stereotactic frame is illustrated with the fiducial markers. (Lyman *et al.*, 1989.)

lated from the treatment plan. If the two BEVs depict the same port location and angulation, the treatment proceeds. Conversely, the patient setup and position is adjusted until the DRR and radiograph are identical.

As in x-ray SRS, the frame immobilizes the patient and establishes a reference for target localization. The distinguishing feature is that the frame is noninvasive and is used for single or multiple fractions.

5. Treatment

A lesion is treated with four ports or beams that traverse only one hemisphere and converge on the target. Each port is conformed to the three-dimensional shape of the target; hence, the need for multiple isocenters is eliminated. Intracranial lesions are treated with multiple fractions, with the total photon-equivalent dose between 15 Gy and 25 Gy. Field sizes range from 8 mm to 60 mm. The treatment dose is calibrated to an isodose surface value between 70–90% of the maximum dose. (Chen *et al.*, 1979 and Goitein *et al.*, 1982) The CT scan data are acquired with a 5-mm slice thickness to facilitate the compensator fabrication for each port. AVM treatments are planned from angiograms and MRI (Phillips *et al.*, 1989). The AVM's surface is contoured at the levels of MR scans corresponding to the CT scans and is incorporated into the CT data set.

B. Linear Accelerators in Radiosurgery

The use of linear accelerators in radiosurgery was first proposed theoretically by Larsson *et al.* in 1974. The first reports on clinical linac-based radiosurgery were published 10 years later in 1984 by Betti and Derechinsky and in 1985 by Colombo *et al.* and Hartmann *et al.* These reports were all based on a technique referred to as the multiple noncoplanar converging arcs radiosurgical technique. The center of the target is placed stereotactically at the machine isocenter and a series of arcs, each with a different stationary treatment-chair position or treatment-couch position, spreads the dose outside the target over as large a volume as possible. Soon thereafter, linac-based radiosurgery started in North America in Boston with a variation on the multiple arcs technique (Houdek *et al.*, 1985; Lutz *et al.*, 1988; and Schell *et al.*, 1991) and in Montreal with the dynamic rotation technique (Podgorsak *et al.*, 1987 and 1988).

Several of the current linac-based radiosurgery techniques are discussed in detail. The discussion focuses on pedestal- and couched-mounted frame systems. A discussion of the physics for radiosurgery with linear accelerators has recently been published by Podgorsak (1992).

1. Pedestal-Mounted Frame Techniques

- *The initial configuration at the Joint Center For Radiation Therapy*

A system has been developed for stereotactically described delivery of prescribed doses of radiation to precisely located volumes ranging from 0.6 cm^3 to 14 cm^3 in the brain (Lutz *et al.*, 1988 and Winston and Lutz, 1988). A Brown–Roberts–Wells (BRW) stereotactic apparatus and a 6-MV linear accelerator equipped with a special collimator (1.25–4.0 cm in diameter) have been adapted. The 20-mm collimator produces a nearly spherical volume of 3.6 cm^3 within the 80% isodose surface for a five-arc geometry with 40 degrees between each arc plane. Outside the treatment volume, the dose declines to 50% of the peripheral target over a distance of 3–4 mm. The target can be located with computed tomography or cerebral angiography. Radiation is delivered with an arcing beam of x rays, with the turntable (patient support assembly) in a different position for each arc. Typically, there are four arc positions, but there are no restrictions. The exact pattern of arcs and arc-weights depends on the treatment goals. The entire system has been extensively tested for accurate alignment and dose distribution. Errors have been measured for the alignment of the apparatus and the process of localization. Safety of operation was emphasized throughout the design and testing phases.

Apparatus

A 6-MV Linear Accelerator (Varian Associates, Inc., Palo Alto, California) was chosen as the source for ionizing radiation on the basis of availability. Good mechanical accuracy is essential. The three principal mechanical axes (gantry, turntable, and collimator) should intersect at a common point (the isocenter) and remain stable during all rotations (Figure 19). The point in space where the three axes come closest together is designated as the "best compromise" isocenter. A true mechanical isocenter is not achieved because of the 0.5–0.7 mm displacements from gantry sag, gantry and turntable axis precession, and lack of intersection of turntable and gantry axes, even if the mean position of the axes intersect.

The conventional collimator on a linear accelerator is inadequate for radiosurgery because the jaws produce rectangular beams, rather than the desirable circular beams. Tertiary collimation also improves the alignment and minimizes the penumbra of the beam, resulting in a more rapid falloff of radiation outside the lesion. The collimator should mount to the gantry in a precise and reproducible manner. It extends to 23 cm from the isocenter and will accept one cylindrical collimator insert. The 10-cm thick inserts are made from cerrobend, and have a stepwise drilled circular opening. A circular collimator was chosen because it delivers a sharper dose gradient than is possible with a square collimator, where the beams are delivered over a hemisphere. Twelve inserts range in size from 1.25 cm to 4.0 cm at the isocenter, although smaller and larger diameter inserts have also been used.

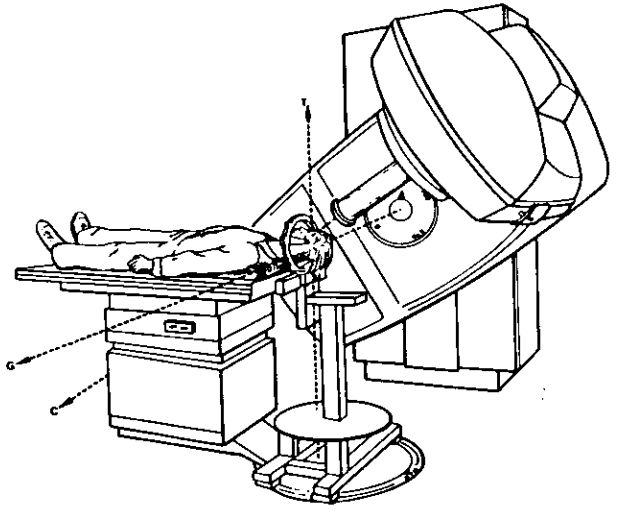

FIGURE 19. The Joint Center hardware configuration is shown with the frame stand mounted on the PSA base plate. The stereotactic frame is attached to the stand and at the locus of the rotation axes of the gantry, table and collimator. (Lutz *et al.*, 1988.)

The central axis of the collimator's insert must be aligned with the line connecting the photon source to the isocenter. Alignment at all gantry and couch positions was evaluated by placing a small spherical steel target precisely at the "best compromise" isocenter and making radiographs of the target using the linear accelerator with the tertiary collimator in place. When the collimator is aligned and the target is at the best isocenter, the circular image of the spherical target should be centered in the circular radiation field regardless of the position of the gantry or couch. The accelerator's light field is usually not adequate for accurate alignment.

An interface base was designed to fix the BRW floor stand to the plate overlying the bearings that support the treatment couch (this establishes the vertical axis of the turntable's rotation). The BRW ring can then be used to attach a patient's head to the floor bearing via the BRW stand. This specially designed base can be pinned and bolted rigidly and with reproducible accuracy to the plate of the couch's floor-bearing. The BRW floor stand has three calibrated orthogonal, manually operated drives that move the head ring, and, hence, any specified point within the patient's head, to the desired Cartesian coordinates (referred to as anteroposterior, lateral, and vertical in BRW terminology). Specifically, these drives are able to place a predetermined target coordinate at the isocenter of the linac. The target positioning is accomplished without reference to the room's alignment lasers because the width of the laser beams and their variability may make them less precise. More importantly, this method of patient positioning permits a rigorous pretreatment verification of the system alignment and setup for each patient. The Varian treatment couch, without additional immobilization, is not sufficiently stable for the precise positioning required. The patient support assembly (PSA) is used to support the patient's trunk and extremities.

Target Localization

A localizer box was designed and constructed for angiographic localization (Figure 20). It attaches to the BRW head ring in the same manner as the CT localizer frame by means of the BRW ball-and-socket mechanism. Each of the four sides of the angiographic box has a set of four lead fiducial markers in a 6 cm × 6 cm square array (any noncolinear arrangement is satisfactory). Localization by angiography requires two different planar angiographs. Cerebral angiographs are typically made in frontal and lateral projections with no requirements for orthogonality, film/target distance, magnification factor, or the orientation of the head with respect to the source or the film. The only requirement is that two sets of markers (one set on each

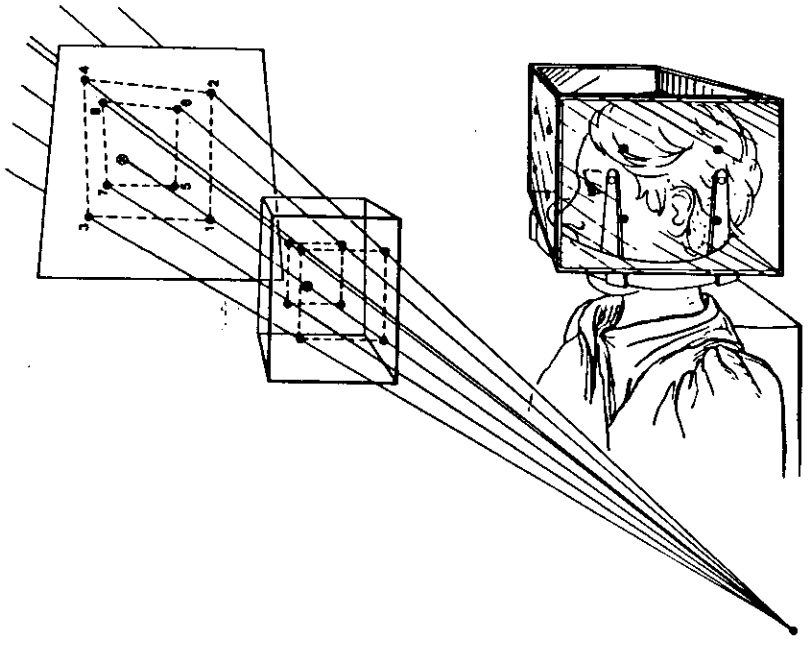

FIGURE 20. The angiographic localizer box is attached to the BRW head ring. Knowledge of the BRW coordinates of the fiducial markers allows for target (AVM) localization from pairs of quasi-orthogonal radiographs. (Lutz *et al.*, 1988.)

side of the box) appear on each radiograph. **One cautionary note: digitized radiographic images may contain geometric distortions.** The unique line passing from the radiation source through the target can be computed when one knows the geometry of the box.

Tumor localization is determined by enhancement on CT and/or MRI. The CT and MRI localizers have unique rod geometries that enable calculation of the coordinate transformation between CT/MRI and the stereotactic frame (Saw *et al.*, 1987). Localization by MRI is also prone to image distortion and should be thoroughly and routinely tested before use.

If a lesion is localized by computed tomography, an appropriately thin slice is used to minimize the error in localization. Once the neurosurgeon and neuroradiologist have selected the CT slice that best locates the lesion, the coordinates of the target center are computed from the positions of the nine localizer rods and the center of the lesion on that slice, as described in the instruction manual for the BRW system.

• *University of Florida Technique*

Apparatus

In 1986, a new linear-accelerator-based system (Friedman, 1989 and Bova, 1991) that expands on the design by Lutz *et al.* (1988) was developed. One of the primary objectives was to provide a mechanical system that would function independently of the linac gantry and patient support systems. The motions requiring precise control were the accuracy of collimation during the arcing of the radiation beam and the rotation of the patient for repositioning between the arcs, both of which were constructed in-house. The first bearing system controls the isocentric accuracy of the collimator. The second bearing system controls the rotations of the head of the BRW floor stand. These two bearing systems are mechanically coupled so that the rotational axes coincide (± 0.2 mm). The two bearing systems alone cannot, however, produce the desired accuracy of a rigid attachment to the linac head. To avoid any torque transfer from the linac head, a gimbal bearing with a sliding collimator mount was developed. This bearing allows the radiosurgery mechanical system, and not the linac head, to determine the isocentric treatment accuracy (see Figure 21).

With this system, standard parts of the BRW stereotactic system are used for either angiographic or CT lesion localization. The BRW head ring is applied in the usual fashion and the angiographic localizer is attached. A standard angiogram is performed and the best anteroposterior (AP) and lateral films for AVM localization are selected. The neurosurgeon defines and outlines the nidus of the AVM with a mouse on the computer system. The fiducial points and target volume appear simultaneously on the computer monitor. The computer calculates the geometric center, the center of mass, or a user-defined center, as well as the demagnified diameter of the field size. The computer also indicates the distance between a line drawn through the center point on each radiograph.

A series of cerrobend collimators, 15 cm long and ranging in diameter from 5 mm to 30 mm (in 2-mm increments), was constructed. Single-beam profiles were obtained for each collimator using film, thermoluminescent dosimeter, and electronic diode measurements.

After dosimetry planning, the system was assembled and tested with the radiographic method of Lutz *et al.* (1988). The patient is then attached to the floor stand and the prescribed arcs of radiation are delivered. The patient is attached to the accelerator for about 20 min during the procedure.

Radiation Beam Accuracy

From the verification films, the displacement of the center of the target image from the center of the radiation field is measured. The measured error is 0.2 mm ± 0.1 mm with a maximum error of 0.5 mm.

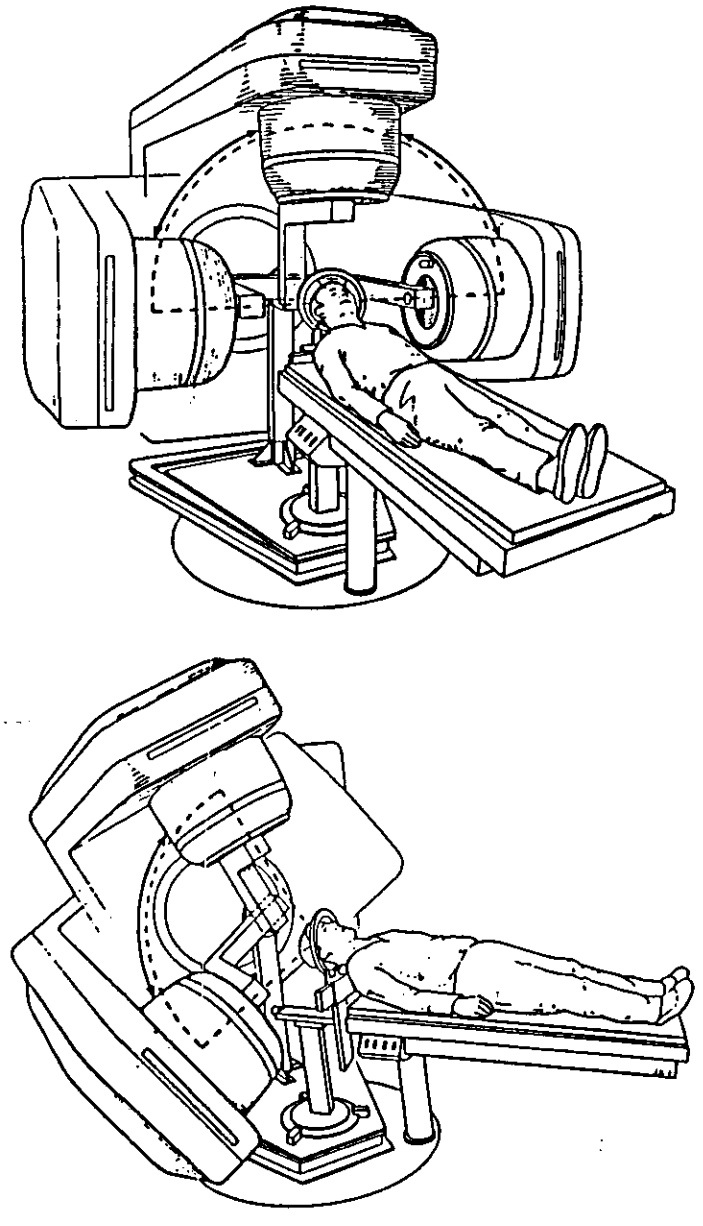

FIGURE 21. The University of Florida system is shown with the gymbal-mounted collimator arm attached to the linac. (Friedman and Bova, 1989.)

2. *Couch-Mounted Frame System*

• *Dynamic Stereotactic Radiosurgery at McGill University*

Apparatus

The dynamic stereotactic radiosurgical technique was developed in 1986 at McGill University in Montreal (Podgorsak *et al.*, 1987, 1990, and 1992). This technique uses a 10-MV linac (Varian, Clinac-18) as the radiation source and two types of commercially available stereotactic frames (OBT frame, Tipal Instruments, Montreal and Leksell frame, Elekta Instruments, Stockholm) for target localization, treatment set-up, and patient immobilization during treatment. In contrast to the multiple noncoplanar converging arcs technique, which spread the dose outside the target area with a series of arcs, dynamic rotation delivers the dose during a simultaneous and continuous rotation of both the gantry and the couch during treatment.

The additions and modifications required to make the linac useful for dynamic radiosurgery are relatively simple and consist of extra 10-cm thick lead collimators to define the small circular fields at the isocenter (0.5–3.5 cm in diameter), a remote controlled motorized couch-rotation capability with a variable speed control, a couch-angle readout and a couch-height readout on the machine console, brackets to fasten the stereotactic frame to the treatment couch, and brakes to immobilize the longitudinal and lateral couch motions.

The stereotactic frames are compatible with modern imaging equipment, such as CT, MRI, and DSA, so as to allow for accurate target localization (Olivier *et al.*, 1987 and Peters *et al.*, 1987) and, so long as appropriate brackets are available, to fasten the frame to the treatment couch to ensure immobilization during the radiosurgical procedure. The frame attachment to the floor stand used in most multiple converging arcs techniques is not possible for dynamic rotation because in dynamic rotation the linac head must pass below the patient. Not being able to attach the frame to the floor stand could be considered a drawback of dynamic rotation, assuming that the floor stand offers better frame stability. However, couch mounting on a properly locked couch offers equal stability and is considerably safer than the floor-stand mounting in cases of inadvertent vertical couch motions.

The stereotactic frames used for dynamic radiosurgery at McGill are compatible with CT, MRI, and DSA, and their mass is only 800 g, making them easily supportable by the patient when moving from diagnostic to therapeutic equipment.

The frame is fastened to the patient's head with three to five carbon pins that penetrate diagonally into the frame's cubic structure. Standard fiducial-marker plates are used to determine the coordinates of the target with CT or MRI, whereas for target localization with the DSA, special magnification plates are used. Information on the target position obtained with diagnostic

procedures is transferred to special target-localization plates that are used in conjunction with wall- and ceiling-mounted lasers for placement of the target center into the linac isocenter before treatment.

Treatment Technique

The patient is placed supine onto the treatment couch and the stereotactic frame is fastened to the couch such that the patient's head overhangs the end of the couch as shown in Figure 11. The appropriate couch position is obtained with the help of wall- and ceiling-mounted laser positioning devices and the target localization plates on which the target centers are indicated. Once the center of the target coincides with the linac isocenter, special brakes immobilize the lateral and longitudinal couch motions and the target localization plates are removed from the frame to minimize the interference of the stereotactic equipment with the radiation beam. The couch is then rotated to 75°, the gantry to 30°, and the dynamic stereotactic radiosurgical procedure is ready to begin.

During the treatment, the couch rotates 150°, from +75° to –75°, while the gantry simultaneously rotates 300°, from 30° to 330°. Thus, each degree of couch rotation corresponds to 2° of gantry rotation. Several successive positions through which the couch and gantry move during the complete radiosurgical procedure are shown in Figure 11, starting (a) with the gantry and couch angles of 30° and +75°, respectively, through (b) 90° and +45°, respectively, (c) 180° and 0°, respectively, (d) 270° and –45°, respectively, and (e) stopping at 330° and –75°, respectively.

During radiosurgery, the radiation beam always points to the target volume. The beam entry trace on the patient's head, however, exhibits a peculiar trace (baseball seam), shown schematically in Figure 2 (g). All points of the beam entry lie in the upper hemisphere, which results in the beam exit points all lying in the lower hemisphere. This means that in the dynamic rotation, even though all beams intersect in the target volume, parallel and opposing beams never degrade the optimal steepness of the dose falloff outside the target volume.

A couch-mounted frame system is also available from RSA, Inc. (Burlington, MA). This system continues to employ a radio-opaque target simulator system to verify the target alignment in the x-ray beam. This approach offers hard-copy documentation of the target placement in the radiation beam.

C. Dedicated Radioisotope SRS Unit—The Gamma Knife Technique

1. Apparatus

The major components of the Leksell stereotactic gamma knife are the radiation unit, four collimator helmets, a patient treatment table, a hydraulic system, and a control panel (Bradshaw, 1986; Lunsford *et al.*, 1987 and 1989; and Wu *et al.*, 1990). The radiation unit consists of an almost spherical housing with a shielded entrance door. Inside the housing is a hemispherical central body, which contains the 201 ^{60}Co sources (Figure 1). The housing and the central body are made of cast iron; the entrance door is cast steel. The radiation unit weighs approximately 16,800 kg. The treatment table weighs an additional 1,500 kg. The housing opens like a clam shell for accessing the sources. The upper half of the housing has an outer radius of 82.5 cm and an inner radius of 42.5 cm. The lower half contains the shielded entrance door and a removable sump plug to retrieve objects accidentally dropped into the unit.

The central body, with an outer radius of 42 cm, fits closely with the inner radius of the upper half of the housing; its inner radius is 22.5 cm. The angulation and diameter of the 201 beam channels are machined precisely (tolerance of 0.026 mm) in the central body. Each beam channel consists of the source/bushing assembly: a 65-mm thick, 96% tungsten alloy precollimator and a 92-mm thick lead collimator. All 201 beam channels are focused to a single point at the center of the radiation unit (focal distance is 40.3 cm). The sources lie in an arc ± 48° from the central beam along the long axis of the treatment table and ± 80° along the transverse axis of the table. No primary beams of radiation are directed out of the shielding door. The central axis of the 201 beams intersect at the focus with a mechanical precision of ± 0.3 mm.

The final collimation is accomplished with one of four collimator helmets. Each helmet has an identical 6-cm thick cast iron shield with an inner radius of 16.5 cm and an outer radius of 22.5 cm. The 201 channels are drilled in each helmet. Removable, 6-cm-thick final collimators are 96% tungsten alloy. They have circular apertures that produce nominal 4-, 8-, 14-, or 18-mm diameter fields at the focus. The apertures of individual collimators can be replaced with occlusive plugs to prevent irradiation of critical structures, such as the lens of the eye, or to alter the shape of the isodose distribution. Each helmet is equipped with a pair of trunnions, which serve as the fixation points for the stereotactic frame in the X dimension (right–left).

Micro switches on each helmet verify alignment between the helmet and central body with a positioning accuracy of ± 0.1 mm. Each ^{60}Co source consists of 20 pellets, 1 mm in diameter and height, stacked on top of one another, and encased in a double-walled stainless steel capsule. Each source fits into the source-bushing assembly at the top of each central body collimator. The short distance from the collimator helmet to the patient reduces the beam penumbra to from 1 to 2 mm for all sizes of collimator helmets. The steel door in the radiation unit is 18.5 cm thick. The opening and closing of the door and the movement of the treatment table in and out of the unit is controlled hydraulically. In the event of a power failure during a

treatment session, reserve hydraulic pressure automatically releases the treatment table and closes the shielding door. If reserve pressure is also lost, a hand pump is available to close the door. Failure of all back-up systems requires manually releasing the table and removing the patient from the unit.

2. *Target Localization*

With Leksell's stereotactic frame attached to the patient's skull, a diagnostic imaging procedure, such as CT, MRI, or angiography is performed to localize the target. A three-dimensional Cartesian coordinate system (X, Y, Z) is used to locate the target coordinates in Leksell's stereotactic frame. The Z-axis (superior–inferior) of the coordinate system lies along the axis of the patient, the X-axis (left–right) is in the coronal plane, and the Y-axis (anterior–posterior) is in the sagittal plane. The frame coordinate system is oriented such that the center of the helmet (the focus of the 201 sources) is X = 100, Y = 100, and Z = 100. ***This system eliminates the use of negative coordinates.***

The target is moved to the focal point of the unit by setting the X, Y, and Z coordinates of the stereotactic frame and fixing the frame to the trunnions of the helmet. The angle made by the frame between the central source ray and the horizontal plate is called the "gamma angle" and is read from indicators on the trunnions. The gamma angle is determined by tilting the patient's head. When shining a small pen light through each collimator in the helmet, radiation beams that would pass through the lens of the eye can be predicted. The appropriate collimators are then replaced with solid plugs to prevent the direct exposure of the lens to radiation. If more than one target is to be irradiated, this process is repeated for each target.

3. *Dose Calibrations and Measurements*

To determine the best dosimetry system for the measurements at the small focal point of beams, several different detectors were investigated. These included an ion chamber, a silicon diode, LiF thermoluminescent dosimeter chips, and film. All of these detectors were calibrated in a phantom against an ion chamber whose calibration is traceable to the National Institute of Science and Technology (NIST).

The dose output for the gamma knife was first measured using the 18-mm collimator helmet. A spherical polystyrene phantom 16 cm in diameter was constructed to simulate a human head. The phantom was fixed between the trunnions along the lateral direction and was movable within the helmet. The ion chamber (coupled to an electrometer) used for calibration and measurement was a 0.07-cm^3 micro-chamber small enough for this purpose.

Before measuring dose rates, the dosimetry system was calibrated. The ion chamber was placed in a polystyrene block phantom at a depth of 8.0 cm to simulate the radius of the spherical phantom. A small 5 × 5 cm^2 ^{60}Co beam was used for irradiation. With the same physical setup, the exposures were repeated using a 0.6-cm^3, Farmer-type ionization chamber and an electrometer, which has a calibration traceable to NIST. Hence, the dosimetry system was appropriately cross-calibrated. With the micro-chamber in place at the center of the spherical phantom, which was centered at the focal point of the 18-mm collimator helmet, dose rates were measured repeatedly at different positions. The trunnions were adjusted to vary the dose until the maximum dose rate was found.

Because the chamber volume was large relative to the region of uniform dose of other collimator helmets, an additional electronic method was used to measure the dose rate at the focus of the 4-, 8-, and 14-mm helmets. A small diode was used in a manner similar to the micro-chamber. Its response in a polystyrene block phantom at a depth of 8 cm on the cobalt unit was compared to that in the spherical phantom at the focus of the gamma knife. The current mode of the electrometer was used for all dose rate measurements with diodes.

Standard (3 mm × 3mm × 1 mm) LiF TLD chips also were used and calibrated in the polystyrene block phantom at a depth of 8 cm for the 5 cm × 5 cm field. The TLDs were appropriately annealed and sorted so that the entire group responded within ± 2% of the mean TLD response. The TLDs were given the same exposures that the chambers were given in the polystyrene block phantom. A dose-to-water versus TLD response curve was determined and fit to a least-square line.

A TLD was placed at the center of the 8-cm radius polystyrene sphere and exposed at the focus of the gamma knife unit. The 18-mm helmet was used with all 201 cobalt source collimators open. The TLD response curve was used to determine the dose rate to water per minute at the center of the polystyrene sphere. The average reading of 11 TLDs, exposed at every 30° along the x-axis of the spherical phantom, determined the dose rate.

To determine the "true" dose rate at the focus of the unit, the transit dose (the dose accumulated during the table's entry and exit from the focus) was subtracted from the total accumulated dose at the focus. The shutter error was determined as for the ^{60}Co teletherapy machine, using the difference in exposures measured in an interval of time with one ON-OFF sequence and several ON-OFF sequences to determine the transit dose.

4. *Absorbed Dose Profiles*

Because the gamma knife unit contains 201 ^{60}Co sources, with each collimated beam focusing at a central point, the dose profile of each individual beam is a building block for the total dose distribution of multiple beams with various plug patterns.

To measure a single beam dose profile, 200 of the 201 collimator openings of the 18-mm helmet were plugged, leaving the central one open. Film was cut to fit a special polystyrene cassette, which was placed at the center of a polystyrene sphere, 8 cm in diameter, to simulate a human head. Approximately 1 Gy was delivered to irradiate the film to obtain an optical density of approximately 2. Profiles were measured along the X- and Y-axes with a 0.75-mm aperture, using a scanning densitometer. The density-dose conversion relation was obtained from calibrated films of the same package exposed to the ^{60}Co teletherapy unit. The true single-beam profiles for each collimator size can be obtained by subtracting the background radiation, which was measured with all 201 collimators plugged, from the single-beam profiles shown in Figure 22, and plotted and illustrated in Figure 23. The dimensions of the 50% isodose, or full-width-of-half-maximum (FWHM), and the penumbra size, defined by the distance between 20% and 80%, are measured. Their FWHMs are 4.0 mm, 8.4 mm, 14.0 mm, and 18.0 mm for 4-mm, 8-mm, 14-mm, and 18-mm collimator helmets, respectively. The penumbras are in the 1–2 mm range, which is, comparably speaking, large for small collimator helmets, but small for large collimator helmets.

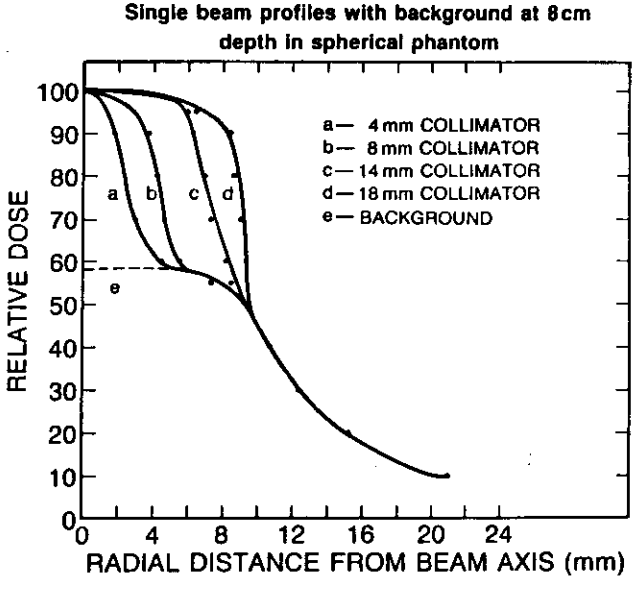

FIGURE 22. Dose profiles of a single beam measured with all but one collimator of the helmet closed. Due to transmission through the 200 collimator plugs, the single beam profiles exhibit high backgrounds. (Wu *et al.*, 1990.)

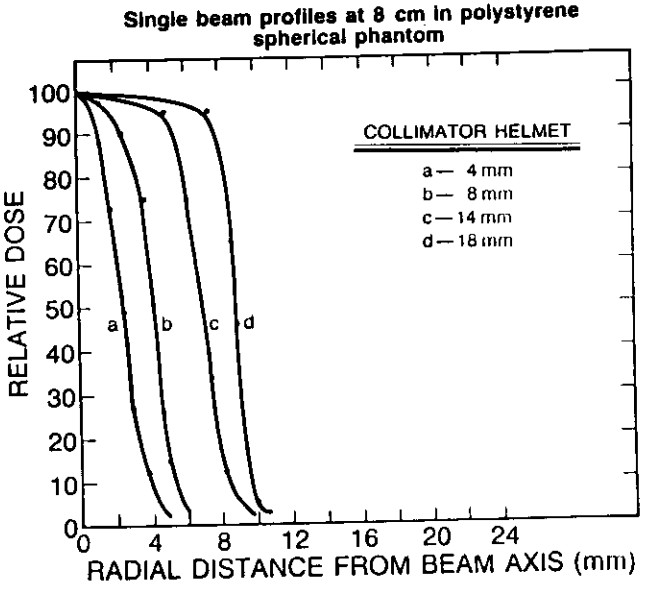

FIGURE 23. The single beam data with the background transmission subtracted. The sizes are defined by the 50% widths, and penumbrae by the 80%–20% distances. (Wu *et al.*, 1990.)

Figure 22 shows the dose profiles of the single beams for all collimator sizes. Shoulders appear on both sides of all beam profiles because of the radiation transmitted through the plugs and are particularly apparent for the 4- and 8-mm helmets. The shoulders are substantial, representing almost 60% of the maximum intensity of a single beam, because radiation is transmitted through all 201 plugs, rather than just one plug.

Most of the 201 collimators remain open during patient treatment. Therefore, we measured dose profiles as well as isodose distributions from films irradiated in two perpendicular planes; that is, the X-Y and X-Z planes at the center of a polystyrene 8-cm sphere in the gamma knife. The dose profiles along the X-axis of all four collimators (helmet at the focus) are shown in Figure 23.

Figure 23 shows isodensity scans of the X-axis dose profiles for the 4-mm, 8-mm, 14-mm, and 18-mm collimators. The corresponding Y-axis dose profiles (not shown) are much sharper at the edges as a result of the collimator pattern that spreads out ± 80° in X direction and ± 48° in Y direction. The Z-axis dose profiles may be slightly skewed toward the top because all of the sources are positioned at the upper hemisphere. However, the small diameters of the beams make this insignificant.

The relative output factors for the four helmets were measured using 1 mm × 1 mm × 1 mm TLD chips and a diode coupled to an electrometer at the focus for each helmet. Both the diode and the TLD chips were calibrated at a depth of 8 cm in a polystyrene block phantom with the small beam of a ^{60}Co teletherapy machine against ion-chamber measurements. The output values are very close to those obtained for a single beam and to those provided by the manufacturer, but there is a 3.5% variation for the 4-mm collimator helmet.

5. Mechanical Alignment Accuracy

To illustrate the qualitative accuracy of gamma knife irradiation, a small lead sphere, 4 mm in diameter, was placed at the center of a 20-cm diameter spherical phantom and exposed exactly at the focus. A strip of film was taped to the bottom of the phantom to catch the exit beams from each of the sources. The 8-mm collimator helmet was used.

An aluminum film cassette was made and placed into a film can. The cassette has a pinhole indicating the focal point of a helmet. A cut-out film was then loaded in the cassette, exposed with a 8-mm collimator helmet, and scanned with a microdensitometer with a 0.75-mm aperture. The position of the pinhole in relation to the focus was determined. Figure 14 shows that the density profile is determined by the half width of the half of the maximum. The position of the mechanical focal point is indicated by the pinhole, which is shown as a dip in the plot. Thus, the deviation of the radiation focus from the mechanical focus along the X-axis can be determined. This measurement was repeated along the Z-axis. The overall deviation from alignment of the unit was calculated from the square root of the sum of the squares from the deviations of X- and Z-axes and found to be approximately 0.25 mm.

6. Results

All three dosimetric tools—ion chamber, diode, and TLDs—were used to measure the output at the focus of the 18-mm helmet. Each response in the gamma knife was related to the dose in water measured by the Farmer ionization chamber on the ^{60}Co unit according to the most recent American Association of Physicists in Medicine protocol. The deviations among the dosimetric tools were less than 0.5%. We detected no appreciable directional dependence of the ion chamber, TLD, and diode measurements within the geometry of the gamma knife.

XVI. APPENDIX V

EXAMPLE GAMMA KNIFE QA PROGRAM

The quality assurance (QA) program that we have implemented in our facility (Univ. of Pittsburgh) includes the topics of physics, dosimetry and safety. The actual program is divided between daily, monthly, semi-annual and annual checks. Each item is not only assigned a frequency as dictated by regulating requirements as a good health physics practice or common sense, but also tolerances as applicable.

PHYSICS:	
Timer Constancy	Monthly
Timer Linearity	Monthly
Timer Accuracy	Monthly
On-Off Error	Monthly – 0.03 min
Trunnion Centricity	Monthly ± 0.5 mm
Radiation Output	Monthly ± 2%
Relative Helmet Factors	Annual ± 3%
Anticipated Output vs. Measured	Monthly ± 3%
DOSIMETRY:	
Computer Output vs. Measured	Monthly ± 3%
Radiation/Mechanical Isocenter Coincidence	Annual ± 0.4 mm
Dose Profiles	After source change or in the acceptance test
SAFETY:	
Timer Termination of Exposure	Daily
Door Interlock	Daily 0.5 cm trip point
Emergency Off Buttons	Daily
Beam Status Lights	Monthly
Emergency Release Rod	Monthly
Audio-Visual Communication Systems	Daily
Permanent Radiation Monitor	Annual functional test
Helmet Microswitch	Monthly 0.1 mm trip point
Hand Held Radiation Monitor	Daily ± 10% Annual
Couch Movement Time Deviation	Monthly < 0.5 min from intial couch movement calibration

SAFETY (*Continued*):

Emergency Instructions	Monthly semi-annual training
Operating Instruction Availability	Monthly
NRC Postings	Monthly
Leak Tests	6 mos. <0.005 μCi
Emergency Power	Annual
Test timers' battery backup through power loss/return cycle	Monthly

* Many of the checks are not required by regulation.

XVII. APPENDIX VI

EXAMPLE RADIOSURGERY PROCEDURES AND CHECKLISTS

(University of Florida - Gainesville)

Procedure for Patient's Room/Clinic

General patient preparation and ring attachment.

- ☐ Administer pre-operative medication.
- ☐ Attach head ring using most posterior and most anterior position.
- ☐ Make sure the word ANTERIOR is above the patient's nose.
- ☐ Ensure that top of CT localizer cage clears top of patient's head.
- ☐ Ensure the angio localizer cage clears patient's head and nose.
- ☐ Attach emergency wrench to head ring.
- ☐ Transport patient to angiography/CT.

Procedure for Patients Undergoing Angiography

Obtaining anterior and lateral angiograms for localization.

- ☐ Make patient's head as comfortable as possible with cushions/braces.
- ☐ Radiologist perform selective transfemoral catheterization.
- ☐ Attach ring support brace.
- ☐ Attach angio localizer cage.
- ☐ Position patient in fields.
- ☐ Take non-injected scout films to verify patient positioning.
- ☐ Ensure full size cut film.
- ☐ Adjust patient as necessary to include target and all 8 fiducial points on both films. Retake scouts if needed.
- ☐ Run injected angio series.
- ☐ Select best target views for later localization.
- ☐ Transport patient to CT.

Procedure for CT Scanning (all patients)

Taking CT scans for reconstruction in treatment planning (CT localization optional).

- ☐ OPTIONAL—Start IV for contrast injection (mandatory for CT localization).
- ☐ Attach CT table adapter to table.
- ☐ Place patient on table and attach head ring to table adapter.
- ☐ Attach CT localizer cage to head ring.
- ☐ Take scout view of patient's head.
- ☐ Examining scout view, adjust gantry tilt as necessary to make gantry plane parallel to head ring plane.
- ☐ Take scans of patient's head according to one of the following:
  - If angio localization is intended, take 5 mm thick scans 5 mm apart starting above the patient's head and ending at the ring. If contrast is desired, begin injecting 1 or 2 slices above the top of the target. Radiologist input may be helpful.
  - If CT will be used for localization, proceed as above except in the vicinity of the target using 3 mm thick scans 3 mm apart for increased resolution. Begin contrast injection before starting 3 × 3 scans.
- ☐ Remove CT localizer cage from ring.
- ☐ Unbolt patient from table adapter and remove patient.
- ☐ Remove adapter from table.
- ☐ Archive the complete CT examination to 1/2" tape for use in treatment planning.
- ☐ Take patient to room or outpatient holding area to wait during treatment planning process.

Procedure for Treatment Planning

Plan the patient's treatment using CAD (Computer-Aided Dosimetry) tools. There are two basic types of plans: angio localization and CT localization. This procedure indicates the differences between the two.

- ☐ Sign on to the Sun system with user name and password.
- ☐ Start the appropriate planning script with either the command **strs/utils/goangio** or **strs/utils/goctloc**.
- ☐ Answer the questions as the script prompts for the patient's name and hospital number.
- ☐ For angiogram localization:
  - The script will automatically start the angio localization program. Verify that the digitizer control box is turned on. Tape

patient films to the digitizer, side by side. For each of the two films:

a) OPTIONAL—Select contour entry and enter the patient's exterior or skull contour for frame of reference.
b) Select point entry and enter all 8 of the fiducial points.
c) The program will prompt if it discovers that the view is upside down based on the positions of the fiducial points.
d) Select target entry and trace the outline of the patient's lesion. When finished, hit the target trace button again to compute the geometric center and center of mass for the view.

- Examine the BRW coordinates and skew distance in the checklist window. Cycle between geometric center and center of mass to minimize the skew distance.
- OPTIONAL—If the skew distance seems excessively large or other considerations make the computed center unacceptable, the user may enter a user center to lock in the isocenter location. Save the data before exiting the angio program.
- The entire angio procedure may be repeated if desired.

☐ The script will automatically start the tape reading program.
☐ Input the required data to select a patient and examination from those available on the tape.
☐ The program will reconstruct all slices from the examination and place them on the disk.
☐ The script will automatically start the CT processing program.
☐ To process the CT's:

- Adjust mean and window for comfortable viewing.
- Trash images until an image with separated rods is visible.
- Select the position button and enter the position of the localizing rods beginning with the thick rod and proceeding clockwise.
- Save the processed image.
- Press the run button to continue processing the remaining images.
- If an image is present after the run, press trash until the program exits.

☐ To perform CT localization:

- The script will automatically start the CT localization program.
- Adjust mean and window for comfortable viewing.
- Page through axial slices until target appears largest.
- Outline the target with TRACE function. When through, press TRACE again to compute geometric center and center of mass.
- Position cursor over either of the two centers and pivot the image to para-sagittal view.

- Repeat the trace procedure for this view.
- As was described in angio localization, select between geometric center, center of mass, or a user input center to obtain the best isocenter location.
- Save the data before exiting.
- The entire CT localization process may be repeated, if desired.

☐ If more than 1 pass was made through the selected localization program, the script will prompt for selection of one of the sets of data.
☐ The script will automatically start the dosimetry program.
☐ Perform the treatment plan in accordance with detailed instructions on the use of the gamma 2 program.
☐ Remember to generate a hard copy of the dose distribution and save the data before exiting the program.
☐ The script will prompt for a dose prescription and isodose line. Enter the prescribed dose and the percent line to which the dose value is given.
☐ When the script prompts, request a hard copy of the treatment information.

Procedure at Radiation Therapy of Gainesville

Assemble apparatus onto accelerator, verify alignment, and treat patient.

☐ Make sure the film processor is turned on.
☐ Move the tool cart into the accelerator room for easy access to tools and parts.
☐ Remove the table top and place it to one side, out of the way.
☐ Remove the touch guard from the accelerator.
☐ Remove the inside corner floor boards.
☐ Replace with radiosurgery notched floor boards.
☐ Place radiosurgery table top onto table, making sure that adapter slides down onto alignment cone.
☐ Raise the table to level 15.
☐ Rotate the table to 50°.
☐ Position A-frame over floor, making sure that rear feet slide all the way into 'U' brackets in pit.
☐ Insert leveling ratchet into needle bearing in A-frame with the handle pointing towards the accelerator.
☐ Roll alignment apparatus over A-frame being careful not to bump table or A-frame.
☐ Carefully lower apparatus onto A-frame. Maintain alignment of holes in plate with holes in A-frame so that pins may be easily inserted.

- ☐ Insert three alignment T-pins through apparatus base plate into the A-frame.
- ☐ Remove wheels from apparatus and place to one side.
- ☐ Install table float modification in control system.
- ☐ Check floor stand leveling. If necessary, adjust level with ratchet by reaching through access hole in base plate.
- ☐ Set accelerator collimator rotation to 0° and primary field size to 5 × 5 cm.
- ☐ Attach gimble bearing plate to accelerator collimator.
- ☐ Remove collimator clamp from apparatus arm. Insert designated collimator through hole in arm into gimble bearing. Make sure that collimator seats firmly on lower lip of hole in arm. Reinstall the collimator clamp and tighten.
- ☐ While one person sets floor stand coordinates to target coordinates, another person setup phantom pointer on phantom base to the same coordinates.
- ☐ Install phantom pointer on floor stand using adapter.
- ☐ Place a piece of white paper behind phantom target ball. Turn on field light and rotate gantry about target, observing location of ball's shadow on paper. If shadow appears to move relative to field, re-check floor stand settings and phantom setting. Repeat until successful.
- ☐ Attach film holder to apparatus arm.
- ☐ Prepare a strip of film approximately 2" wide.
- ☐ Insert film strip into film holder. At several different gantry angles, expose the film to 55 MU, repositioning the strip for each exposure.
- ☐ Develop film. Examine film and verify that the phantom ball is centered in the radiation field in each exposure. Retain film strip for patient records.
- ☐ Remove film holder from apparatus arm.
- ☐ Remove phantom pointer and adapter from floor stand.
- ☐ Place patient on table and clamp head ring to floor stand.
- ☐ After adjusting table height to maximize patient comfort, securely clamp retaining collar to table ram, preventing table slippage.
- ☐ Recheck floor stand level, adjusting if necessary as above.
- ☐ Turn on lasers and observe the position of the lasers on the patient's skin. Verify that the position is in accordance with the known position of the target. Turn off lasers.
- ☐ Following the computer generated list of actions, treat the patient using the following procedure for each arc:
  1. Set floor stand coordinates to new isocenter if required for this arc.
  2. Rotate floor stand and table to correct angle.

  3. Recheck coordinates on floor stand.
  4. Manually move gantry completely through the range of the arc.
  5. Set machine for correct MU's and rotation direction. Note that the gantry should always rotate away from the floor stand.
  6. Administer radiation.
- ☐ After last arc, unbolt patient from floor stand.
- ☐ Remove table stop collar and lower table to a safe level.
- ☐ Remove head ring from patient and remove patient from table.
- ☐ Following the reverse of the assembly procedure, disassemble the apparatus and store the components.
- ☐ Remove the table float modification from the control system.

Parts List for Stands

- ☐ Appropriate medication for anxiety.
- ☐ Xylocaine.
- ☐ Syringe.
- ☐ Head Ring Assembly.
- ☐ Wrench.
- ☐ CT Localizer Cage.
- ☐ Angio Localizer Cage.
- ☐ Angio Table Support Bracket.
- ☐ CT Table Adapter.
- ☐ Ruler.
- ☐ Computer Tape.

ISOEFFECTIVE DOSE CURVES

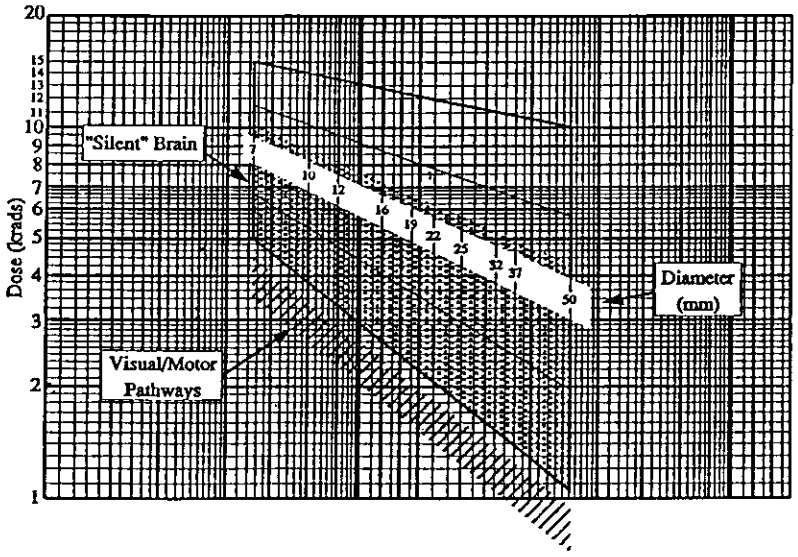

AVM dose determination. Isoeffective doses for proton beams of various diameters from 7 mm to 50 mm. The *bottom* line of the 4-sided figure represents the one percentile isoeffective dose for cerebral necrosis in the normal brain. Note that for a small beam (7 mm), the one percentile dose is 5000 rads. For a larger 50 mm beam, the one percentile isoeffective dose is 1100 rads. Isoeffective dose is different for each different beam diameter. Since the injured brain has a larger threshold for necrosis than normal brain, we operate with a margin below the one percentile line to provide a margin of safety.

GRAPH OF FIELD SIZE VS. COLLIMATOR SIZE

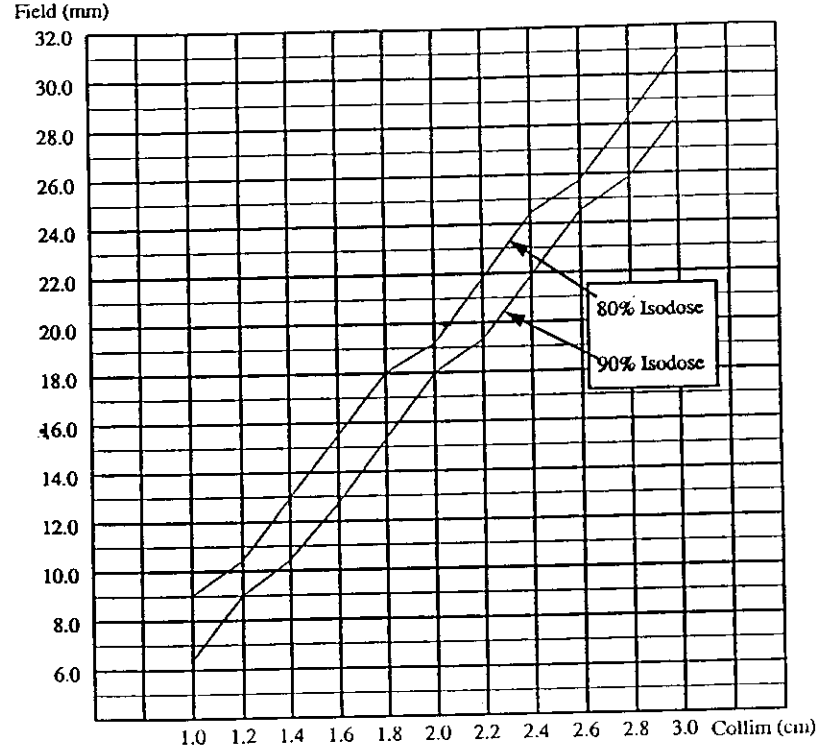

Note—Field size measured in transaxial plane through isocenter in lateral direction. Isodose curves generated by standard four arc distribution.

MAXIMUM ANGLE FOR VERTICAL OFFSET

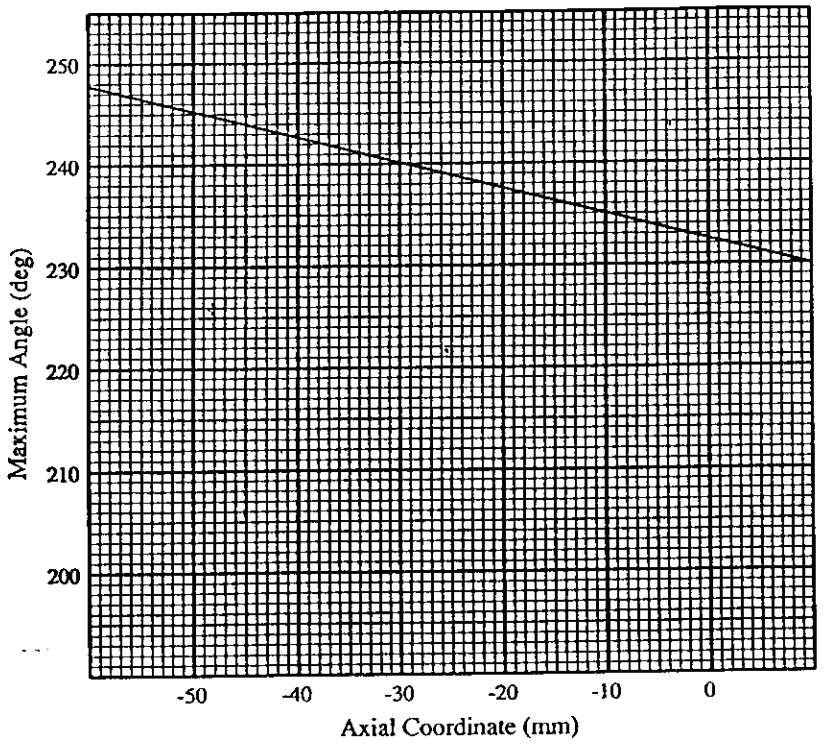

Maximum angle to which the gantry can be rotated based on the axial coordinate setting of the floor stand. This constraint must be taken into account when defining arcs in the patient's treatment plan.

XVIII. APPENDIX VII

DYNAMIC STEREOTACTIC BRAIN IRRADIATION PATIENT CHART (SAMPLE)

McGill University
Department of Radiation Oncology
Division of Physics

Patient #: _____
Patient name: _____
Hospital: _____
Patient #: _____
Diagnosis: _____

Treatment #: _____
Treatment unit: _____
Total prescribed dose (cGy): _____
Dose Maximum (cGy): _____
Prescribed isodose line (IL): _____

Number of Treatments Treatment number						
Date of treatment						
Prescribed dose for this treatment (TD)						
Physicians						
Physicists						

Collimator diameter Δ: _____ cm Linac collimator: ☐ 4 x 4 cm^2 ☐ 5 x 5 cm^2

Collimator Diameter (cm):	0.5	0.8	1	1.25	1.5	1.75	2	2.25	2.5	2.75	3	3.5	4
Relative Dose Factor RDF (Δ):	0.54	0.69	0.74	0.79	0.82	0.85	0.87	0.88	0.89	0.9	0.91	0.92	0.94

Stereotactic frame: OBT Leksell

Localization box: _____ Coordinates: x = _____ ; y = _____ ; z = _____

Tumor volume: _____ cm^3
Target volume: _____ cm^3

Couch height: ☐ ☐ ☐ ☐ ☐ ☐

DYNAMIC STEREOTACTIC BRAIN IRRADIATION PATIENT CHART (SAMPLE) *CONTINUED*

Calculate total required MU from equation:

$$MU = \frac{100xTD}{D_{max}(10)xRDF(D)xILxC_f} = \_\_\_\_\_ = \square$$

where D_{max} (10) = 1.05 cGy/MU, TD is the prescribed tumor dose. IL is the prescribed isodose line, RDF(A) is the relative dose factor for the collimator and C_f is the correction factor for the stereotactic frame (0.98).

Gantry angular interval: $A = 180 - \theta_i$ = ...

Maximum MU per gantry angular interval: $B = (180 - \theta_i) \times 4.99$ = ...

Estimated number of angular intervals required: $C = \frac{\text{Total MU}}{B} = \_\_\_\_ =$ .....

Adjusted C upwards to the nearest even number: D = ...

Calculated MU per angular interval: $E = \frac{\text{Total MU}}{D} = \_\_\_\_ =$

Calculated and set MU per degree: $\frac{E}{A}$ _____ (must be less than 4.99) =

	FRACTIONAL TREATMENT MU (DOS 1)			FRACTIONAL TREATMENT MU (DOS 1)	
1	1. Gantry (CW) θ_i to 180°		6	11. Gantry (CCW) θ_i to 180°	
	2. Gantry (CW) 180° to θ_f			12. Gantry (CCW) 180° to θ_i	
2	3. Gantry (CCW) θ_f to 180°		7	13. Gantry (CW) θ_i to 180°	
	4. Gantry (CCW) 180° to θ_i			14. Gantry (CW) 180° to θ_f	
3	5. Gantry (CW) θ_i to 180°		8	15. Gantry (CCW) θ_f to 180°	
	6. Gantry (CW) 180° to θ_f			16. Gantry (CCW) 180° to θ_i	
4	7. Gantry (CCW) θ_f to 180°		9	17. Gantry (CW) θ_i to 180°	
	8. Gantry (CCW) 180° to θ_i			18. Gantry (CW) 180° to θ_f	
5	9. Gantry (CW) θ_i to 180°		10	19. Gantry (CCW) θ_f to 180°	
	10. Gantry (CW) 180° to θ_f			20. Gantry (CCW) 180° to θ_i	

TOTAL MU GIVEN

REFERENCES

1. *AAPM Policy Statement*, 1985. The roles, responsibilities, and status of the clinical medical physicist. 1985 Presidential Ad Hoc Committee, E. C. McCullough, B. E. Bjarngaard and J. A. Deye.
2. *AAPM Report 13*. Physical aspects of quality assurance in radiation therapy. (American Association of Physicists in Medicine, New York, 1984).
3. *AAPM Report 21*: A protocol for absorbed dose from high-energy beams. Report of AAPM Task Group 21. Med. Phys. **10**:741 (1983).
4. *AAPM Report 40*. Comprehensive QA for Radiation Oncology: Report of AAPM Radiation Therapy Committee Task Group 40, 1993 (submitted for publication).
5. *AAPM Report 45*. AAPM code of practice for radiotherapy accelerators: Report of AAPM Radiation Therapy Task Group No. 45, 1993 (submitted for publication).
6. *ACMP Report 2*. Radiation control and quality assurance in radiation oncology; a suggested protocol. (American College of Medical Physics, Madison, WI, 1986).
7. E. Alexander III, J. S. Loeffler, and L. D. Lunsford, *Stereotactic radiosurgery*. (McGraw Hill, New York, NY, 1993).
8. G. Arcovito, A. Piermattei, G. D'Abramo, and F. A. Bassi, "Dose measurements and calculations of small radiation fields for 9-MV x rays," Med. Phys. **12**, 779 (1985).
9. J. L. Barcia-Salorio, P. Roldan, G. Henandez, and G. L. Lopez, "Radiosurgical treatment of epilepsy," Appl. Neurophysiol. **48**, 400 (1985).
10. A. S. Beddar, "Dosimetry of stereotactic radiation fields using a miniature plastic scintillator detector," Med. Phys. **19**, 790 (1992) (abstract).
11. O. O. Betti and V. E. Derechinsky, "Hyperselective encephalic irradiation with linear accelerator," Acta. Neurochirurgica., Suppl. **33**, 385 (1984).
12. O. O. Betti, C. Munari, and R. Rosler, "Stereotactic radiosurgery with the linear accelerator: treatment of arteriovenous malformations," Neurosurgery. **24**, 311 (1989).
13. B. E. Bjarngard, J. S. Tsai, and R. K. Rice, "Doses on central axis of narrow 6-MV x-ray beams," Med. Phys. **17**, 794 (1990).
14. F. J. Bova and W. A. Friedman, "Stereotactic angiography: an inadequate database for radiosurgery?" Int. J. Radiat. Oncol. Biol. Phys. **20**, 891 (1991).
15. J. D. Bradshaw, "The stereotactic radiosurgery unit in Sheffield," Clin. Radiol. **37**, 277 (1986).
16. D. J. Brenner, M. K. Martel, and E. J. Hall, "Fractionated regimens for stereotactic radiotherapy of recurrent tumors in the brain," Int. J. Radiat. Oncol. Biol. Phys. **21**, 819 (1991).
17. M. Carol, Stereotactic Surgery and Radiosurgery, (Med. Phys. Pub. Co., Madison, WI, 1993), pp. 249–326.
18. G. T. Y. Chen, R. P. Singh, J. R. Castro, *et al.*, "Treatment planning for heavy ion therapy," Int. J. Radiat. Oncol. Biol. Phys. **5**, 1809 (1979).
19. G. Chierego, C. Marchetti, R. C. Avanzo, *et al.*, "Dosimetric considerations on multiple arc stereotaxic radiotherapy," Radiotherapy and Oncology. **12**, 141 (1988).
20. F. Colombo, A. Benedetti, L. Casentini, *et al.*, "Linear accelerator radiosurgery of arteriovenous malformations," Appl. Neurophysiol. **50**, 257 (1987).
21. F. Colombo, A. Benedetti, F. Pozza, *et al.*, "External stereotactic irradiation by linear accelerator," Neurosurgery. **16**, 154 (1985).
22. F. Colombo, A. Benedetti, F. Pozza, *et al.*, "Stereotactic radiosurgery utilizing a linear accelerator," Appl. Neurophysiol. **48**, 133 (1985).
23. R. Cox, W. P. Haneman, and S. W. Brain, "Dose distributions produced by a robot-mounted linac (abstract)," Med. Phys. **20**, 889 (1993).
24. D. J. Dawson, N. J. Schroeder, and J. D. Hoya, "Penumbral measurements in water for high-energy x rays," Med. Phys. **13**, 101 (1986).
25. C. E. DeMagri, V. Smith, M. C. Schell, *et al.*, "Interlock system for linear accelerator radiosurgery." To be submitted to Int. J. Radiat. Oncol. Biol. Phys. 1995.
26. R. Drzymala, "Quality assurance for linac-based stereotactic radiosurgery in quality assurance in radiotherapy physics," Proc. American College of Medical Physics Symp., G. Starkshall and J. Horton, eds. (Medical Physics Pub., Madison, WI, 1991).

27. H. Ehricke, L. R. Schad, G. Gademann, *et al.*, "Use of MR angiography for stereotactic planning," J. Comp. Asst. Tomography. **16**, 35 (1992).
28. J. I. Fabrikant, J. T. Lyman, and Y. Hosobuchi, "Stereotactic heavy-ion Bragg peak radiosurgery for intracranial vascular disorders: method for treatment of deep arteriovenous malformations," Br. J. Radiol. **57**, 479 (1984).
29. J. I. Fabrikant, J. T. Lyman, and K. A. Frankel, "Heavy charged-particle Bragg peak radiosurgery for intercranial vascular disorders," Radiat. Res. Suppl. **104**, S244 (1985).
30. J. C. Flickinger and J. Loeffler, 34th annual scientific meeting—American Society for Therapeutic Radiology and Oncology, Stereotactic adiosurgery; refresher course #410, November 1992.
31. J. C. Flickinger, A. Maitz, L. D. Kalend, *et al.*, "Treatment volume shaping with selective beam blocking using the Leksell Gamma Unit," Int. J. Radiat. Oncol. Biol. Phys. **19**, 783 (1990).
32. J. C. Flickinger, M. C. Schell, and D. A. Larson, "Estimation of complications for linear accelerator radiosurgery with the integrated logistic formula," Int. J. Radiat. Oncol. Biol. Phys. **19**, 143 (1990).
33. W. A. Friedman, and F. J. Bova, "The University of Florida radiosurgery system," Surg. Neurol. **32**, 334 (1989).
34. B. G. Fuller, I. D. Kaplan, J. Adler, *et al.*, "Stereotactic radiosurgery for brain metastases: the importance of adjuvant whole brain irradiation," Int. J. Radiat. Oncol. Biol. Phys. **23**, 413 (1992).
35. R. L. Galloway and R. J. Maciunas, "Stereotactic neurosurgery," Biomedical Engineering. **18**, 181 (1990).
36. M. Goitein, M. Abrams, R. Gentry, *et al.*, "Planning treatment with heavy charged particles," Int. J. Radiat. Oncol. Biol. Phys. **8**, 2065 (1982).
37. E. C. Halperin, G. Bentel, E. R. Heinz, *et al.*, "Radiation therapy treatment planning in supratentorial glioblastoma multiforme: an analysis based in postmortem. Topographic anatomy with CT correlations," Int. J. Radiat. Oncol. Biol. Phys. **17**, 1347 (1989).
38. M. I. Hariz, R. Henricksson, P. O. Lofroth, *et al.*, "A non-invasive method for fractionated stereotactic irradiation of brain tumors with linear accelerator," Radiotherapy and Oncology. **17**, 57 (1990).
39. G. H. Hartmann, B. Bauer-Kirpes, C. F. Serago, *et al.*, "Precision and accuracy of stereotactic convergent beam irradiations from a linear accelerator," Int. J. Radiat. Oncol. Biol. Phys. **28**, 481 (1993).
40. G. H. Hartmann, W. Schlegel, V. Sturm, *et al.*, "Cerebral radiation surgery using moving field irradiation at a linear accelerator facility," Int. J. Radiat. Oncol. Biol. Phys. **11**, 1185 (1985).
41. F. H. Hochberg and A. Pruitt, "Assumptions in the radiotherapy of glioblastoma," Neurology. **30**, 907 (1980).
42. Y. Hosobuchi, J. Fabricant, and J. Lyman, "Stereotactic heavy-particle irradiation of intracranial arteriovenous malformations," Appl. Neurophysiol. **50**, 248 (1987).
43. P. V. Houdek, "Computer controlled stereotactic radiotherapy system," Int. J. Radiat. Oncol. Biol. Phys. **19**(Suppl. 1) (1990) (abstract).
44. P. V. Houdek, J. V. Fayos, B. J. M. Van, *et al.*, "Stereotactic radiotherapy technique for small intracranial lesions," Med. Phys. **12**, 469 (1985).
45. P. V. Houdek, J. M. VanBuren, and J. V. Fayos, "Dosimetry of small radiation fields for 10-MV x rays," Med. Phys. **10**, 333 (1983).
46. S. K. Jani, *Handbook of dosimetry data for radiotherapy*. (CRC Press, Boca Raton, FL., 1993).
47. JCAHO quality assurance standards. Joint commission on the accreditation of healthcare organizations, radiation oncology services. 1987 (unpublished).
48. JCAHO quality assurance standards. Joint commission on the accreditation of healthcare organizations, radiation oncology services. 1992 (unpublished).
49. D. Jones, D. A. Christopherson, J. E. Raisis, *et al.* "The use of an external reference frame system in brain implants," Endocurie. Hypertherm. Oncol. **5**, 221 (1989).
50. E. D. Jones, "Risk analysis in regulating the use of nuclear medical devices. Fission energy and systems safety program." (Lawrence Livermore National Lab., Livermore, CA, 1994). NRC FIN L-1938. Report in progress, (submitted for publication).

51. F. M. Kahn, W. Schwchand, J. Lee, *et al.*, "Revision of tissue-maximum ratio and scatter-maximums ratio concepts for cobolt 60 and higher energy x-ray beams," Med. Phys. **7**, 230 (1980).
52. A. Kalend, A. Zheng, A. Wu, *et al.*, "A miniature air ionization chamber for absolute dose measurement in radiosurgery," Med. Phys. **20**, 926, (1993) (abstract).
53. D. Kamerer, L. D. Lunsford, and M. Miller, "Gamma Knife: an alternative treatment for acoustic neuromas," Ann. Otol. Rhinol. Laryngol. **97**, 631 (1988).
54. P. J. Kelly, C. Daumas-Dupport, D. B. Kispert, *et al.*, "Image-based stereotactic biopsies in untreated intracranial gliol neoplasms," J. Neurosurg. **66**, 865 (1987).
55. D. W. Kerst, "Betatron-Quastler era at the University of Illinois," Med. Phys. **2**, 297 (1975).
56. M. L. Kessler and P. L. Carson, "Test object design and performance simulation for 3-D imaging systems: spiral rod image distortion phantom," Annual meeting of the Radiological Society of North America (1992) (abstract).
57. L. Kihlstrom, "Stereotactic radiosurgery – epidemeologic considerations," Karolinska Stockholm Hospital, 1986.
58. R. N. Kjellberg, "Stereotactic bragg peak proton beam radiosurgery for cerebral arteriovenous malformations," Ann. Clin. Res. **47**, 17 (1986).
59. R. N. Kjellberg, K. R. Davis, S. Lyons, *et al.*, "Bragg peak proton beam therapy for arteriovenous malformation of the brain," Clin. Neurosurg. **31**, 248 (1983).
60. H. Kooy, L. Nedzi, L. A. Nedzi, *et al.*, "Treatment planning for stereotactic radiosurgery of intracranial lesions," Int. J. Radiat. Oncol. Biol. Phys. **21**, 683 (1991).
61. H. Kooy, M. van Herk, P. Barnes, *et al.*, "Image fusion for stereotactic radiotherapy and radiosurgery treatment planning," Int. J. Radiat. Oncol. Biol. Phys. (1993).
62. D. A. Larson, P. H. Gutin, S. A. Leibel, "Stereotactic irradiation of brain tumors," Cancer. **65**, 792 (1990).
63. B. Larsson, K. Linden, and B. Sarby, "Irradiation of small structures through the intact skull," Acta Radiologica. Ther. Phys. Biol. **13**, 512 (1974).
64. D. D. Leavitt, F. A. Gibbs, M. P. Heilbrun, *et al.*, "Dynamic field shaping to optimize radiosurgery," Int. J. Radiat. Oncol. Biol. Phys. **21**, 1247 (1991).
65. D. D. Leavitt, J. R. Stewart, J. H. Moeller, *et al.*, "Electron arc therapy: implementation and evaluation of a dynamic multi-vane collimator system," Int. J. Radiat. Oncol. Biol. Phys. **17**, 1089 (1989).
66. D. G. Leksell, "Stereotactic radiosurgery. Present status and future trends," Neurol. Res. **9**, 60 (1987).
67. L. T. Leksell, "Stereotactic radiosurgery," J. Neurol. Neurosurg. Psychiatry. **46**, 797 (1983).
68. L. T. Leksell, "The stereotactic method and radiosurgery of the brain," Acta Chir. Scand. **102**, 316 (1951).
69. R. Levy, J. Fabricant, K. Frankel, "Stereotactic heavy charged particle Bragg peak radiosurgery for the treatment of intracranial arteriovenous malformations in childhood and adolescence," Neurosurg. **24**, 841 (1989).
70. L. D. Lunsford, and D. A. Larson, "Consensus Statement on Stereotactic Radiosurgery Prepared by The American Association of Neurological Surgeons Task Force on Stereotactic Radiosurgery and The American Society for Therapeutic Radiology and Oncology Task Force on Stereotactic Radiosurgery," Neurosurgery **34**, 193 (1994).
71. L. D. Lunsford, A. Maitz, G. Linder, "First United States 201 source ^{60}Co Gamma Unit for radiosurgery," Appl. Neurophysiol. **50**, 253 (1987).
72. L. D. Lunsford, J. Flickinger, G. Lindner, *et al.*, "Stereotactic radiosurgery of the brain using the first United States 201 ^{60}Co source Gamma Knife," Neurosurgery. **24**, 151 (1989).
73. W. Lutz, K. R. Winston, N. Maleki, "A system for stereotactic radiosurgery with a linear accelerator," Int. J. Radiat. Oncol. Biol. Phys. **14**, 373 (1988).
74. G. Luxton, P. Zbigniew, G. Jozsef, *et al.*, "Stereotactic radiosurgery: principles and comparison of treatment methods," Neurosurgery. **32**, 241 (1993).
75. J. T. Lyman and A. Wolbarst, "Optimization of radiation therapy, III: a method of assessing complication probabilities from dose-volume histograms," Int. J. Radiat. Oncol. Biol. Phys. **13**, 103 (1987).

76. J. T. Lyman, M. H. Phillips, K. A. Frankel, *et al.*, "Stereotactic frame for neuroradiology and charged particle Bragg peak radiosurgery of intracranial disorders," Int. J. Radiat. Oncol. Biol. Phys. **16**, 1615 (1989).
77. J. T. Lyman and C. Y. Chong, "ISAH: a versatile treatment positioner for external radiation therapy," Cancer. **34**, 12 (1974).
78. R. J. Maciunas, R. L. Galloway, J. W. Latimer, "The application accuracy of stereotactic frames," Neurosurgery. **35**, 682 (1994).
79. T. R. Mackie, P. J. Reckwerdt, S. Swerdloff, *et al.*, "Tomotherapy: a proposal for optimized dose delivery of radiotherapy," Med. Phys. **20**, 875 (1993).
80. M. R. McKenzie, L. Souhami, E. B. Podgorsak, *et al.*, "Photon radiosurgery: a clinical review," Canadian J. Neurol. Sci. **19**, 212 (1992).
81. MEDCO (private communication).
82. H. Meertens, "Digital processing of high-energy photon beam images," Med. Phys. **12**, 11 (1985).
83. C. M. Meger-Wells and T. R. Mackie, "Dosimetry of stereotactic radiosurgery beams using a plastic scintillation detector," Med. Phys. **20**, 890 (1993).
84. M. Mehta, J. Mascíopinto, K. Bastin, *et al.*, "Glioblastoma treated with external beam radiotherapy and stereotactic radiosurgery boost," Int. J. Radiat. Oncol. Biol. Phys. **27**, 152 (suppl.) (1993).
85. J. Milan and R. E. Bentley, "The storage and manipulation of radiation dose data in a small digital computer," Br. J. Radiol. **47**, 115 (1974).
86. L. A. Nedzi, H. Kooy, E. Alexander III, *et al.*, "Dose volume consideration in field shaping for stereotactic radiosurgery using a linear accelerator," Radiosurgery update, Pine Manor College, Chestnut Hill, MA, June, 1990.
87. L. A. Nedzi, H. Kooy, E. Alexander III, *et al.*, "Variables associated with the development of complications from radiosurgery of intracranial tumors," Int. J. Radiat. Oncol. Biol. Phys. **21**, 591 (1991).
88. L. A. Nedzi, H. Kooy, E. Alexander III, *et al.*, "Dynamic field shaping for stereotactic radiosurgery: a modeling study," Int. J. Radiat. Oncol. Biol. Phys. **25**, 859 (1993).
89. P. F. J. New, R. G. Ojemann, K. R. Davis, *et al.*, "MR and CT of occult vascular malformations of the brain," Am. J. Radiology. **147**, 985 (1986).
90. A. Niemierko and M. Goitein, "The influence of the size of the grid used for dose calculation on the accuracy of dose estimation," Med. Phys. **16**, 239 (1989).
91 A. Olivier, A. de Lotbiniere, T. Peters, *et al.*, "Combined use of digital subtraction angiography and MRI for radiosurgery and stereoencephalography," Appl. Neurophysiol. **50**, 92 (1987).
92. L. E. Olsson, J. Arndt, A. Fransson, *et al.*, "Three-dimensional dose mapping from gamma knife treatment using a dosimeter gel and MR-imaging," Radiotherapy and Oncology. **24**, 82 (1992).
93. S. Otto-Oelschlager, W. Schlegel, W. Lorenz, "Different collimators in convergent beam irradiation of irregularly shaped intracranial target volumes," Radiotherapy and Oncology. **30**, 175 (1994).
94. T. M. Peters, J. Clark, B. Pike, *et al.*, "Stereotactic surgical planning with magnetic resonance imaging, digital subtraction angiography and computed tomography," Appl. Neurophysiol. **50**, 33 (1987).
95. M. H. Phillips, K. A. Frankel, J. T. Lyman, *et al.*, "Comparison of different radiation types and irradiation geometries in stereotactic radiosurgery," Int. J. Radiat. Oncol. Biol. Phys. **18**, 211 (1990).
96. M. H. Phillips, K. A. Frankel, J. T. Lyman, *et al.*, "Heavy charged-particle stereotactic radiosurgery: cerebral angiography and CT in the treatment of intracranial vascular malformations," Int. J. Radiat. Oncol. Biol. Phys. **17**, 419 (1989).
97. B. Pike, T. M. Peters, E. B. Podgorsak, *et al.*, "Stereotactic external beam calculations for radiosurgical treatment of brain lesions," Appl. Neurophysiol. **50**, 269 (1987).
98. B. Pike, E. B. Podgorsak, T. M. Peters, *et al.*, "Dose distributions in dynamic stereotactic radiosurgery," Med. Phys. **14**, 780 (1987).
99. E. B. Podgorsak, "Physics for radiosurgery with linear accelerators," Neurosurgery Clinics of North America. **3**, 9 (1992), edited by L.D. Lunsford, "Stereotactic Radiosurgery."

100. E. B. Podgorsak, A. Olivier, M. Pla, "Physical aspects of dynamic stereotactic radiosurgery," Appl. Neurophysiol. **50**, 263 (1987).
101. E. B. Podgorsak, A. Olivier, M. Pla, *et al.*, "Dynamic stereotactic radiosurgery," Int. J. Radiat. Oncol. Biol. Phys. **14**, 115 (1988).
102. E. B. Podgorsak, G. B. Pike, A. Olivier, *et al.*, "Radiosurgery with high energy photon beams: a comparison among techniques," Int. J. Radiat. Oncol. Biol. Phys. **16**, 857 (1989).
103. E. B. Podgorsak, G. B. Pike, M. Pla, *et al.*, "Radiosurgery with photon beams: physical aspects and adequacy of linear accelerators," Radiotherapy and Oncology. **17**, 349 (1990).
104. I. Rabinowitz, J. Broomberg, M. Goitein, *et al.*, "Accuracy of radiation field alignment in clinical practice," Int. J. Radiat. Oncol. Biol. Phys. **2**, 67 (1985).
105. R. K. Rice, J. L. Hansen, G. K. Svensson, *et al.* "Measurements of dose distributions in small beams of 6-MV x rays," Phys. Med. Biol. **32**, 1087 (1987).
106. W. M. Saunders, K. R. Winston, R. L. Siddon, *et al.*, "Radiosurgery for arteriovenous malformations of the brain using a standard linear accelerator: rationale and technique," Int. J. Radiat. Oncol. Biol. Phys. **15**, 441 (1988).
107. C. B. Saw, K. Ayyangar, N. Suntharalingam, "Coordinate transformations and calculation of the angular and depth parameters for a stereotactic system," Med. Phys. **14**, 1042 (1987).
108. L. R. Schad, H. Ehricke, B. Wowra, *et al.*, "Correction of spatial distortion in magnetic resonance angiography for radiosurgical treatment planning of cerebral arteriovenous malformations," Magnetic Resonance Imaging. **10**, 9 (1992).
109. M. C. Schell and H. Kooy, "Stereotactice radiosurgery quality improvement: interdepartmental collaboration," Int. J. Radiat. Oncol. Biol. Phys. **28**, 551 (1994).
110. M. C. Schell, J. H. Evans, M. K. Martel, *et al.*, "A methodology for the analysis of stereotactic radiosurgery beam data," Submitted to Med. Phys., 1994.
111. M. C. Schell, V. Smith, D. A. Larson, *et al.*, "Evaluation of radiosurgery techniques with cumulative dose volume histograms in linac-based stereotactic external beam irradiation," Int. J. Radiat. Oncol. Biol. Phys. **20**, 1325 (1991).
112. J. G. Schwade, P. V. Houdek, H. J. Landy, *et al.*, "Small-field stereotactic external beam radiation therapy of intracranial lesions: fractionated treatment with a fixed-halo immobilization device," Radiology. **176**, 563 (1990).
113. C. F. Serago, P. V. Houdek, G. H. Hartmann, *et al.*, "Tissue maximum ratios (and other parameters) of small circular 4, 6, 10, 15 and 24 MV x-ray beams for radiosurgery," Phys. Med. Biol. **37**, 1943 (1992).
114. C. F. Serago, A. A. Lewin, P. V. Houdek, *et al.*, "Improved linac dose distributions for radiosurgery with irregularly shaped fields," Int. J. Radiat. Oncol. Biol. Phys. **19**, 134 (1990) (abstract).
115. C. F. Serago, A. A. Lewin, P. V. Houdek, *et al.*, "Stereotactic radiosurgery: dose volume analysis of linear accelerator techniques," Med. Phys. **19**, 181 (1992).
116. C. F. Serago, A. A. Lewin, P. V. Houdek, *et al.*, "Stereotactic target point verification of an x-ray and CT localizer," Int. J. Radiat. Oncol. Biol. Phys. **20**, 517 (1991).
117. E. Shaw, R. Kline, M. Gillin, *et al.*, "Radiation therapy oncology group: radiosurgery quality assurance guidelines," Int. J. Radiat. Oncol. Biol. Phys. **27**, 1231 (1993).
118. R. L. Siddon and N. H. Barth, "Stereotaxic localization of intracranial targets," Int. J. Radiat. Oncol. Biol. Phys. **13**, 1241 (1987).
119. K. E. Sixel and R. Podgorsak, "Buildup region of high-energy x-ray beams in radiosurgery," Med. Phys. **20**, 761 (1993).
120. K. E. Sixel, "Physical parameters of narrow photon beams in radiosurgery," M. Sc. thesis, McGill University, Montreal, Canada, 1990.
121. V. Smith, M. C. Schell, and D. A. Larson, "The role of tertiary collimation for linac-based radiosurgery," American Association of Physicists in Medicine Annual Meeting, 1989.
122. A. Sofat, G. Kratimenos, and D. G. Thomas, "Early experience with the Gill–Thomas Locator for computed tomography-directed stereotactic biopsy of intracranial lesions," Neurosurgery **31**, 972 (1992).
123. L. Souhami, A. Olivier, E. B. Podgorsak, *et al.*, "Radiosurgery of cerebral arteriovenous

malformations with the dynamic stereotactic irradiation," Int. J. Radiat. Oncol. Biol. Phys. **19**, 775 (1990).
124. L. Steiner, *Radiosurgery in cerebral arteriovenous malformations. Textbook of cerebrovascular surgery*, edited by Flam and Fein, (Springer Verlag, New York, 1986).
125. V. Sturm, B. Kober, K. H. Hover, *et al.*, "Stereotactic percutaneous single dose irradiation of brain metastases with a linear accelerator," Int. J. Radiat. Oncol. Biol. Phys. **13**, 279 (1987).
126. T. S. Sumanaweera, J. R. Adler, S. Napel, *et al.*, "Characterization of spatial distortion in magnetic resonance imaging and its implications for stereotactic surgery," Neurosurgery **35**, 696 (1994).
127. G. K. Svensson, "Physical aspects of quality assurance," For the committee on quality assurance in radiation oncology. American College of Radiology, 1990.
128. J. Tsai, B. A. Buck, G. K. Svensson, *et al.*, "Quality assurance in stereotactic radiosurgery using a standard linear accelerator," Int. J. Radiat. Oncol. Biol. Phys. **21**, 737 (1991).
129. J. Van Dyk, R. B. Barnett, J. E. Cygler, *et al.*, "Commissioning and quality assurance of treatment planning computers," Int. J. Radiat. Oncol. Biol. Phys. **26**, 261 (1993).
130. K. E. Wallner, J. H. Galicich, M. G. Malkin, *et al.*, "Inability of computed tomography appearance of recurrent malignant astrocytoma to predict survival following reoperation," J. Clin. Oncology **7**, 1492 (1989).
131. K. E. Wallner, J. H. Galicich, M. G. Malkin, *et al.*, "Patterns of failure following treatment for glioblastoma multiforme and anaplastic astrocytoma," Int. J. Radiat. Oncol. Biol. Phys. **16**, 1405 (1989).
132. L. Walton, C. K. Bomford, and D. Ramsden, "The Sheffield stereotactic radiosurgery unit: physical characteristics and principles of operation," Br. J. Radiol. **60**, 897 (1987).
133. R. R. Wilson, "Radiological use of fast protons," Radiology **40**, 487 (1946).
134. K. R. Winston and W. Lutz, "Linear accelerator as a neurosurgical tool for stereotactic radiosurgery," Neurosurgery **22**, 454 (1988).
135. A. Wu, A. H. Maitz, A. M. Kalend, *et al.*, "Physics of gamma knife approach on convergent beams in stereotactic radiosurgery," Int. J. Radiat. Oncol. Biol. Phys. **18**, 941 (1990).
136. D. Yeung, J. Palta, J. Fontanesi, *et al.*, "Systematic analysis of errors in target localization and treatment delivery in stereotactic radiosurgery (SRS)," Int. J. Radiat. Oncol. Biol. Phys. **28**, 493 (1994).

No. 22 "Rotation Scintillation Camera Spect Acceptance Testing and Quality Control," Task Group of the Nuclear Medicine Committee (1987)

No. 23 "Total Skin Electron Therapy: Technique and Dosimetry," AAPM Radiation Therapy TG #30 (1988)

No. 24 "Radiotherapy Portal Imaging Quality," AAPM Radiation Therapy TG #28 (1988)

No. 25 "Protocols for the Radiation Safety Surveys of Diagnostic Radiological Equipment," AAPM Diagnostic X-Ray Imaging Committee TG #1 (1988)

No. 26 "Performance Evaluation of Hyperthermia Equipment," AAPM Hyperthermia TG #1 (1989)

No. 27 "Hyperthermia Treatment Planning," AAPM Hyperthermia Committee TG #2 (1989)

No. 28 "Quality Assurance Methods and Phantoms for Magnetic Resonance Imaging," AAPM Nuclear Magnetic Resonance Committee TG #1 (1990)

No. 29 "Equipment Requirements and Quality Control for Mammography," AAPM Diagnostic X-Ray Imaging Committee TG #7 (1990)

No. 30 "E-mail and Academic Computer Networks," AAPM Computer Committee TG #1 (1990)

No. 31 "Standardized Methods for Measuring Diagnostic X-Ray Exposures," AAPM Diagnostic X-Ray Imaging Committee TG #8 (1991)

No. 32 "Clinical Electron-Beam Dosimetry," Radiation Therapy Committee TG #25 (1991)

No. 33 "Staffing Levels and Responsibilities in Diagnostic Radiology" Diagnostic X-Ray Imaging Committee TG #5 (1991)

No. 34 "Acceptance Testing of Magnetic Resonance Imaging Systems" AAPM Nuclear Magnetic Resonance TG #6 (1992)

No. 35 "Recommendations on Performance Characteristics of Diagnostic Exposure Meters" AAPM Diagnostic X-Ray Imaging TG #6 (1992)

No. 36 "Essentials and Guidelines for Hospital Based Medical Physics Residency Training Programs," AAPM Presidential Ad Hoc Committee (1992)

No. 37 "Auger Electron Dosimetry" AAPM Nuclear Medicine Committee TG #6 (1993)

No. 38 "The Role of the Physicist in Radiation Oncology," Professional Information and Clinical Relation Committee TG #1 (1993)

No. 39 "Specification and Acceptance Testing of Computed Tomography Scanners," Diagnostic X-Ray Imaging Committee TG #2 (1993)

No. 40 "Radiolabeled Antibody Tumor Dosimetry," AAPM Nuclear Medicine Committee TG #2 (1993)

No. 41 "Remote Afterloading Technology," Remote Afterloading Technology TG #41 (1993)

No. 42 "The Role of the Clinical Medical Physicist in Diagnostic Radiology," AAPM Professional Information and Clinical Relations Committee TG #2 (1993)

No. 43 "Quality Assessment and Improvement of Dose Response Models," $25, (1993). Published by Medical Physics Publishing. They can be contacted at (800) 442-5778 or fax (608) 265-2121

No. 44 "Academic Program for Master of Science Degree in Medical Physics," AAPM Education and Training of Medical Physicists Committee (1993)

No. 45 "Management of Radiation Oncology Patients with Implanted Cardiac Pacemakers," AAPM Task Group #4 (1994)

No. 46 "Comprehensive QA for Radiation Oncology," AAPM Radiation Therapy Committee TG #40 (1994)

No. 47 "AAPM Code of Practice for Radiotherapy Accelerators," AAPM Radiation Therapy TG #45 (1994)

No. 48 "The Calibration and Use of Plane-Parallel Ionization Chambers for Dosimetry of Electron Beams," AAPM Radiation Therapy Committee TG #39 (1994)

No. 49 "Dosimetry of Auger-Electron-Emitting Radionuclides," AAPM Nuclear Medicine TG #6 (1995)

No. 50 "Fetal Dose from Radiotherapy with Photon Beams," AAPM Radiation Therapy Committee TG #36 (1995)

No. 51 "Dosimetry of Interstitial Brachytherapy Sources," AAPM Radiation Therapy Committee TG #43 (1995)

No. 52 "Quantitation of SPECT Performance," AAPM Nuclear Medicine Committee TG #4 (1995)

No. 53 "Radiation Information for Hospital Personnel," AAPM Radiation Safety Committee (1995)

No. 54 "Stereotactic Radiosurgery," Radiation Therapy Committee TG #42 (1995)

****

Return to: American Institute of Physics
c/o AIDC
P. O. Box 20
Williston, VT 05495-0020
(800) 809-2247 phone
(802) 864-7626 FAX

Name: _____

Address: _____

_____

____ copies of _____ @ ____

____ copies of _____ @ ____

____ copies of _____ @ ____

Prepayment required
U.S. check or International
Money Order

Amount enclosed _____